Investigating the Influence of Hydrophobicity on the Thermoresponsive Behavior of Statistical Copolymers

by

Irem Akar



A thesis submitted to the University of Birmingham for the degree of

DOCTOR OF PHILOSOPHY

School of Chemistry

College of Engineering and Physical Sciences

University of Birmingham

January 2023

UNIVERSITY OF
BIRMINGHAM

University of Birmingham Research Archive

e-theses repository

This unpublished thesis/dissertation is copyright of the author and/or third parties. The intellectual property rights of the author or third parties in respect of this work are as defined by The Copyright Designs and Patents Act 1988 or as modified by any successor legislation.

Any use made of information contained in this thesis/dissertation must be in accordance with that legislation and must be properly acknowledged. Further distribution or reproduction in any format is prohibited without the permission of the copyright holder.

Abstract

Thermoresponsive polymers have gained interest over many decades and have been used in diverse applications such as bioseparation, tissue engineering and drug delivery owing to their readily tunable nature. Several ways to tune the thermoresponsive behavior of polymers have been reported, providing a wide range of opportunities to design polymeric systems as required for specific applications. The aim of this project was to investigate the effect of polymer hydrophobicity on tuning the thermoresponsive behavior of statistical amphiphilic copolymers achieved *via* reversible addition-fragmentation chain-transfer (RAFT) polymerization and explore the biological efficacy of thermoresponsive nanoparticles functionalized with therapeutic moieties. Importantly, a computational tool was used for the determination of hydrophobicity of the produced copolymers, and it was aimed to correlate the values that represented polymer hydrophobicity to the measured macroscopic changes in the polymer solution upon change in temperature. The findings of these studies are expected to provide insight into the design of new functional copolymers with required thermoresponsiveness. Moreover, thermoresponsive nanoparticles were developed *via* polymerization-induced thermal self-assembly (PITSA) benefiting the versatile, easy applicable and robust nature of this technique. Functionalization of these nanoparticles with therapeutic synthetic peptides was achieved to explore the stability and of the nanoparticles. These studies are expected to contribute to future studies in creating functional drug delivery systems.

This thesis is dedicated to my family.

Acknowledgements

It feels surreal to be at this point, writing the acknowledgement part of my thesis but here I am. First, I would like to thank my supervisor, Professor Rachel O'Reilly, for accepting me to work in her group, believing in my skills (often more than me) and for her constant support for me to improve myself in so many ways.

I would like to thank my MSci supervisor Professor Binnur Aydoğan Temel for opening the way for me to apply to this PhD and for always supporting me. I would like to thank my mentors in the group, Dr. Jeffrey Foster, Dr. Robert Keogh and Dr. Jonathan Husband for putting up with all the silly questions of a bioengineer who tries to survive in chemistry! Special thanks to Jon for all the fun times spent trying to fix the peptide synthesizer (*i.e.*, finger crossing for it to work).

I also would like to thank our collaborator Prof. Robert T. Mathers for transferring his experiences about the computational calculations, always be willing to provide his help selflessly and for all the fruitful discussions we had throughout my PhD. I would like to thank Dr. Amanda K. Pearce, Dr. Calum Ferguson and Dr. Julia Rho for their guidance and help on my projects. And I would like to thank Dr. Sam Parkinson, Dr. Simon Dale and Ms. Alisha Miller for proofreading my introduction and Alisha also for her help with my TEMs. I would also like to thank Ms. Bethany Crow for her kindness and help with my HPLC measurements.

I can't thank enough especially to Ms. Tessa Kintail for always being kind and open to help, fixing all my problems and making life easier for everyone in the groups. I would like to thank Ms. Julia Valverde and Dr. Daniel Smith for their massive help. I would also like to thank Dr. Cécile S. Le Duff for our nice conversations, both scientific and personal.

Next, I would like to thank all the past and present members of both groups for always be willing to talk about science, life, problems, music, or anything one could ask for. I feel so

lucky to have worked with people who are always supportive to each other. But my very special thanks go to my two beloved people, members of the Dramaaa team: Dr. Marjolaine Thomas (I will make you proud on the Türkiye leg of the cucumber study but only if you send more grandma selfies) and mi niño Señorito David Andres Londoño de la Cruz, aka Davisito, (builder of my classical music playlist, my "The Office" mait and Brummie bab). I couldn't think of being friends with anyone this close at this point of my life but you two came as a surprise. Thank you for all our memories and can't wait for the new ones.

I would also like to thank Gabige (Ms. Bige Garbonova and Ms. Gabriela Batı, I think!) and Mr. Daniele Giannantonio for being amazing friends, for all our adventures, fun times, and delicious foods with additional thanks to Daniele for the best tiramisu I've ever had in my life! I would like to thank Ms. Ana Cubillo Alvarez and Ms. Siriporn Chaimueangchen, my Wales trip partners (I will always remember the "Four Cheese").

I would like to thank Dr. Maria Pervez, Dr. Turgay Yıldırım and Dr. İlknur Yıldırım for their help to me to settle in when I first arrived in the UK and for their continuous support. I would like to thank my MSci student Xiyue Leng, not only for making me gain experience on mentoring but also for her friendship and always smiley face.

A special thanks for my friends, my housemates, my sisters Ms. Merve Koçbıyık and Ms. İlay Sema Ünal. I was lucky to meet them on this PhD journey and travel around the UK together. I want to add that I have no regrets for dragging you after me to every bakery. Thank you for always being there for me.

I would like to thank my family, especially my parents İlknur and Adnan Akar, and my siblings Rümeysa, Ömer Faruk and Kerem Akar for always supporting me, listening to me whine but still love me (I hope!). I am forever grateful! My special thanks go to Talha Ceylan and Ahsen Nur Ürey for always being a phone call away whenever I needed them. I love you all so much!

Lastly, I would like to thank my funder Turkish Ministry of National Education, without their support this PhD wouldn’t be possible.

Table of Contents

Table of Contents I

List of Figures III

List of Schemes IV

List of Symbols and Abbreviations V

List of Publications X

Declaration of Authorship XI

Chapter 1. Introduction 1

1.1 Introduction to synthetic polymers 2

1.2 Polymerization techniques 4

1.2.1 Step-growth polymerization 4

1.2.2 Chain-growth polymerization 4

1.2.2.1. Reversible-Deactivation Radical Polymerization (RDRP) 7

1.2.2.1.1 Reversible Addition-Fragmentation Chain Transfer (RAFT) Polymerization 10

1.3 Block copolymer self-assembly in solution 13

1.4 Polymerization-Induced Self-Assembly (PISA) 16

1.4.1 Polymerization-induced thermal self-assembly (PITSA) 19

1.5 Stimuli-responsive polymers 21

1.5.1 Thermoresponsive polymers 21

1.6 Polymer hydrophobicity 25

1.6.1 Predictive models used for investigating polymer hydrophobicity 26

1.6.1.1. Mather's hydrophobicity parameter (MHP) 28

1.7 Summary 30

1.8 References 31

Chapter 2. Grafting Density Governs the Thermoresponsive Behavior of P(OEGMA-*co*-RMA) copolymers 46

2.1 Manuscript details and overview 47

2.2 Supporting Information 51

Chapter 3. LogP_{oct}/SA Predicts the Thermoresponsive Behavior of P(DMA-*co*-RA) Statistical Copolymers 52

3.1 Manuscript details and overview 53

3.2 Supporting Information 56

Chapter 4. Preparation of Functional Nanoparticles of P(DMA-*co*-HA) Copolymers via Polymerization-Induced Thermal Self-Assembly 57

4.1 Manuscript details and overview 58

4.2 Supporting Information 60

Chapter 5. Conclusion and Outlook 61

List of Figures

Figure 1.1. Examples of compositions, topologies and functionalizations of polymers. Reproduced from ref.[12] 3

Figure 1.2. Change in the polymer molecular weight with increasing monomer conversion for step-growth, conventional chain-growth and living polymerizations.....5

Figure 1.3. Guideline for selection of R– and Z– groups of RAFT agents for different polymerizations. Figure reproduced from ref.[41] 13

Figure 1.4. Different morphologies obtained by using block copolymer self-assembly methods. Figure reproduced from ref.[46] 14

Figure 1.5. Effect of different packing parameters on the resulting morphologies of amphiphilic block-copolymer based nano-objects. Figure reproduced from ref.[48] 15

Figure 1.6. Different morphologies created *via* RAFT-mediated PISA. Figure reproduced from ref.[63] 17

Figure 1.7. Phase diagram, and associated TEM images of various compositions of GMA-HPMA nanostructures obtained by RAFT-PISA. Figure reproduced from ref.[50] 18

Figure 1.8. a) The mechanism of formation of particles *via* RAFT-PITSA and b) different morphologies obtained upon increasing the hydrophobic block length. Figure reproduced from ref.[68] 20

Figure 1.9. LCST and UCST points of thermoresponsive polymers. Figure reproduced from ref.[94] 23

Figure 1.10. A flow diagram showing the steps of calculating Log*P*/SA values of polymers. Adapted from ref.[144].....29

List of Schemes

Scheme 1.1. Mechanism of free radical polymerization (FRP). Reproduced from ref.[27].....7

Scheme 1.2. Mechanism of atom-transfer radical polymerization (ATRP). Reproduced from ref.[36] 9

Scheme 1.3. Mechanism of nitroxide-mediated polymerization (NMP). Reproduced from ref.[38] 9

Scheme 1.4. Schematic representation of RAFT polymerization mechanism. Figure reproduced from ref.[29].....11

List of Symbols and Abbreviations

% w/w	Solids concentration
[M]	Monomer concentration
$[M]_0$	Initial monomer concentration
°C	Degrees Celsius
a_0	Area of the hydrophilic head group
AA	Acrylic acid
AIBN	2,2'-Azobis(2-methylpropionitrile)
ATRP	Atom transfer radical polymerization
BA	Benzyl acrylate
BCP	Block copolymer
BMA	*n*-Butyl methacrylate
$CDCl_3$	Deuterated chloroform
CDSA	Crystallization-Driven Self-Assembly
$CHCl_3$	Chloroform
CTA	Chain transfer agent
D_{ave}	Average diameter recorded by TEM
DEGMA	Di(ethylene glycol) methacrylate
D_h	Hydrodynamic volume
DLS	Dynamic light scattering

$Đ_M$	Molar-mass dispersity by SEC
DMA	*N*,*N*-Dimethyl acrylamide
DMF	Dimethylformamide
DP	Degree of polymerization
EMA	Ethly methacrylate
eq.	Equivalents
FRP	Free radical polymerization
FT-IR	Fourier transform infrared
g	Gram(s)
h	Hour(s)
HA	Hexyl acrylate
HMA	Hexyl methacrylate
HPLC	High pressure liquid chromatography
H_2O	Water
k_p	Propagating rate constant
LAMs	Less activated monomers
l_c	Length of the hydrophobic chain
LCST	Lower critical solution temperature
LMA	Lauryl methacrylate
LogP_{oct}	Octanol-water partition coefficient

Log*P*/SA	Surface area normalized octanol-water partition coefficient
m/z	Mass-to-charge ratio
Macro-CTA	Macromolecular chain transfer agent
MAMs	More activated monomers
mg	Miligram(s)
min	Minute(s)
mL	Mililiter(s)
MMA	Methyl methacrylate
M_n	Average molecular weight
mol	Mole(s)
M_t^m/L	Transition metal complex
M_w	Weight average molecular weight
MW	Molecular weight
MWCO	Molecular weight cut-off
N_2(g)	Nitrogen gas
*n*BuA	*n*-Butyl acrylate
*n*BMA	*n*-Butyl methacrylate
nm	Nanometer(s)
NMP	Nitroxide-mediated radical polymerization
NMR	Nuclear magnetic resonance

OEGMA	Oligoethylene glycol mono methyl ether methacrylate
p	Packing parameter
PD	Polydispersity
PEG	Poly(ethylene glycol)
PEO	Poly(ethylene oxide)
PFPA	Pentafluorophenyl acrylate
PISA	Polymerization-induced self-assembly
PITSA	Polymerization-induced thermal self-assembly
$Pm^{\bullet}$	Growing radical chain
PMMA	Poly(methyl methacrylate)
$Pn^{\bullet}$	Growing radical chain
PNIPAM	Poly(*N*-isopropylacrylamide)
PRE	Persistent radical effect
RT	Room temperature
RAFT	Reversible addition fragmentation chain transfer
RDRP	Reversible deactivation radical polymerization
RI	Refractive index
ROMP	Ring-opening metathesis polymerization
SEC	Size exclusion chromatography
T	Temperature

*t*BuA	*tert*-Butyl acrylate
T_{CP}	Cloud point temperature
TEA	Triethylamine
TEM	Transmission electron microscope
T_g	Glass transition temperature
THFA	Tetrahydrofurfuryl acrylate
UA	Uranyl acetate
UCST	Upper critical solution temperature
UV-Vis	Ultraviolet-visible
V_m	Molar volume
δ	Hildebrand solubility parameter
δ_d	Dispersion force
δ_h	Hydrogen bonding force
ΔG	Gibb's free energy of mixing
ΔH	Enthalpy of dissolution
δ_p	Polar force
ΔS	Entropy change
λ	Wavelength
µDSC	Micro differential scanning calorimetry
µl	Microliter(s)

List of Publications

4. Akar, I.; Pearce, A. K.; Ferguson, C.; O'Reilly, R. K. Preparation of Functional Nanoparticles of P(DMA-*co*-HA) Copolymers *via* Polymerization-Induced Thermal Self-Assembly.

   Manuscript prepared.

3. Akar, I.; Foster, J. C.; Leng, X.; Pearce, A. K.; Mathers, R. T.; O'Reilly, R. K. LogP_{oct}/SA Predicts the Thermoresponsive Behavior of P(DMA-*co*-RA) Statistical Copolymers. *ACS Macro Lett*. 2022, 11 (4), 498-503.

2. Foster, J. C.; Akar, I.; Grocott, M. C.; Pearce, A. K.; Mathers, R. T.; O'Reilly, R. K. 100th Anniversary of Macromolecular Science Viewpoint: The Role of Hydrophobicity in Polymer Phenomena. *ACS Macro Lett*. 2020, 9, 11, 1700-1707.

1. Akar, I.; Keogh, R.; Blackman, L. D.; Foster, J. C.; Mathers, R. T.; O'Reilly, R. K. Grafting Density Governs the Thermoresponsive Behavior of P(OEGMA-*co*-RMA) Statistical Copolymers. *ACS Macro Lett*. 2020, 9, 8, 1149-1154.

Declaration of Authorship

This thesis is submitted to the University of Birmingham in support of my application for the degree of Doctor of Philosophy. This thesis was composed by myself and has not been submitted previously for the award of any degree.

Parts of this thesis have been published by the author in the form of open-access articles in peer-reviewed scientific journals as stated below. The work presented herein, including project design and performance of experiments, materials characterization, data collection and analysis, figure and manuscript preparation, was carried out by myself except for contributions from other colleagues which are outlined below in further detail.

Chapter 2 – "Reprinted with permission from: Akar, I.; Keogh, R.; Blackman, L. D.; Foster, J. C.; Mathers, R. T.; O'Reilly, R. K. Grafting Density Governs the Thermoresponsive Behavior of P(OEGMA-*co*-RMA) Statistical Copolymers. ACS Macro Lett. 2020, 9, 8, 1149-1154. Copyright 2020 American Chemical Society." (link)

LogP_{oct}/SA calculations was performed with assistance from Prof. Robert T. Mathers at Pennsylvania State University. Statistical analysis on experimental and literature data for OEGMA based copolymers was performed by Dr. Jeffrey C. Foster.

Chapter 3 – "Reprinted with permission from: Akar, I.; Foster, J. C.; Mathers, Leng, X.; Pearce, A.K.; R. T.; O'Reilly, R. K. Grafting Density Governs the Thermoresponsive Behavior of P(OEGMA-*co*-RMA) Statistical Copolymers. ACS Macro Lett. 2020, 9, 8, 1149-1154. Copyright 2020 American Chemical Society." (link)

Chapter 4 – Manuscript prepared: Akar, I.; Pearce, A. K.; Ferguson, C. O'Reilly, R. K. Preparation of Functional Nanoparticles of P(DMA-co-HA) Copolymers via Polymerization-Induced Thermal Self-Assembly.

Chapter 1. Introduction

1.1 Introduction to synthetic polymers

Increasing technological developments have allowed humankind to mimic nature's polymers, such as DNA, proteins and nucleic acids, allowing access to their synthetic counterparts which can be readily synthesized using a library of chemicals.[1]

Polymers are composed of macromolecules with high molar mass which are comprised of monomers; small repeating units linked to each other *via* covalent or non-covalent interactions.[2, 3] The number of repeating units in the chain, known as the degree of polymerization (DP), is used to define synthetic polymers as well as their molecular mass. Molecular weight distribution, also known as dispersity ($Đ_M$), of the polymers is another key property when defining polymers.[4] $Đ_M$ is the ratio of weight-average molar mass (M_w) to number-average molar mass (M_n) and represents the distribution of molecular mass across all polymer chains. $Đ_M = 1$ in the case of a "monodisperse" polymer, *i.e.,* all polymer chains in a sample are of the same molecular weight and is a rare occurrence for synthetic polymers. Synthetic polymers are generally "polydisperse" meaning they contain chains with different lengths and molecular weights.[5] Physicochemical properties of polymers can be heavily dependent upon DP and $Đ_M$. Having higher molecular masses compared to their component repeating units provides polymers with different macroscopic properties such as chemical resistance, viscosity, and mechanical strength. Glass transition temperature (T_g) is another unique property of polymers, and is defined as the temperature at which polymer chains lose short range mobility.[6]

Polymer properties and their applications can be altered by their composition, architecture, and functionality (Figure 1.1). These elements can be controlled to design polymers with required properties for specific applications.[7] Polymers with different compositions, such as homopolymers or copolymers, or special arrangement such as alternating or random

(statistical) copolymers, can easily be synthesized by tuning monomer sequence.[8] The composition can also be tuned by varying tacticity which refers to arrangement of pendant groups along the polymer chain, leading to isotactic, syndiotactic and atactic polymers. All the pendant groups are located on the same side of the polymer backbone for isotactic polymers while syndiotactic polymers have alternating pendant groups and atactic polymers have randomly arranged pendant groups along the backbone. Additionally, polymers can be designed to have different architectures such as linear, star, bottlebrush *etc.* that gives them different properties.[9, 10] Finally, polymers can be functionalized through reactive components *via* post-polymerization modifications resulting in polymers with diverse characteristics.[11] Ability to synthesize polymers with different architectures enables the utilization of such synthetic polymers for various industrial applications.

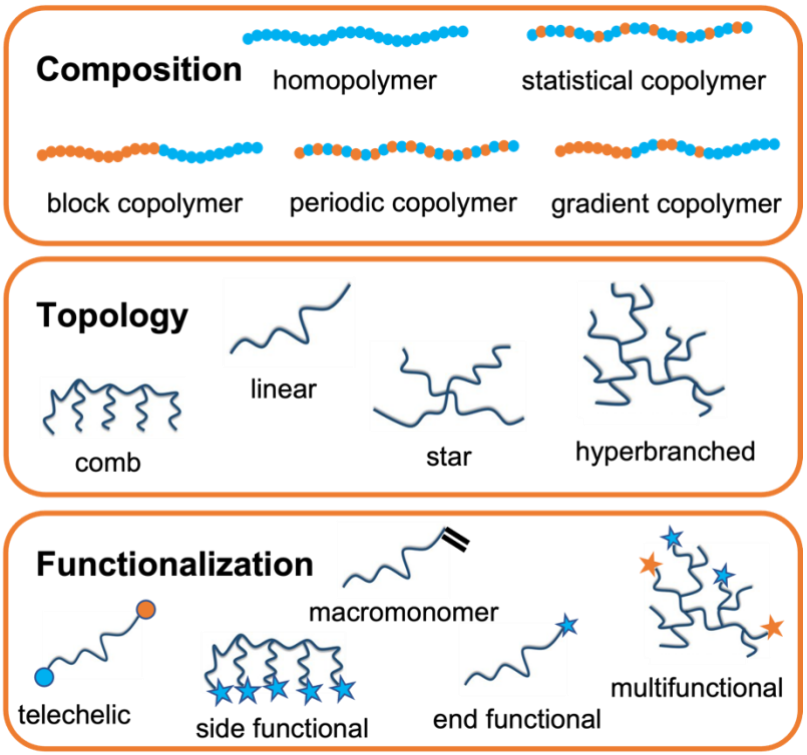


Figure 1.1. Examples of compositions, topologies and functionalizations of polymers. Reproduced from ref.[12]

1.2 Polymerization techniques

1.2.1 Step-growth polymerization

Step-growth polymerization has been widely used especially in industry to synthesize well-known polymers such as polyesters, polyurethanes, polyureas and polyamides. These polymers are obtained either by polycondensation or polyaddition reactions.[13] In polycondensation reactions a small molecule, typically water, is released, whereas in polyaddition reactions monomers with different functionalities polymerize without generating byproducts.[14]

In step-growth polymerizations, monomers initially react with each other to form dimers, trimers and oligomers, yielding high molecular weight polymer chains only at the end of the polymerization when all monomers are consumed. Thus, high levels of conversion are required to obtain high molecular weight polymers *via* step-growth polymerizations.[15, 16]

The requirement of high monomer purity with precise stoichiometry of monomers and lack of control over the molecular weight render step-growth polymerization a challenging method to access well-defined polymers compared to chain-growth polymerizations.

1.2.2 Chain-growth polymerization

Chain-growth polymerizations, such as "living" polymerization, free radical polymerization (FRP), and reversible deactivation radical polymerization (RDRP), involve multiple reaction stages including initiation and propagation that occur simultaneously.[17] Chain-growth polymerizations except for the "living" polymerizations also include a termination stage. Throughout a chain-growth polymerization, monomer concentration decreases constantly until all monomers are consumed and high molecular weight polymers form.[18] In the case of conventional chain-growth polymerizations, high molecular weight polymers can form at the early stages upon addition of monomers to the initiated polymer chains followed by rapid growing of these chains (Figure 1.2.). Unlike step-growth polymerizations, an initiator is

required for monomers to polymerize where activated intermediates are generated upon external application of heat, light, electromagnetic radiation *etc.* and concentration of the initiator plays a key role for the polymerization rate. All chain growth polymerizations start with the generation of these activated species such as a free radical, cation or anion in the initiation step. In the propagation step, monomers react with the active site of these generated species to form a growing polymer chain. Contrary to step-growth polymerizations, termination reactions also occur during radical step growth polymerizations. This is not observed during "living" polymerization as a consequence of the charged nature of the active species. Thus, in the case of "living" polymerization, the polymer chains remain active at full conversion enabling chain extension with addition of monomers. Also, because the initiation rate is much higher than the propagation rate, polymer chains grow from uniformly distributed initiated chains allowing formation of polymer chains with narrow molecular weight distributions.[19]

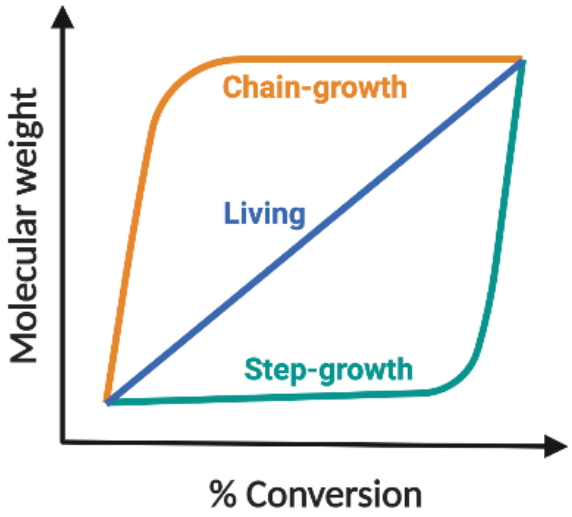
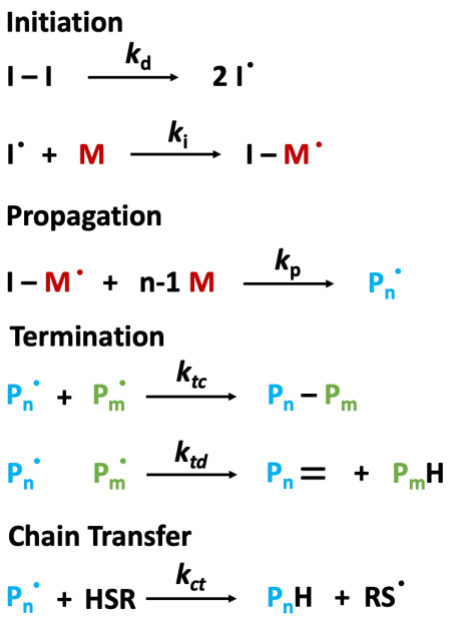


Figure 1.2. Change in the polymer molecular weight with increasing monomer conversion for step-growth, conventional chain-growth and living polymerizations.

Well-established examples of the living polymerization techniques are group transfer polymerization, anionic and cationic polymerization, and ring-opening metathesis

polymerization (ROMP).[20-23] Aside of the advantages of control over molecular weight, dispersity and end-group functionality, requirement of strict reaction conditions such as complete removal of oxygen, water, and other impurities can limit the application of living polymerization.[19]

FRP is another chain-growth polymerization method which is one of the most utilized polymerization methods in industry to obtain high molecular weight polymers such as polystyrene, poly(vinyl acetate), and poly(vinyl chloride). As in all conventional chain-growth polymerizations, FRP involves initiation, propagation, and termination steps (Scheme 1.1).[24, 25] Polymerization reaction starts with generation of free radicals upon decomposition of an initiator molecule. These radicals then react with monomer leading to the formation of propagating radicals. During the propagation step, monomers are added to these propagating radicals to form the growing polymer chains. Termination reactions occur *via* an irreversible reaction between either two growing chains (recombination) or other terminating species (disproportionation) forming "dead" polymers.[25] Active radicals can also be transferred to another chain, the solvent, a monomer, or a chain transfer agent (CTA). This phenomenon is known as chain transfer events often causing lower molecular weight polymers than theoretically expected.[26]



Scheme 1.1. Mechanism of free radical polymerization (FRP). Reproduced from ref.[27]

In FRP, chain transfer and termination are second order reactions while the propagation is a first-order reaction. Also, because the rate of the initiation is the lowest amongst the others, chain transfer and termination reactions have faster kinetics than propagation or initiation reactions. This poor control results in formation of non-uniform polymers with broad molecular weight distributions, diverse compositions, and topologies. Because of these limitations, FRP is not a robust polymerization method for the synthesis of well-defined block copolymers with tunable properties.[28]

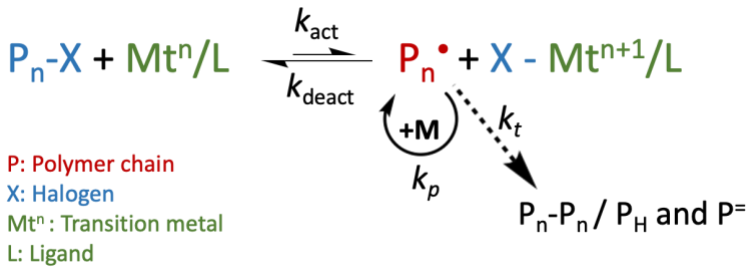
1.2.2.1 Reversible-Deactivation Radical Polymerization (RDRP)

Possessing numerous advantages of FRP and living polymerizations, reversible-deactivation radical polymerization (RDRP) techniques are one of the most robust tools for the synthesis of well-defined polymers. RDRP methods are preferable because of their facile applicability such as good control of polymer molecular weight and composition under a range of conditions, availability to a wide range of monomers and functional groups, and applicability in various reaction conditions such as bulk, solution, emulsion or suspension.[29]

RDRP are chain growth polymerizations but have the same linear relationship between the molecular weight and monomer conversion as living polymerizations as shown above in Figure 1.2. In RDRP, there is a fast and reversible equilibrium between the active propagating chains and deactivated dormant intermediates. Deactivation occurs *via* three different processes, namely deactivation by catalyzed reversible coupling, deactivation by spontaneous reversible coupling and deactivation by degenerative transfer.[30] Atom transfer radical polymerization (ATRP) and nitroxide-mediated radical polymerization (NMP) are examples of RDRP which rely upon deactivation by catalyzed reversible coupling, and deactivation by spontaneous reversible coupling, respectively.[31, 32] These polymerizations progress based upon this phenomenon called persistent radical effect (PRE), meaning radical species that are generated cannot self-terminate but will only terminate with the propagating polymer chains.[33] ATRP and NMP are briefly explained below whereas RAFT polymerization, which was utilized in all Chapters 2, 3 and 4 of this thesis is discussed in detail in Section 1.2.2.1.1.

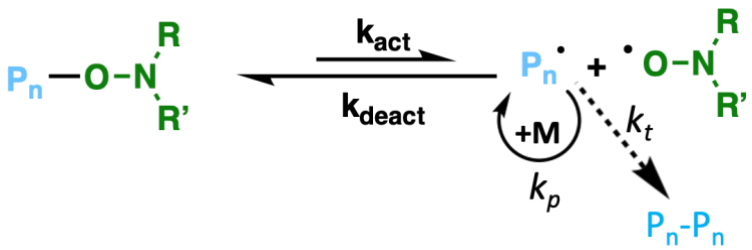
ATRP was discovered independently by Krzystof Matyjaszewski and Mitsuo Sawamoto and Jin-Shan Wang in 1995.[34] In ATRP, transition metal complexes such as copper, iron, ruthenium, and osmium are used as catalysts, with a secondary or tertiary alkyl halide (R-X) used as the initiator.[35] Radicals ($R^{\bullet}$) and oxidized transition metals are generated by the transition metal complex (M_t^m/L) through a reversible redox reaction of alkyl halides with transition metal complexes. Then, monomers are attacked by the produced radicals to form the propagating polymer chains ($P_n^{\bullet}$). These chains can continue to propagate, or they regenerate the catalyst by reacting with the oxidized transition metals, capping the polymer chain with a halogen (Scheme 1.2.). In this reversible main equilibrium state, the halide is transferred between the propagating polymer chains and the transition metal complexes resulting in limited termination reactions and a high degree of polymerization control. Because the concentration of radicals is significantly decreased compared to FRP, termination reactions are reduced to a

much greater extent than propagation. This is because the fast transfer of halides between the metal activator and the propagating chains drives the equilibrium toward the deactivated species.[34]



Scheme 1.2. Mechanism of atom-transfer radical polymerization (ATRP). Reproduced from ref.[36]

In NMP, a stable nitroxide acts as the persistent radical and reversibly caps the growing polymer chains in the same way as the halide atoms act in ATRP (Scheme 1.3). Alkoxyamines are used as initiators in NMP for producing nitroxide radicals and initiating species. Unlike ATRP, a catalyst is not required, and radicals are formed upon homolysis at high temperatures. Then, the propagating radicals can either react with monomers or with the nitroxide radicals resulting in the formation of polymer chains end-capped by nitroxides. Reversible termination results in a low radical concentration which decreases the irreversible termination reactions. This causes main equilibrium to be driven towards the deactivated species and provides good control over the polymerization.[37]



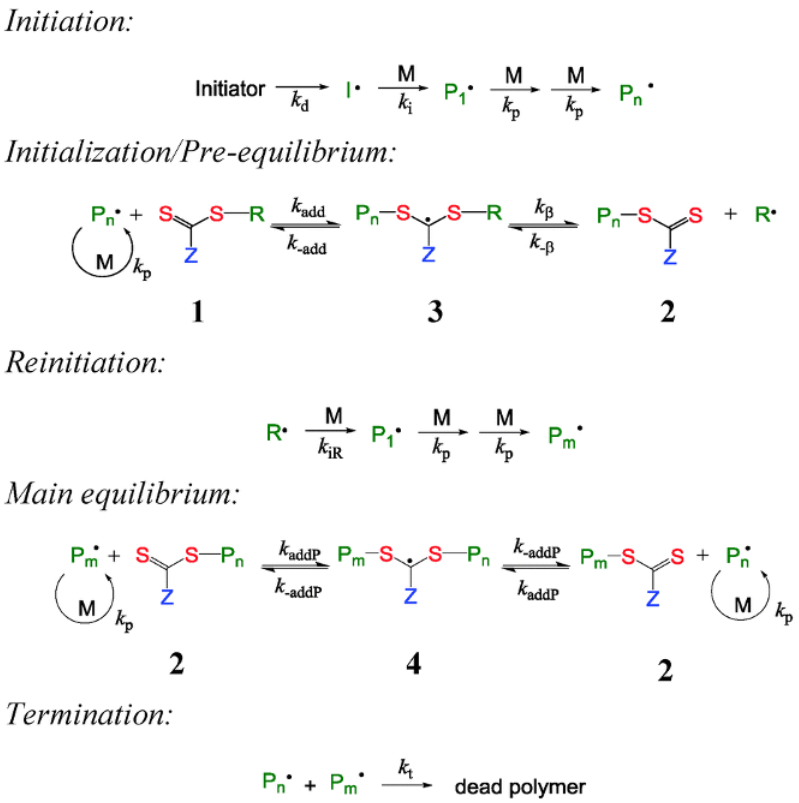
Scheme 1.3. Mechanism of nitroxide-mediated polymerization (NMP). Reproduced from ref.[38]

1.2.2.1.1 Reversible Addition-Fragmentation Chain Transfer (RAFT) Polymerization

Reversible Addition-Fragmentation Chain Transfer (RAFT) polymerization has been widely used since its discovery in 1998 owing to its significant advantages: applicable for numerous monomers, providing access to polymers with low dispersity, and allowing easy functionalization of polymer end groups.[39, 40] One key advantage of RAFT polymerization over the other RDRP techniques is the fact that reagents like metal ligands or harsh reaction conditions such as high temperature are not required when performing RAFT. Another difference is that the equilibrium between active and dormant species is under a degenerative chain transfer mechanism. In a degenerative transfer system, the number of radicals remain constant during the activation-deactivation process because radicals are not created or consumed. Therefore, to initiate the RAFT polymerization an external radical source is required. Another important element is the chain transfer agent (CTA), also known as RAFT agent. CTAs play a key role in reducing the radical-radical terminations by ensuring the rapid transfer of radicals between the propagating polymer chains and the dormant species allowing good control over the polymerization.[29]

RAFT polymerization follows the same mechanism as FRP in that it includes initiation, propagation and termination steps. In the initiation step, free radicals ($I^{\bullet}$) are generated upon thermolysis, photolysis *etc.* of the initiator (I-I) (Scheme 1.4). These radicals react with vinyl monomers (M) to form an active propagating polymer chain ($P_n^{\bullet}$) and active chains reversibly react with the RAFT agents, a thiocarbonylthio group such as dithioesters and trithiocarbonates, in the pre-equilibrium step to form intermediate radicals.[41] These intermediate species can then fragment to form a polymeric CTA (macro-CTA) and a CTA-derived radical ($R^{\bullet}$). Next, during the reinitiation step, the CTA-derived radical reacts with monomers to produce propagating polymer chains ($P_m^{\bullet}$). In the main equilibrium step, the CTA-derived radical intermediate rapidly fragments to add either $P_n^{\bullet}$ or $P_m^{\bullet}$ chains onto its C=S

bond. The rate of this propagation step is greater than the rate of the fast addition where the radical intermediate is formed. This affords a reduction in termination reactions such as the bimolecular coupling of $P_n^{\bullet}$ and $P_m^{\bullet}$, leading to relatively good control over the polymer dispersity as each propagating polymer radical has equal chance of activating due to the symmetrical structure of the CTA-derived radical intermediate.[29]



Scheme 1.4. Schematic representation of RAFT polymerization mechanism. Figure reproduced from ref.[29]

The R– and Z– groups of a CTA play an important role in the RAFT polymerization mechanism by ensuring rapid completion of pre-equilibrium and reinitiation steps, allowing the system to reach the main equilibrium state. Another parameter which should be considered for a well-controlled polymerization is the type of monomers used.[42] Therefore, it is key to match appropriate CTAs and monomers when targetting well-defined polymers *via* RAFT polymerization. Regarding the monomer type, there are two classes of monomers known as more activated monomers (MAMs) and less activated monomers (LAMs) used as RAFT

monomers. Styrene, (meth)acrylates, (meth)acrylamides, isoprene, and butadiene are some examples for MAMs that bear a vinyl bond attached to either another double bond, aromatic ring, carbonyl and nitrile groups. Vinyl acetate, *N*-vinylpyrrolidone, alkenes and vinyl chloride are examples of LAMs have a double bond next to either a sulfur with a lone electron pair or nitrogen, oxygen, halogen, saturated carbons.[41]

Trithiocarbonates (Z═S-alkyl) or aromatic dithioesters (Z═aryl) are the most suitable RAFT agents for the well-controlled polymerization of MAMs as MAMs usually produce more stable radicals during their polymerization. However, since the use of these CTAs inhibit the polymerization of LAMs, less reactive xanthates (Z═OR) and dithiocarbamates (Z═NR′$_2$) are preferred for the polymerization of LAMs since they have poor homolytic leaving groups because of their high reactivity. Therefore, use of highly reactive CTAs with LAMs or less reactive CTAs with MAMs would lead to retardation and slow fragmentation which results in poor control over the polymerization, or no polymerization at all. This highlights the importance of selecting an appropriate "Z" group in the CTA which is responsible for the stability of the intermediate radical species. On the other hand, the selection of "R" group is also key as it controls the fragmentation of the intermediates by acting as a good homolytic leaving group. A guideline for selection of both "Z" and "R" groups is shown in Figure 1.3.[41]

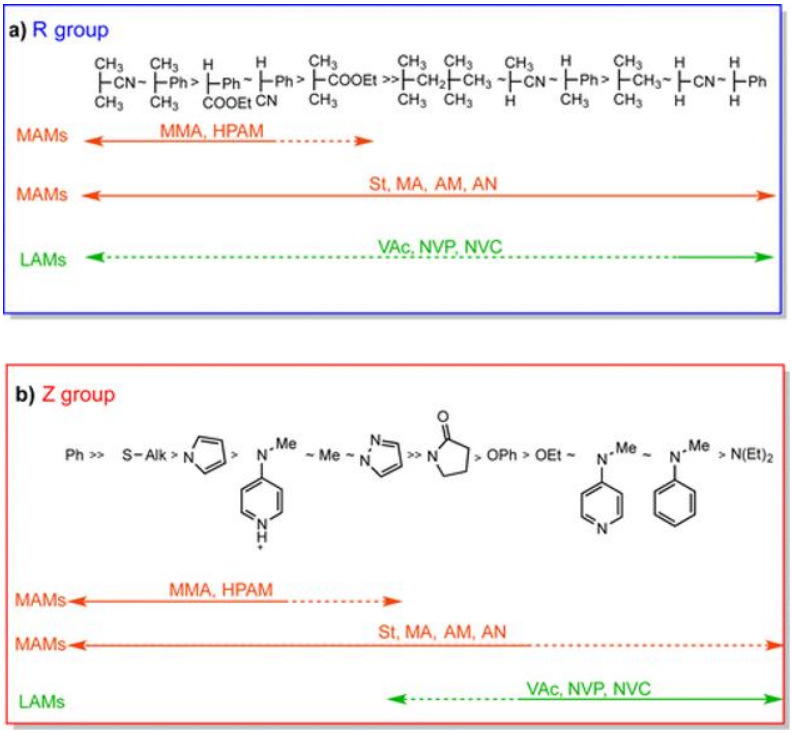


Figure 1.3. Guideline for selection of R– and Z– groups of RAFT agents for different polymerizations. Figure reproduced from ref.[41]

In summary, RAFT polymerization is a very useful tool for the synthesis of well-designed polymers as it is applicable to a vast number of monomers and solvents and allows for easy post-polymerization functionalization of polymer chain ends. Moreover, eliminating the use of metals or harsh conditions, and displaying high functional group tolerance are further advantages of the RAFT polymerization. Due to these reasons, RAFT polymerization has been used for many applications such as paints, cosmetics, lubricants, biosensors, and polymer therapeutics through the construction of complex structures like block and branched architectures and stimuli-responsive polymers.[43-45]

1.3 Block copolymer self-assembly in solution

The ability to design and synthesize various macromolecular architectures such as block copolymers (BCPs) has been greatly facilitated by the developments in controlled and living polymerization techniques such as RAFT. BCPs can be designed to contain blocks with

different solvophilicity similar to amphiphilic small molecule surfactants that have a solvophilic head and a solvophobic tail. In selected solvents, this results in aggregation of such amphiphilic BCPs, known as solution self-assembly. The driving force that governs this phenomenon is the requirement of minimizing unfavorable thermodynamic interactions such as hydrophobe-water interactions in aqueous solutions.[46, 47]

Diverse morphologies such as spherical micelles, rods, lamellae, vesicles and other complex structures have been achieved using amphiphilic BCP self-assembly processes in water (Figure 1.5).

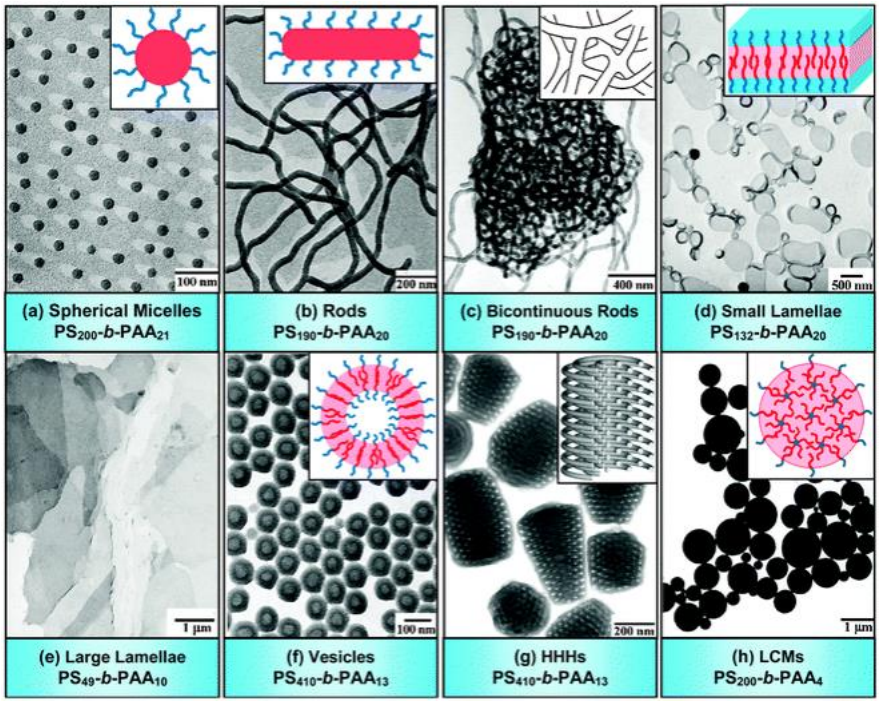


Figure 1.4. Different morphologies obtained by using block copolymer self-assembly methods. Figure reproduced from ref.[46]

The self-assembly behavior of BCPs depends on various parameters such as molecular weight, composition and architecture of the copolymers, solvent quality and volume fraction of the constituent blocks, known as the packing parameter (p) (Figure 1.6.).[46, 48] p is the ratio of the volume of the hydrophobic chain, v; to the optimal area of the hydrophilic head group, a_0; and

the length of the hydrophobic chain, l_c. The interfacial curvature of the particles increases as the packing parameter decreases ($p \leq 1/3$) leading to formation of spherical micelles. Worms and vesicles form for the packing parameters of $1/3 < p < 1/2$ and $1/2 \leq p < 1$, respectively.[47] Overall, various morphologies can be obtained by tuning the length of the two blocks, solvophobicity of the hydrophobic block and the total solid contents.[49, 50]

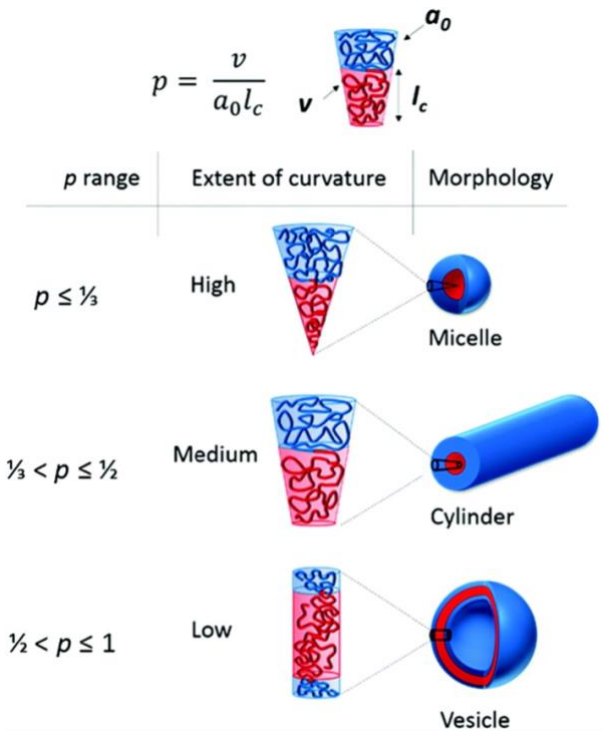


Figure 1.5. Effect of different packing parameters on the resulting morphologies of amphiphilic block-copolymer based nano-objects. Figure reproduced from ref.[48]

Polymeric nano-objects can be prepared by conventional self-assembly methods such as solvent-switch, direct dissolution and thin-film rehydration, or alternative methods such as nanoprecipitation, dispersion/emulsion polymerization, crystallization-driven self-assembly (CDSA).[51-55] These nano-objects can be utilized in a variety of areas such as imaging, sensing, catalysis, and drug delivery owing to their unique properties such as tunable lipophilicity, enhanced therapeutic efficiency, ability to control and functionalize their structures.[56]

Even though conventional BCP self-assembly methods have been utilized extensively, there are a number of disadvantages, for example time consuming multi-step procedures including synthesis and purification of polymers prior to self-assembly and the requirement of dilute polymerization solutions for self-assembly. Recently, a new method for self-assembly known as polymerization-induced self-assembly (PISA) has been developed which overcomes many of the disadvantages attributed to conventional self-assembly methods.[57]

1.4 Polymerization-Induced Self-Assembly (PISA)

Polymerization induced self-assembly (PISA) is a method which can be used to produce different nanostructures from block copolymers by driving a physical self-assembly process upon an increase of the solvophobic part of the block copolymers as the polymerization progresses. Polymerization of a solvent-miscible monomer from a pre-synthesized macroCTA leads to self-assembly of the block copolymer as the second block becomes insoluble in the solvent at a critical degree of polymerization.[58] PISA is a one-pot synthetic method which has many benefits compared to conventional self-assembly methods in the formation of different morphologies owing to the following advantages; it can be performed at high solid concentrations (up to 50% w/w), it can be carried out in both polar and non-polar organic solvents as well as aqueous environments, it is compatible with reversible-deactivation radical polymerization methods such as ATRP,[59] NMP,[60] and RAFT[61], synthesis is possible at concentrated environments facilitating industrial scale-up, and it is able to form a wide range of nano-object morphologies (Figure 1.7).[57, 62]

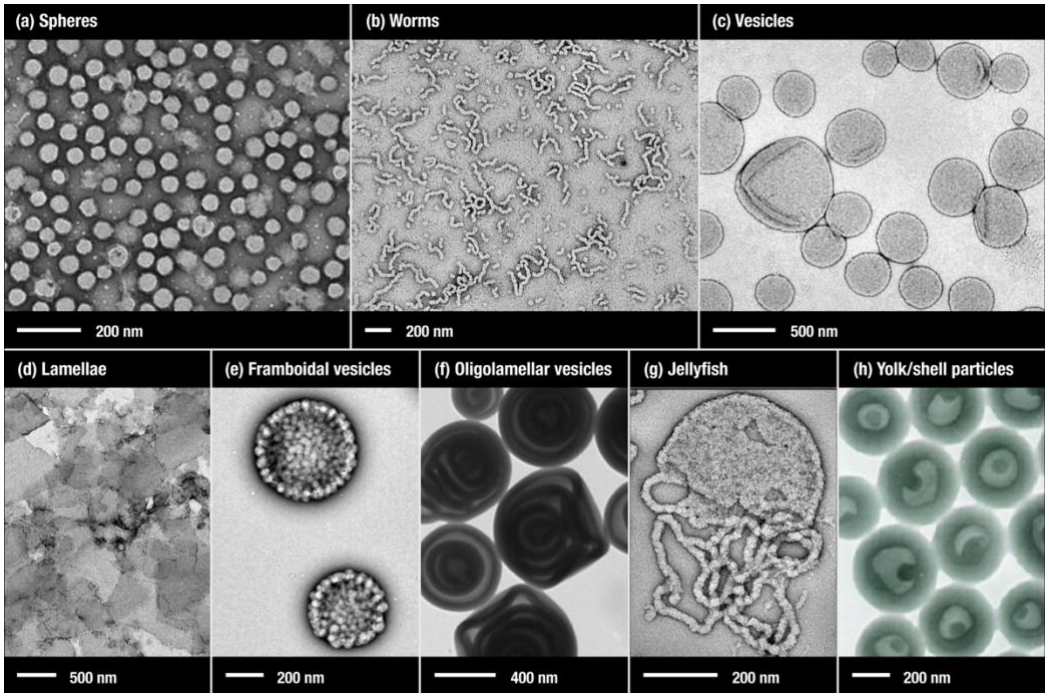


Figure 1.6. Different morphologies created *via* RAFT-mediated PISA. Figure reproduced from ref.[63]

RAFT polymerization has been widely used in PISA under both emulsion and dispersion polymerization conditions.[57, 63, 64] Chain extension of a solvophilic macroCTA (stabilizer block) produces amphiphilic block copolymers which then self-assemblies to form nano-objects, such as spherical micelles, nanoworms, and vesicles upon continuous growth of the solvophobic block. Like conventional BCP self-assembly techniques, the volume fraction of the stabilizer and core-forming blocks (*i.e.*, packing parameter, *p*) governs the final morphology of the nanoparticles. Higher order morphologies such as worms, vesicles, lamellae, *etc.* can be obtained by tuning the parameters such as the length of core and corona forming blocks, the total solids content and the solvophobicity of the core block (Figure 1.8).

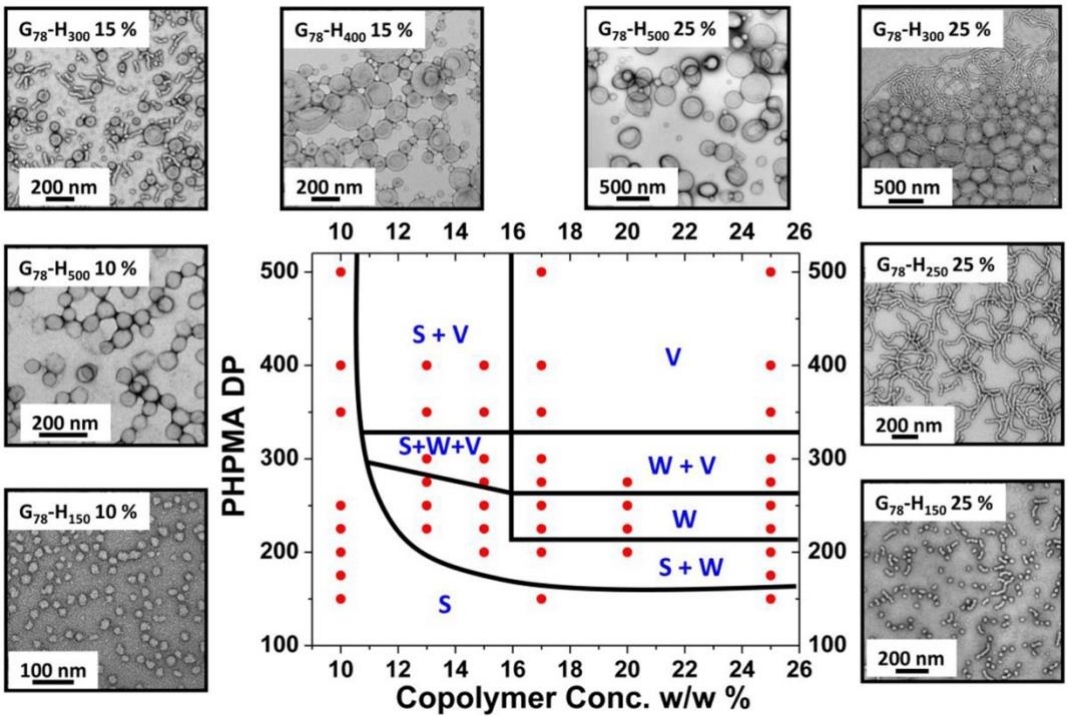


Figure 1.7. Phase diagram, and associated TEM images of various compositions of GMA-HPMA nanostructures obtained by RAFT-PISA. Figure reproduced from ref.[50]

Additionally, an *in silico* method has been reported by the O'Reilly group which can predict both core- and corona-forming monomers that can be used in PISA. This is done by calculating a hydrophobicity proxy known as the surface area normalized octanol-water partition coefficient (Log*P*/SA). Using this computational method, it has been shown that at certain core block lengths, higher order morphologies are formed from polymers with high Log*P*/SA values. It has been shown that this tool is capable of predicting new monomers for different RDRP based PISA methods facilitating the development of PISA as a tool for designing nano-objects.[65]

In summary, PISA has been proven to be a robust and versatile method for the production of nano-objects with various morphologies, of which can be used in several areas, including drug delivery systems, nanoreactors, stimuli responsive nanomaterials, and imaging agents.[66, 67]

1.4.1 Polymerization-induced thermal self-assembly (PITSA)

Polymerization-induced thermal self-assembly (PITSA) is a solution self-assembly method that combines the advantages of PISA with the unique properties of thermoresponsive polymers.[68] Thermoresponsive polymers display a distinct behavior where they reversibly undergo a phase transition beyond a critical temperature point. This can either be an upper critical solution temperature (UCST) or lower critical solution temperature (LCST).[69] Combining the behavior of thermoresponsive polymers with the versatility of PISA enables the synthesis of nanoparticles that self-assemble *via* a phase transition upon change of temperature beyond a critical point.[68]

PITSA takes advantage of the reversible phase transition behavior of thermoresponsive polymers. Entropy changes in the system upon reaching a critical temperature point drives the phase transition which contributes to the formation of nanoparticles. Furthermore, the nanoparticles are not stable after the reaction owing to the reversible nature of the thermally triggered assemblies. For example, in case of LCST polymers, polymers self-assemble above a critical temperature where the polymer chains are no longer soluble and aggregate in the polymerization solution and disassemble when the reaction temperature decreases below that critical temperature.[69]

In order for the particles to remain stable at room temperature, macroinitiators can be functionalized with crosslinkable moieties prior to PITSA so that, once the solution reaches the specific temperature required for self-assembly, the particles can be crosslinked.[68, 70] One example of this is a study by Sumerlin and coworkers where they investigated the self-assembly behavior of the most common thermoresponsive polymer, poly(*N*-isopropylacrylamide) (PNIPAM). In this study, they induced self-assembly of a growing NIPAM polymer using a thermal trigger and investigated how the resulting nano-object morphologies differ with the

PNIPAM degree of polymerization (Figure 1.9). They conducted PITSA using a hydrophilic macro-CTA containing *N*,*N*-dimethylacrylamide (DMA) and acrylic acid (AA) and chain extended with NIPAM. Self-assembly of the polymer chains was achieved above the LCST of the growing PNIPAM block and the particles were crosslinked through the AA groups using an amine to prevent disassembling when the temperature was reduced to below the LCST of NIPAM.[68]

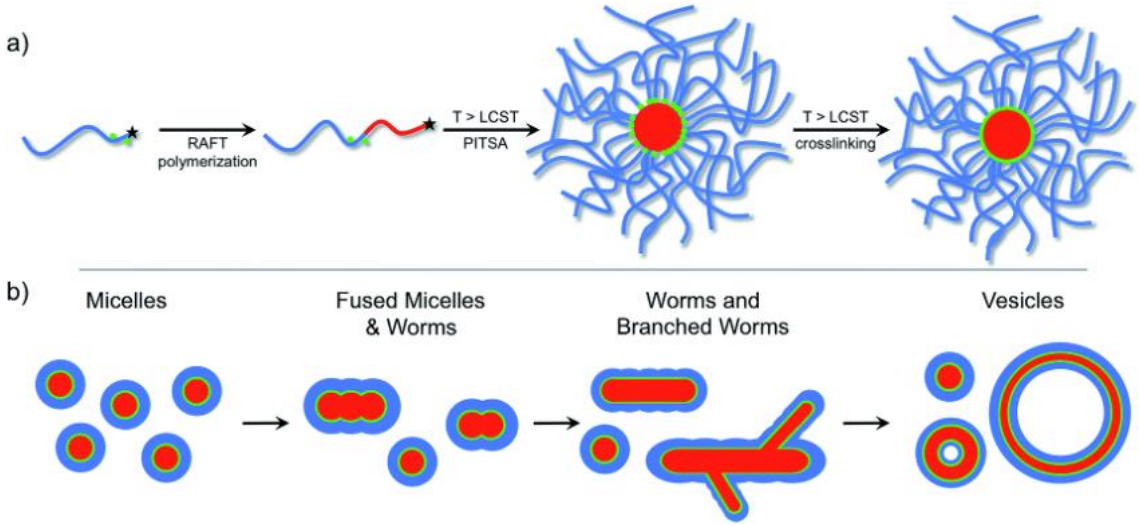


Figure 1.8. a) The mechanism of formation of particles *via* RAFT-PITSA and b) different morphologies obtained upon increasing the hydrophobic block length. Figure reproduced from ref.[68]

Another example of PITSA is the study by Theato and coworkers where they reported the PITSA of copolymers containing DMA, NIPAM and pentafluorophenyl acrylate (PFPA) monomers which were crosslinked *via* reacting the PFPA units with hexamethylenediamine. They also investigated the effect of the changing the PNIPAM DP on the resulting polymeric nanoparticles where they showed that the increase in the PNIPAM DP resulted in a morphology change from spherical micelles to fused spherical-worm like micelles, to worms and then to vesicles.[70]

In summary, PITSA is a convenient method for facile production of thermoresponsive nano-objects that may find application in several diverse areas, especially in drug delivery systems.[71,

[72] The ability to tune the thermoresponsive behavior by altering polymer properties, such as hydrophobicity, also renders PITSA a versatile technique to design functional nanoparticles. However, lack of diversity of the range of monomers that can be employed in PITSA for different applications and a great number of parameters that are required to be controlled for tuning the thermoresponsive behavior of the polymers can be counted as possible limitations of this technique.

1.5 Stimuli-responsive polymers

Natural polymers such as proteins, peptides, nucleic acids adapt to environmental changes by changing their conformation.[73] This inspired chemists to mimic this behavior using synthetic polymers. Synthetic polymers also have potential to be suitably designed to respond to different stimuli such as temperature, light, pH, redox state, ultrasound, or magnetic field.[74-78]

Temperature is the most extensively studied stimulus since its earliest report in 1967,[79] mostly because phase transitions of polymeric systems can be designed to respond at physiologically relevant temperatures. This allows their utilization for biological applications such as controlled drug delivery, smart surfaces and bioseparations.[72, 80-84]

1.5.1 Thermoresponsive polymers

The first reported, and subsequently most studied thermoresponsive polymer was PNIPAM by Heskins and Guillet.[85] Production of diverse thermoresponsive systems has accelerated with the progress in the area of RDRP methods such as ATRP[86] and RAFT[44] facilitating the design of macromolecular structures and also the advantages that “click” chemistry has provided for easy functionalization of macromolecules has led to even more improvements in the design of thermoresponsive systems.[87]

Thermoresponsive polymers display two distinct behaviors in solution: upper critical solution temperature (UCST) or lower critical solution temperature (LCST) providing a versatile

synthetic platform for tunable polymer structures.[76, 88] UCST and LCST are the temperature points at which above or below polymers are completely miscible with solvent, respectively (Figure 1.10).[89] However, relatively high temperature requirements for UCST-based systems make them unfavorable. For this reason and because of the abundance and wider applications of LCST polymers, the LCST transition is particularly more attractive than the UCST.[69]

In case of the LCST, below the critical temperature there is a negative Gibb's free energy of mixing, $\Delta G = \Delta H - T\Delta S$, therefore the polymer and solvent spontaneously mix. Above the critical temperature, the Gibb's free energy becomes positive leading to phase separation. In an LCST polymer-solvent mixture, the enthalpy of dissolution (ΔH) and entropy change (ΔS) are negative. The entropy decreases in the system due to hydrogen bonding of the solvent to the polymer chains. As temperature (T) increases hydrogen bonds between the water molecules and the polymer chains are disrupted and hydrophobic interactions between the polymer chains dominate leading to the collapse and aggregation of the chains. This means phase separation is more favorable at elevated temperature, because of the domination of the entropic term ($-T\Delta S$) caused by water molecules becoming less ordered above a certain temperature.[90-92] The temperature at which the clear polymer solution undergoes a phase transition and becomes cloudy is known as cloud point temperature (T_{CP}) and often used as a proxy of the LCST. This is because determining the LCST is laborious since it is the lowest point of T_{CP} versus polymer concentration curve and requires multiple experiments to measure it, whereas the T_{CP} is a macroscopic effect that can be detected easily.[69, 93]

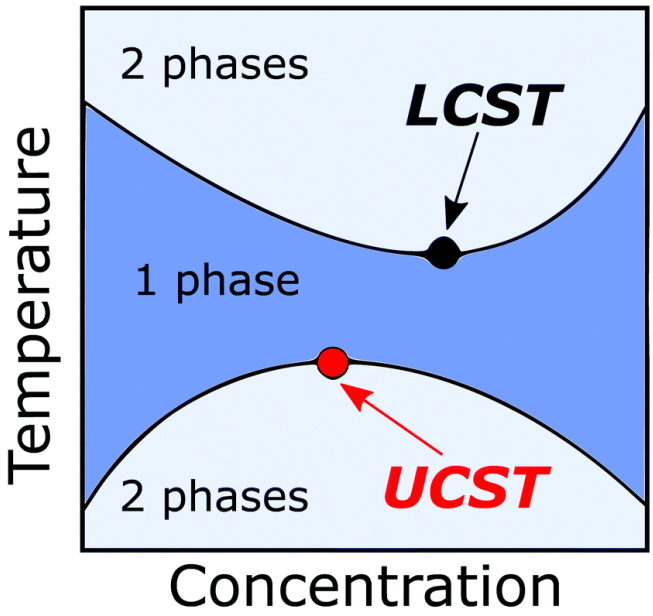


Figure 1.9. LCST and UCST points of thermoresponsive polymers. Figure reproduced from ref.[94]

Tuning the T_{CP} of thermoresponsive polymers can be achieved *via* several methods such as changing polymer molecular weight, solution concentration, or varying polymer composition.[95-99] For example, Gibson *et. al.* and Hoogenboom *et. al.* investigated the effect of the molecular weight on thermoresponsive behavior of P(*N*-vinyl piperidone), P(*N*-isopropylacrylamide), P(*N*-vinylcaprolactam), P(oligo(ethyleneglycol)methacrylate) and P(2-cyclopropyl-2oxazoline) polymers showing that the T_{CP} decreases as the molecular weight of the polymers increased.[95, 98] This happens because the phase separation occurs quickly since long polymer chains can form inter- and/or intramolecular aggregation at low temperature.[100] There are also polymers with molecular weight-independent thermoresponsive behavior such as poly(oligo ethylene glycol methyl methacrylate) (POEGMA)[101] and PNIPAM[102, 103]. Additionally, in some cases polymer LCST can increase with increasing molecular weight as a study by Ni *et. al.* showed that the LCST of the poly(2-(methylamino)ethyl methacrylate) (PDMAEMA) polymers increased when the polymer molecular weight increased.[104] However, these differences in molecular weight-dependence might be caused by non-elimination of parameters such as influence of hydrophobicity of end groups and tacticity of polymers.[105-107]

Another parameter that influences the thermoresponsive behavior is polymer architecture.[108, 109] Especially the difference in the thermal response of linear and brushy versions of the polymers have been reported in many studies.[108, 110-112] This difference is a result of the effect of interactions between the neighboring chains on the phase transition process and depends highly upon the packing of the side chains *i.e.* grafting density.[113] In thermodynamics point of view, a change in the polymer topography such as altering the grafting density, will have an effect on the entropy of the system resulting in a change in the phase transition behavior of the polymers, thus affecting their LCST.[108] Oligo(ethylene glycol) methacrylate (OEGMA) has been widely used for synthesis of brush polymer architectures, where grafting density plays a key role in altering the thermoresponsive behavior.[114-117] Thermoresponsive behavior of OEGMA-based homopolymers is dependent on the length of OEGMA chains whereas in the case of OEGMA-based copolymers thermoresponsive behavior depends upon the monomer composition. As an example, Luzon *et. al.* compared linear and hyperbranched copolymers of di(ethylene glycol) methacrylate (DEGMA) and OEGMA for their thermoresponsive behavior. It was shown that the T_{CP} of polymers increased in both linear and hyperbranched polymer series as the hydrophilic OEGMA composition increases. However, a 5-10 °C decrease in the T_{CP} of hyperbranched polymers compared to their linear analogs was reported.[116]

Another method to control the LCST behavior is the introduction of comonomers into polymer structure which has been widely and effectively used. Increasing hydrophilic composition of the polymer causes an increase in LCST, hence the T_{CP}, because more energy is required to break the H-bonding of hydrated polymer chains. Conversely, increasing the hydrophobic nature of the polymer leads to a decrease in the T_{CP} due to increasing hydrophobic interactions between the chains.[118]

Hoogenboom et al. reported the tuning of LCST by using comonomers to alter polymer composition. They synthesized statistical copolymers of 2-ethyl-2-oxazoline (EtOx) and 2-*n*-

propyl-2-oxazoline (*n*PropOx) with varied compositions and found that the T_{CP} of the copolymers decreased as more of the hydrophobic *n*PropOx was introduced to the polymer structure.[98] This inverse relationship between polymer hydrophobicity and the T_{CP} has facilitated altering the thermoresponsive behavior of copolymers leading to many reports in the literature.[116, 119-123] This relationship has also been intensely investigated in this thesis, therefore the next section covers polymer hydrophobicity in detail.

1.6 Polymer hydrophobicity

Hydrophobicity is one of the most important parameters that can help to explore polymer structure-property relationships amongst many other properties of polymers that influence their behavior such as self-assembly, stimuli-responsiveness, degradation behavior, biological activity, mechanical properties and solubility.[4, 124, 125]

The term "hydrophobicity" has been used for over 100 years in many scientific disciplines such as chemistry, physics, biochemistry, and materials science for applications such as self-assembly, protein folding, thermal transitions.[124] However, there is still an uncertainty in the predictive models used to explain these phenomena. Prediction of the behavior of small molecules in solution has been explained well by Hildebrand and Hansen solubility parameters and partition coefficients (Log*P* values).[126-128] However, prediction of hydrophobicity has its limits when translating from small molecules, with rigid structures, to large macromolecules like polymers which have flexible structures.[129] Different predictive models are discussed briefly in the following section. Mather's hydrophobicity parameter (MHP), which is surface area normalized Log*P* (Log*P*/SA), and its predictive capability is discussed in more detail since it was extensively used in this thesis for the prediction of hydrophobicity of several statistical copolymer series.

1.6.1 Predictive models used for investigating polymer hydrophobicity

Hydrophobicity of small molecules and macromolecules have been evaluated in three categories: theory, simulation and experimental.[124, 130-132] There are several methods to quantify hydrophobicity experimentally and each of these methods contributes to the measurements in different aspects based on their strengths and limitations. Some of these methods include contact angle measurements, which is amongst the most widely used experimental method due to its facile applicability,[133] swelling of crosslinked polymer networks,[134] HPLC measurements (mostly used to determine the hydrophobicity of biomolecules),[135] and solvatochromic dyes that investigate the hydrophobicity based upon the change in absorbance/fluorescence.[136] In recent work by our group it was shown that combining these experimental methods with theory and simulations would provide more powerful tools for designing functional, responsive materials.[124]

The pioneering theoretical evaluation of hydrophobicity was reported in 1950s by Hildebrand in an approach named the Hildebrand solubility parameter (δ), which combines enthalpy (ΔH) and molar volume (V_m) for predicting the solubility of small molecules (Equation 1).[137]

$$\delta = \sqrt{\frac{\Delta H_v - RT}{V_m}} \qquad \text{(Equation 1)}$$

Hansen extended the scope of the Hildebrand parameter by including the parameters of polar (δ_p), dispersion (δ_d), and hydrogen bonding (δ_h) forces between the solute and solvent molecules.[138] Later, octanol-water partition coefficients (LogP_{oct}) which involve a free-energy approach to define hydrophobicity were introduced by medicinal and pharmaceutical chemists during the 1980s and 1990s (Equation 2). LogP_{oct} represents how a molecule partitions between lipophilic (mostly *n*-octanol) and aqueous phases (Equation 3) having negative values for soluble compounds and positive for insoluble ones.[139]

$$LogP_{oct} = \frac{(-\Delta G_{transfer})}{RT\ ln10} \qquad \text{(Equation 2)}$$

$$\text{Log}P_{oct} = \text{Log}\left(\frac{[\text{solute}_{\text{octanol}}]}{[\text{solute}_{\text{water}}]}\right) \qquad \text{(Equation 3)}$$

Then, in 1999 Lum, Chandler and Weeks (LCW) reported how hydrophobicity relates to the length scale. In LCW theory, hydrophobicity phenomenon is explained by investigating the solvation behavior of small and large hydrophobic solutes in water. Hydrogen bonds in water molecules are reorganized differently when around small or large hydrophobic solutes. This revealed the information that hydrophobicity scales with molecular volume and surface area for small and large length scales, respectively.[140, 141]

Based on this fact, Mathers and coworkers have reported the Mathers hydrophobicity parameter (MHP) which is determined by surface area normalization of the calculated Log*P* values (Log*P*/SA).[142] MHP brought a different insight to hydrophobicity models than the Hildebrand and Hansen parameters for the fact that Log*P* values are proportional to the Gibbs free energy (ΔG), contrary to the Hildebrand and Hansen parameters which depend on enthalpy (ΔH) and molar volume (V_m).

In recent work by our group, information gathered from all hydrophobicity models was utilized to represent polymer hydrophobicity more accurately. Five important parameters were highlighted for determining the most versatile hydrophobicity parameter.[124] First, the structure of the polymer should be determined by using experimental data to factor in the effects of stereochemistry, branching, cross-linking and polymer composition. Second, as LCW theory suggests hydrophobicity of the polymers are proportionate to their volumes below a specific length scale and their surface areas above that length scale. Therefore, an accurate model with appropriate length should be built to represent the polymer chains. A thermodynamic parameter is the third component that a robust model should include for that it allows accurate

quantification and a theoretical basis for prediction. The fourth component is a structural parameter that will account for molecular size. A structural parameter is measured after molecular dynamic (MD) simulations for more accurate measurements. MD simulations are frequently used to determine the physical properties such as surface area (SA) of macromolecules. Finally, the model should represent the role of temperature to better reflect the direct relationship between hydrophobic interactions and temperature.[124]

Considering all of these parameters, both Hildebrand solubility parameter and MHP were shown to be effective tools to explain polymer hydrophobicity. Since MHP was extensively used in this thesis to explain thermoresponsive behavior of polymers, it is discussed in detail in the next section.

1.6.1.1 Mather's hydrophobicity parameter (MHP)

Mather's hydrophobicity parameter (MHP), *i.e.*, Log*P*/SA, has been proven to be very useful as it fits the five components discussed previously. Representing the hydrophobicity of polymers by Log*P*/SA combines insights from different aspects: physical chemistry *via* LCW theory for designing molecular models to accurately represent the actual polymer, medicinal chemistry *via* prediction of Log*P* values, MD simulations by using force fields that minimizes energy for molecular models to find their best conformation, and surface area calculation that uses the information from protein modeling. In Figure 1.10, the mechanism of calculating the Log*P*/SA is explained: an oligomer model with an appropriate size (5-10 monomer units for linear polymers, up to 20-25 units for comonomers or branching) is created prior to Log*P*/SA calculations. For the amphiphilic copolymers, oligomer models are designed to contain appropriate ratios of all comonomers. Log*P* of the polymers is calculated computationally using an atom-based approach (ALogP98 method)[128] for all molecular models containing C, H, N, and O atoms. Then, Log*P* of each polymer is normalized by their surface area.[65, 143-145]

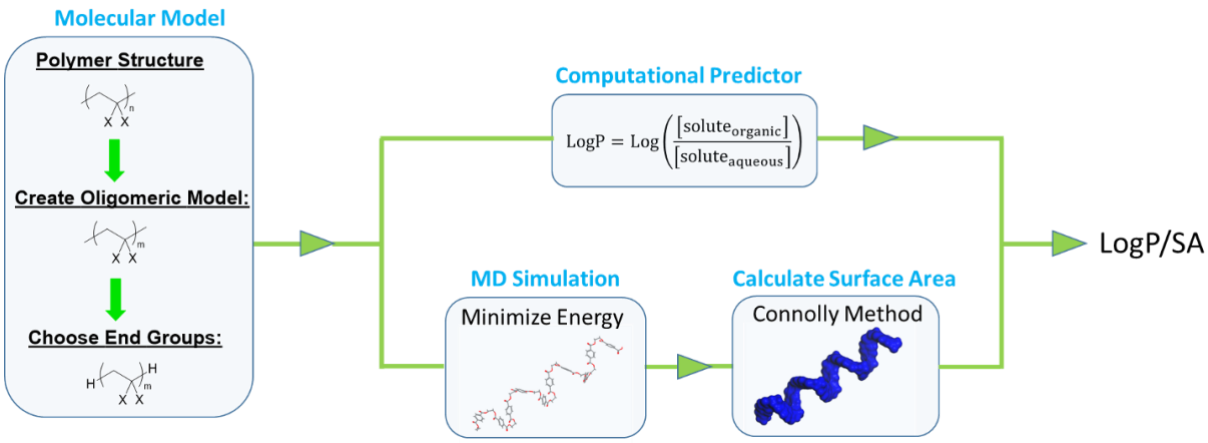


Figure 1.10. A flow diagram showing the steps of calculating Log*P*/SA values of polymers. Adapted from ref.[144]

It has been reported that Log*P*/SA functions well for relating polymer hydrophobicity to experimental observations such as polymer degradation, polymer surface energy, self-assembly and LCST behavior of the polymers.[124] Also, the inverse relationship between the T_{CP} and polymer hydrophobicity inspired many researchers to design polymers with tunable thermoresponsive behaviors as mentioned previously. Based on this, the calculated MHP and measured T_{CP} values have been used as proxies in the Chapters 2 and 3 of this thesis to represent the inverse relationship between the hydrophobicity and LCST behavior of polymers.

1.7 Summary

Within this Chapter, key concepts investigated in the experimental Chapters of this thesis have been reviewed. First, fundamentals about synthetic polymers have been introduced briefly, followed by common polymerization techniques including the mechanisms of controlled polymerizations. RAFT polymerization has been explained extensively, as it has been used heavily for the preparation of block copolymers in all experimental chapters of this thesis. Then, self-assembly of block copolymers was briefly explained prior to the description of PISA. More specifically, PITSA was described under a separate topic since it was used in this thesis in Chapter 4 for the synthesis of thermoresponsive nanoparticles. To better emphasize the thermoresponsive behavior of the polymers that was benefited in PITSA method, stimuli responsive polymers were introduced and thermoresponsive polymers were explained in detail including the theory of thermoresponsive behavior of polymers in solution. As one of the methods to control thermoresponsive behavior of polymers, polymer hydrophobicity and its effect on the thermoresponsive behavior were explained. The evolution of determination of hydrophobicity has been introduced and finally, the concept of Log*P*/SA, *i.e.*, Mather's Hydrophobicity Parameters (MHP) was highlighted since this parameter was used to determine the hydrophobicity of copolymers prepared in Chapters 2 and 3.

1.8 References

1. Bassas-Galia, M.; Follonier, S.; Pusnik, M.; Zinn, M. 2 - Natural polymers: A source of inspiration. In *Bioresorbable Polymers for Biomedical Applications*, Perale, G., Hilborn, J. Eds.; Woodhead Publishing, 2017; pp 31-64.

2. Brunsveld, L.; Folmer, B. J. B.; Meijer, E. W.; Sijbesma, R. P. Supramolecular Polymers. *Chem. Rev.* **2001**, *101* (12), 4071-4098.

3. Aida, T.; Meijer, E. W.; Stupp, S. I. Functional Supramolecular Polymers. *Science* **2012**, *335* (6070), 813-817.

4. Gentekos, D. T.; Sifri, R. J.; Fors, B. P. Controlling polymer properties through the shape of the molecular-weight distribution. *Nat. Rev. Mater.* **2019**, *4* (12), 761-774.

5. Gentekos, D. T.; Dupuis, L. N.; Fors, B. P. Beyond Dispersity: Deterministic Control of Polymer Molecular Weight Distribution. *J. Am. Chem. Soc.* **2016**, *138* (6), 1848-1851.

6. Mark, J. E. *Physical properties of polymers handbook*; Springer, 2007.

7. Matyjaszewski, K. Macromolecular engineering: From rational design through precise macromolecular synthesis and processing to targeted macroscopic material properties. *Prog. Polym. Sci.* **2005**, *30* (8), 858-875.

8. Lutz, J.-F.; Ouchi, M.; Liu, D. R.; Sawamoto, M. Sequence-Controlled Polymers. *Science* **2013**, *341* (6146), 1238149.

9. Hadjichristidis, N.; Iatrou, H.; Pitsikalis, M.; Mays, J. Macromolecular architectures by living and controlled/living polymerizations. *Prog. Polym. Sci.* **2006**, *31* (12), 1068-1132.

10. Syrett, J. A.; Haddleton, D. M.; Whittaker, M. R.; Davis, T. P.; Boyer, C. Functional, star polymeric molecular carriers, built from biodegradable microgel/nanogel cores. *Chem. Commun.* **2011**, *47* (5), 1449-1451.

11. Gauthier, M. A.; Gibson, M. I.; Klok, H.-A. Synthesis of Functional Polymers by Post-Polymerization Modification. *Angew. Chem. Int. Ed.* **2009**, *48* (1), 48-58.

12. Matyjaszewski, K. Architecturally Complex Polymers with Controlled Heterogeneity. *Science* **2011**, *333* (6046), 1104-1105.

13. Hiemenz, P. C.; Lodge, T. P. *Polymer chemistry*; CRC press, 2007.

14. Flory, P. J. Fundamental Principles of Condensation Polymerization. *Chem. Rev.* **1946**, *39* (1), 137-197.

15. Stille, J. K. Step-growth polymerization. *J. Chem. Educ.* **1981**, *58* (11), 862.

16. Billiet, L.; Fournier, D.; Du Prez, F. Step-growth polymerization and 'click' chemistry: The oldest polymers rejuvenated. *Polymer* **2009**, *50* (16), 3877-3886.

17. Odian, G. *Principles of polymerization*; John Wiley & Sons, 2004.

18. Odian, G. Chain-Reaction Polymerization. *Encyclopedia of Polymer Science and Technology* **2002**.

19. Szwarc, M. 'Living'polymers. *Nature* **1956**, *178* (4543), 1168-1169.

20. Hirao, A.; Goseki, R.; Ishizone, T. Advances in Living Anionic Polymerization: From Functional Monomers, Polymerization Systems, to Macromolecular Architectures. *Macromolecules* **2014**, *47* (6), 1883-1905.

21. Chen, Y.; Zhang, L.; Jin, Y.; Lin, X.; Chen, M. Recent Advances in Living Cationic Polymerization with Emerging Initiation/Controlling Systems. *Macromol. Rapid Commun.* **2021**, *42* (13), 2100148.

22. Fuchise, K.; Chen, Y.; Satoh, T.; Kakuchi, T. Recent progress in organocatalytic group transfer polymerization. *Polym. Chem.* **2013**, *4* (16), 4278-4291.

23. Bielawski, C. W.; Grubbs, R. H. Living ring-opening metathesis polymerization. *Prog. Polym. Sci.* **2007**, *32* (1), 1-29.

24. Colombani, D. Chain-growth control in free radical polymerization. *Prog. Polym. Sci.* **1997**, *22* (8), 1649-1720.

25. Helfferich, F. G. *Kinetics of homogeneous multistep reactions*; Elsevier, 2001.

26. Sugihara, Y.; O'connor, P.; Zetterlund, P. B.; Aldabbagh, F. Chain transfer to solvent in the radical polymerization of N-isopropylacrylamide. *J. Polym. Sci., Part A: Polym. Chem.* **2011**, *49* (8), 1856-1864.

27. Nesvadba, P. Radical Polymerization in Industry. *Encyclopedia of Radicals in Chemistry, Biology and Materials* **2012**.

28. Webster, O. W. Living Polymerization Methods. *Science* **1991**, *251* (4996), 887-893.

29. Keddie, D. J. A guide to the synthesis of block copolymers using reversible-addition fragmentation chain transfer (RAFT) polymerization. *Chem. Soc. Rev.* **2014**, *43* (2), 496-505.

30. Corrigan, N.; Jung, K.; Moad, G.; Hawker, C. J.; Matyjaszewski, K.; Boyer, C. Reversible-deactivation radical polymerization (Controlled/living radical polymerization): From discovery to materials design and applications. *Prog. Polym. Sci.* **2020**, *111*, 101311.

31. Matyjaszewski, K.; Xia, J. Atom Transfer Radical Polymerization. *Chem. Rev.* **2001**, *101* (9), 2921-2990.

32. Hawker, C. J.; Bosman, A. W.; Harth, E. New Polymer Synthesis by Nitroxide Mediated Living Radical Polymerizations. *Chem. Rev.* **2001**, *101* (12), 3661-3688.

33. Fischer, H. The Persistent Radical Effect: A Principle for Selective Radical Reactions and Living Radical Polymerizations. *Chem. Rev.* **2001**, *101* (12), 3581-3610.

34. Wang, J.-S.; Matyjaszewski, K. Controlled/"living" radical polymerization. atom transfer radical polymerization in the presence of transition-metal complexes. *Journal of the American Chemical Society* **1995**, *117* (20), 5614-5615.

35. di Lena, F.; Matyjaszewski, K. Transition metal catalysts for controlled radical polymerization. *Prog. Polym. Sci.* **2010**, *35* (8), 959-1021.

36. Pintauer, T.; Braunecker, W.; Collange, E.; Poli, R.; Matyjaszewski, K. Determination of Rate Constants for the Activation Step in Atom Transfer Radical Polymerization Using the Stopped-Flow Technique. *Macromolecules* **2004**, *37* (8), 2679-2682.

37. Nicolas, J.; Guillaneuf, Y.; Lefay, C.; Bertin, D.; Gigmes, D.; Charleux, B. Nitroxide-mediated polymerization. *Prog. Polym. Sci.* **2013**, *38* (1), 63-235.

38. Petton, L.; Ciolino, A. E.; Dervaux, B.; Du Prez, F. E. From one-pot stabilisation to in situ functionalisation in nitroxide mediated polymerisation: an efficient extension towards atom transfer radical polymerisation. *Polym. Chem.* **2012**, *3* (7), 1867.

39. Chiefari, J.; Chong, Y.; Ercole, F.; Krstina, J.; Jeffery, J.; Le, T. P.; Mayadunne, R. T.; Meijs, G. F.; Moad, C. L.; Moad, G. Living free-radical polymerization by reversible addition− fragmentation chain transfer: the RAFT process. *Macromolecules* **1998**, *31* (16), 5559-5562.

40. Barner-Kowollik, C.; Perrier, S. The future of reversible addition fragmentation chain transfer polymerization. *J. Polym. Sci., Part A: Polym. Chem.* **2008**, *46* (17), 5715-5723.

41. Perrier, S. 50th Anniversary Perspective: RAFT Polymerization—A User Guide. *Macromolecules* **2017**, *50* (19), 7433-7447.

42. Keddie, D. J.; Moad, G.; Rizzardo, E.; Thang, S. H. RAFT Agent Design and Synthesis. *Macromolecules* **2012**, *45* (13), 5321-5342.

43. Moad, G.; Rizzardo, E.; Thang, S. H. RAFT Polymerization and Some of its Applications. *Chem. Asian J.* **2013**, *8* (8), 1634-1644.

44. Boyer, C.; Bulmus, V.; Davis, T. P.; Ladmiral, V.; Liu, J.; Perrier, S. Bioapplications of RAFT Polymerization. *Chem. Rev.* **2009**, *109* (11), 5402-5436.

45. Nothling, M. D.; Fu, Q.; Reyhani, A.; Allison-Logan, S.; Jung, K.; Zhu, J.; Kamigaito, M.; Boyer, C.; Qiao, G. G. Progress and Perspectives Beyond Traditional RAFT Polymerization. *Adv. Sci.* **2020**, *7* (20), 2001656.

46. Mai, Y.; Eisenberg, A. Self-assembly of block copolymers. *Chem. Soc. Rev.* **2012**, *41* (18), 5969-5985.

47. Blanazs, A.; Armes, S. P.; Ryan, A. J. Self-Assembled Block Copolymer Aggregates: From Micelles to Vesicles and their Biological Applications. *Macromol. Rapid Commun.* **2009**, *30* (4-5), 267-277.

48. Doncom, K. E. B.; Blackman, L. D.; Wright, D. B.; Gibson, M. I.; O'Reilly, R. K. Dispersity effects in polymer self-assemblies: a matter of hierarchical control. *Chem. Soc. Rev.* **2017**, *46* (14), 4119-4134.

49. Figg, C. A.; Carmean, R. N.; Bentz, K. C.; Mukherjee, S.; Savin, D. A.; Sumerlin, B. S. Tuning Hydrophobicity To Program Block Copolymer Assemblies from the Inside Out. *Macromolecules* **2017**, *50* (3), 935-943.

50. Blanazs, A.; Ryan, A. J.; Armes, S. P. Predictive Phase Diagrams for RAFT Aqueous Dispersion Polymerization: Effect of Block Copolymer Composition, Molecular Weight, and Copolymer Concentration. *Macromolecules* **2012**, *45* (12), 5099-5107.

51. Su, Y.; Jiang, Y.; Liu, L.; Xie, Y.; Chen, S.; Wang, Y.; O'Reilly, R. K.; Tong, Z. Hydrogen-Bond-Regulated Platelet Micelles by Crystallization-Driven Self-Assembly and Templated Growth for Poly(ε-Caprolactone) Block Copolymers. *Macromolecules* **2022**, *55* (3), 1067-1076.

52. Grundy, L. S.; Lee, V. E.; Li, N.; Sosa, C.; Mulhearn, W. D.; Liu, R.; Register, R. A.; Nikoubashman, A.; Prud'homme, R. K.; Panagiotopoulos, A. Z.; et al. Rapid Production of Internally Structured Colloids by Flash Nanoprecipitation of Block Copolymer Blends. *ACS Nano* **2018**, *12* (5), 4660-4668.

53. Luo, M.; Epps, T. H. Directed Block Copolymer Thin Film Self-Assembly: Emerging Trends in Nanopattern Fabrication. *Macromolecules* **2013**, *46* (19), 7567-7579.

54. Varlas, S.; Georgiou, P. G.; Bilalis, P.; Jones, J. R.; Hadjichristidis, N.; O'Reilly, R. K. Poly(sarcosine)-Based Nano-Objects with Multi-Protease Resistance by Aqueous

Photoinitiated Polymerization-Induced Self-Assembly (Photo-PISA). *Biomacromolecules* **2018**, *19* (11), 4453-4462.

55. Bosworth, J. K.; Paik, M. Y.; Ruiz, R.; Schwartz, E. L.; Huang, J. Q.; Ko, A. W.; Smilgies, D.-M.; Black, C. T.; Ober, C. K. Control of Self-Assembly of Lithographically Patternable Block Copolymer Films. *ACS Nano* **2008**, *2* (7), 1396-1402.

56. Agrahari, V.; Agrahari, V. Advances and applications of block-copolymer-based nanoformulations. *Drug Discovery Today* **2018**, *23* (5), 1139-1151.

57. Liu, C.; Hong, C.-Y.; Pan, C.-Y. Polymerization techniques in polymerization-induced self-assembly (PISA). *Polym. Chem.* **2020**, *11* (22), 3673-3689.

58. Charleux, B.; Delaittre, G.; Rieger, J.; D'Agosto, F. Polymerization-Induced Self-Assembly: From Soluble Macromolecules to Block Copolymer Nano-Objects in One Step. *Macromolecules* **2012**, *45* (17), 6753-6765.

59. Wang, G.; Schmitt, M.; Wang, Z.; Lee, B.; Pan, X.; Fu, L.; Yan, J.; Li, S.; Xie, G.; Bockstaller, M. R.; et al. Polymerization-Induced Self-Assembly (PISA) Using ICAR ATRP at Low Catalyst Concentration. *Macromolecules* **2016**, *49* (22), 8605-8615.

60. Qiao, X. G.; Dugas, P. Y.; Charleux, B.; Lansalot, M.; Bourgeat-Lami, E. Nitroxide-mediated polymerization-induced self-assembly of amphiphilic block copolymers with a pH/temperature dual sensitive stabilizer block. *Polym. Chem.* **2017**, *8* (27), 4014-4029.

61. Wan, J.; Fan, B.; Thang, S. H. RAFT-mediated polymerization-induced self-assembly (RAFT-PISA): current status and future directions. *Chem. Sci.* **2022**, *13* (15), 4192-4224.

62. Karagoz, B.; Esser, L.; Duong, H. T.; Basuki, J. S.; Boyer, C.; Davis, T. P. Polymerization-Induced Self-Assembly (PISA) – control over the morphology of nanoparticles for drug delivery applications. *Polym. Chem.* **2014**, *5* (2), 350-355.

63. Canning, S. L.; Smith, G. N.; Armes, S. P. A Critical Appraisal of RAFT-Mediated Polymerization-Induced Self-Assembly. *Macromolecules* **2016**, *49* (6), 1985-2001.

64. Derry, M. J.; Fielding, L. A.; Armes, S. P. Industrially-relevant polymerization-induced self-assembly formulations in non-polar solvents: RAFT dispersion polymerization of benzyl methacrylate. *Polym. Chem.* **2015**, *6* (16), 3054-3062.

65. Foster, J. C.; Varlas, S.; Couturaud, B.; Jones, J. R.; Keogh, R.; Mathers, R. T.; O'Reilly, R. K. Predicting Monomers for Use in Polymerization-Induced Self-Assembly. *Angew. Chem. Int. Ed.* **2018**, *130* (48), 15959-15963.

66. Yeow, J.; Boyer, C. Photoinitiated Polymerization-Induced Self-Assembly (Photo-PISA): New Insights and Opportunities. *Adv. Sci.* **2017**, *4* (7), 1700137.

67. Karayianni, M.; Pispas, S. Block copolymer solution self-assembly: Recent advances, emerging trends, and applications. *J. Polym. Sci.* **2021**, *59* (17), 1874-1898.

68. Figg, C. A.; Simula, A.; Gebre, K. A.; Tucker, B. S.; Haddleton, D. M.; Sumerlin, B. S. Polymerization-induced thermal self-assembly (PITSA). *Chem. Sci.* **2015**, *6* (2), 1230-1236.

69. Roy, D.; Brooks, W. L. A.; Sumerlin, B. S. New directions in thermoresponsive polymers. *Chem. Soc. Rev.* **2013**, *42* (17), 7214-7243.

70. Vakili, M.; Cunningham, V. J.; Trebbin, M.; Theato, P. Polymerization-Induced Thermal Self-Assembly of Functional and Thermo-Responsive Diblock Copolymer Nano-Objects via RAFT Aqueous Polymerization. *Macromol. Chem. Phys.* **2019**, *220* (2), 1800370.

71. Qiao, S.-L.; Mamuti, M.; An, H.-W.; Wang, H. Thermoresponsive Polymer Assemblies: From Molecular Design to Theranostics Application. *Prog. Polym. Sci.* **2022**, *131*, 101578.

72. Bordat, A.; Boissenot, T.; Nicolas, J.; Tsapis, N. Thermoresponsive polymer nanocarriers for biomedical applications. *Adv. Drug Del. Rev.* **2019**, *138*, 167-192.

73. Wei, M.; Gao, Y.; Li, X.; Serpe, M. J. Stimuli-responsive polymers and their applications. *Polym. Chem.* **2017**, *8* (1), 127-143.

74. Dai, S.; Ravi, P.; Tam, K. C. pH-Responsive polymers: synthesis, properties and applications. *Soft Matter* **2008**, *4* (3), 435-449.

75. Gibson, M. I.; O'Reilly, R. K. To aggregate, or not to aggregate? considerations in the design and application of polymeric thermally-responsive nanoparticles. *Chem. Soc. Rev.* **2013**, *42* (17), 7204-7213.

76. Jochum, F. D.; Theato, P. Temperature- and light-responsive smart polymer materials. *Chem. Soc. Rev.* **2013**, *42* (17), 7468-7483.

77. Zhang, A.; Jung, K.; Li, A.; Liu, J.; Boyer, C. Recent advances in stimuli-responsive polymer systems for remotely controlled drug release. *Prog. Polym. Sci.* **2019**, *99*, 101164.

78. Zhang, X.; Han, L.; Liu, M.; Wang, K.; Tao, L.; Wan, Q.; Wei, Y. Recent progress and advances in redox-responsive polymers as controlled delivery nanoplatforms. *Mater. Chem. Front.* **2017**, *1* (5), 807-822.

79. Scarpa, J. S.; Mueller, D. D.; Klotz, I. M. Slow hydrogen-deuterium exchange in a non-. alpha.-helical polyamide. *Journal of the American Chemical Society* **1967**, *89* (24), 6024-6030.

80. Lutz, J.-F. Thermo-Switchable Materials Prepared Using the OEGMA-Platform. *Adv. Mater.* **2011**, *23* (19), 2237-2243.

81. Hatakeyama, H.; Kikuchi, A.; Yamato, M.; Okano, T. Patterned biofunctional designs of thermoresponsive surfaces for spatiotemporally controlled cell adhesion, growth, and thermally induced detachment. *Biomaterials* **2007**, *28* (25), 3632-3643.

82. Nagase, K.; Kobayashi, J.; Okano, T. Temperature-responsive intelligent interfaces for biomolecular separation and cell sheet engineering. *J. R. Soc. Interface* **2009**, *6* (suppl_3), S293-S309.

83. Nagase, K.; Okano, T. Thermoresponsive-polymer-based materials for temperature-modulated bioanalysis and bioseparations. *Mater Chem B.* **2016**, *4* (39), 6381-6397.

84. Nagase, K. Thermoresponsive interfaces obtained using poly(N-isopropylacrylamide)-based copolymer for bioseparation and tissue engineering applications. *Adv. Colloid Interface Sci.* **2021**, *295*, 102487.

85. Heskins, M.; Guillet, J. E. Solution Properties of Poly(N-isopropylacrylamide). *J. Macromol. Sci. A* **1968**, *2* (8), 1441-1455.

86. Siegwart, D. J.; Oh, J. K.; Matyjaszewski, K. ATRP in the design of functional materials for biomedical applications. *Prog. Polym. Sci.* **2012**, *37* (1), 18-37.

87. Li, M.; De, P.; Gondi, S. R.; Sumerlin, B. S. Responsive Polymer-Protein Bioconjugates Prepared by RAFT Polymerization and Copper-Catalyzed Azide-Alkyne Click Chemistry. *Macromol. Rapid Commun.* **2008**, *29* (12-13), 1172-1176.

88. Zhang, Q.; Hoogenboom, R. Polymers with upper critical solution temperature behavior in alcohol/water solvent mixtures. *Prog. Polym. Sci.* **2015**, *48*, 122-142.

89. Zhang, Q.; Weber, C.; Schubert, U. S.; Hoogenboom, R. Thermoresponsive polymers with lower critical solution temperature: from fundamental aspects and measuring techniques to recommended turbidimetry conditions. *Mater. Horiz.* **2017**, *4* (2), 109-116.

90. Hoogenboom, R. Chapter 2 - Temperature-Responsive Polymers: Properties, Synthesis, and Applications. In *Smart Polymers and their Applications (Second Edition)*, Aguilar, M. R., San Román, J. Eds.; Woodhead Publishing, 2019; pp 13-44.

91. Bawa, P.; Pillay, V.; Choonara, Y. E.; du Toit, L. C. Stimuli-responsive polymers and their applications in drug delivery. *Biomed. Mater.* **2009**, *4* (2), 022001.

92. Bromberg, L. E.; Ron, E. S. Temperature-responsive gels and thermogelling polymer matrices for protein and peptide delivery. *Adv. Drug Del. Rev.* **1998**, *31* (3), 197-221.

93. Akar, I.; Foster, J. C.; Leng, X.; Pearce, A. K.; Mathers, R. T.; O'Reilly, R. K. LogPoct/SA Predicts the Thermoresponsive Behavior of P(DMA-co-RA) Statistical Copolymers. *ACS Macro Lett.* **2022**, *11* (4), 498-503.

94. Niskanen, J.; Tenhu, H. How to manipulate the upper critical solution temperature (UCST)? *Polym. Chem.* **2017**, *8* (1), 220-232.

95. Ieong, N. S.; Hasan, M.; Phillips, D. J.; Saaka, Y.; O'Reilly, R. K.; Gibson, M. I. Polymers with molecular weight dependent LCSTs are essential for cooperative behaviour. *Polym. Chem.* **2012**, *3* (3), 794-799.

96. Keogh, R.; Blackman, L. D.; Foster, J. C.; Varlas, S.; O'Reilly, R. K. The Importance of Cooperativity in Polymer Blending: Toward Controlling the Thermoresponsive Behavior of Blended Block Copolymer Micelles. *Macromol. Rapid Commun.* **2020**, *41* (6), 1900599.

97. Kempe, K.; Neuwirth, T.; Czaplewska, J.; Gottschaldt, M.; Hoogenboom, R.; Schubert, U. S. Poly(2-oxazoline) glycopolymers with tunable LCST behavior. *Polym. Chem.* **2011**, *2* (8), 1737-1743.

98. Glassner, M.; Lava, K.; de la Rosa, V. R.; Hoogenboom, R. Tuning the LCST of poly(2-cyclopropyl-2-oxazoline) via gradient copolymerization with 2-ethyl-2-oxazoline. *J. Polym. Sci., Part A: Polym. Chem.* **2014**, *52* (21), 3118-3122.

99. Kostyurina, E.; De Mel, J. U.; Vasilyeva, A.; Kruteva, M.; Frielinghaus, H.; Dulle, M.; Barnsley, L.; Förster, S.; Schneider, G. J.; Biehl, R.; et al. Controlled LCST Behavior and Structure Formation of Alternating Amphiphilic Copolymers in Water. *Macromolecules* **2022**, *55* (5), 1552-1565.

100. Han, S.; Hagiwara, M.; Ishizone, T. Synthesis of Thermally Sensitive Water-Soluble Polymethacrylates by Living Anionic Polymerizations of Oligo(ethylene glycol) Methyl Ether Methacrylates. *Macromolecules* **2003**, *36* (22), 8312-8319.

101. Cook, M. T.; Haddow, P.; Kirton, S. B.; McAuley, W. J. Polymers Exhibiting Lower Critical Solution Temperatures as a Route to Thermoreversible Gelators for Healthcare. *Adv. Funct. Mater.* **2021**, *31* (8), 2008123.

102. Furyk, S.; Zhang, Y.; Ortiz-Acosta, D.; Cremer, P. S.; Bergbreiter, D. E. Effects of end group polarity and molecular weight on the lower critical solution temperature of poly(N-isopropylacrylamide). *J. Polym. Sci., Part A: Polym. Chem.* **2006**, *44* (4), 1492-1501.

103. Zhang, Y.; Furyk, S.; Sagle, L. B.; Cho, Y.; Bergbreiter, D. E.; Cremer, P. S. Effects of Hofmeister Anions on the LCST of PNIPAM as a Function of Molecular Weight. *J. Phys. Chem. C.* **2007**, *111* (25), 8916-8924.

104. Liu, Q.; Yu, Z.; Ni, P. Micellization and applications of narrow-distribution poly[2-(dimethylamino)ethyl methacrylate]. *Colloid. Polym. Sci.* **2004**, *282* (4), 387-393.

105. Xia, Y.; Burke, N. A. D.; Stöver, H. D. H. End Group Effect on the Thermal Response of Narrow-Disperse Poly(N-isopropylacrylamide) Prepared by Atom Transfer Radical Polymerization. *Macromolecules* **2006**, *39* (6), 2275-2283.

106. Pasparakis, G.; Tsitsilianis, C. LCST polymers: Thermoresponsive nanostructured assemblies towards bioapplications. *Polymer* **2020**, *211*, 123146.

107. Ray, B.; Okamoto, Y.; Kamigaito, M.; Sawamoto, M.; Seno, K.-i.; Kanaoka, S.; Aoshima, S. Effect of tacticity of poly (N-isopropylacrylamide) on the phase separation temperature of its aqueous solutions. *Polym. J.* **2005**, *37* (3), 234-237.

108. Chee, C.-K.; Hunt, B. J.; Rimmer, S.; Rutkaite, R.; Soutar, I.; Swanson, L. Manipulating the thermoresponsive behaviour of poly(N-isopropylacrylamide) 3. On the conformational behaviour of N-isopropylacrylamide graft copolymers. *Soft Matter* **2009**, *5* (19), 3701-3712.

109. Qiu, X.-P.; Winnik, F. M. Effect of Topology on the Properties of Poly(N - isopropylacrylamide) in Water and in Bulk. *Macromol* **2009**, *278* (1), 10-13.

110. Luzon, M.; Corrales, T. Thermal studies and chromium removal efficiency of thermoresponsive hyperbranched copolymers based on PEG-methacrylates. *J. Therm. Anal. Calorim.* **2014**, *116* (1), 401-409.

111. Porsch, C.; Hansson, S.; Nordgren, N.; Malmström, E. Thermo-responsive cellulose-based architectures: tailoring LCST using poly(ethylene glycol) methacrylates. *Polym. Chem.* **2011**, *2* (5), 1114-1123.

112. Morgese, G.; Shirmardi Shaghasemi, B.; Causin, V.; Zenobi-Wong, M.; Ramakrishna, S. N.; Reimhult, E.; Benetti, E. M. Next-Generation Polymer Shells for Inorganic Nanoparticles are Highly Compact, Ultra-Dense, and Long-Lasting Cyclic Brushes. *Angew. Chem. Int. Ed.* **2017**, *56* (16), 4507-4511.

113. Humphreys, B. A.; Prescott, S. W.; Murdoch, T. J.; Nelson, A.; Gilbert, E. P.; Webber, G. B.; Wanless, E. J. Influence of molecular weight on PNIPAM brush modified colloidal silica particles. *Soft Matter* **2019**, *15* (1), 55-64.

114. Lutz, J.-F.; Hoth, A. Preparation of Ideal PEG Analogues with a Tunable Thermosensitivity by Controlled Radical Copolymerization of 2-(2-Methoxyethoxy)ethyl Methacrylate and Oligo(ethylene glycol) Methacrylate. *Macromolecules* **2006**, *39* (2), 893-896.

115. Becer, C. R.; Hahn, S.; Fijten, M. W. M.; Thijs, H. M. L.; Hoogenboom, R.; Schubert, U. S. Libraries of methacrylic acid and oligo(ethylene glycol) methacrylate copolymers with LCST behavior. *J. Polym. Sci., Part A: Polym. Chem.* **2008**, *46* (21), 7138-7147.

116. Luzon, M.; Boyer, C.; Peinado, C.; Corrales, T.; Whittaker, M.; Tao, L.; Davis, T. P. Water-soluble, thermoresponsive, hyperbranched copolymers based on PEG-methacrylates: Synthesis, characterization, and LCST behavior. *J. Polym. Sci., Part A: Polym. Chem.* **2010**, *48* (13), 2783-2792.

117. Tian, H.-Y.; Yan, J.-J.; Wang, D.; Gu, C.; You, Y.-Z.; Chen, X.-S. Synthesis of Thermo-Responsive Polymers With Both Tunable UCST and LCST. *Macromol. Rapid Commun.* **2011**, *32* (8), 660-664.

118. Zhao, C.; Ma, Z.; Zhu, X. X. Rational design of thermoresponsive polymers in aqueous solutions: A thermodynamics map. *Prog. Polym. Sci.* **2019**, *90*, 269-291.

119. Jain, K.; Vedarajan, R.; Watanabe, M.; Ishikiriyama, M.; Matsumi, N. Tunable LCST behavior of poly(N-isopropylacrylamide/ionic liquid) copolymers. *Polym. Chem.* **2015**, *6* (38), 6819-6825.

120. Ksendzov, E. A.; Nikishau, P. A.; Zurina, I. M.; Presniakova, V. S.; Timashev, P.; Rochev, Y. A.; Kotova, S.; Kostjuk, S. V. Graft Copolymers of N-Isopropylacrylamide with Poly(d,l-lactide) or Poly(ε-caprolactone) Macromonomers: A Promising Class of Thermoresponsive Polymers with a Tunable LCST. *ACS Appl. Polym. Mater.* **2022**, *4* (2), 1344-1357.

121. Audureau, N.; Coumes, F.; Rieger, J.; Stoffelbach, F. Poly(N-cyanoethylacrylamide), a new thermoresponsive homopolymer presenting both LCST and UCST behavior in water. *Polym. Chem.* **2022**, *13* (8), 1075-1083.

122. Park, J.-S.; Kataoka, K. Comprehensive and Accurate Control of Thermosensitivity of Poly(2-alkyl-2-oxazoline)s via Well-Defined Gradient or Random Copolymerization. *Macromolecules* **2007**, *40* (10), 3599-3609.

123. Legros, C.; De Pauw-Gillet, M.-C.; Tam, K. C.; Taton, D.; Lecommandoux, S. Crystallisation-driven self-assembly of poly(2-isopropyl-2-oxazoline)-block-poly(2-methyl-2-oxazoline) above the LCST. *Soft Matter* **2015**, *11* (17), 3354-3359.

124. Foster, J. C.; Akar, I.; Grocott, M. C.; Pearce, A. K.; Mathers, R. T.; O'Reilly, R. K. 100th Anniversary of Macromolecular Science Viewpoint: The Role of Hydrophobicity in Polymer Phenomena. *ACS Macro Lett.* **2020**, *9* (11), 1700-1707.

125. Lynd, N. A.; Meuler, A. J.; Hillmyer, M. A. Polydispersity and block copolymer self-assembly. *Prog. Polym. Sci.* **2008**, *33* (9), 875-893.

126. Hansen, C. M. The universality of the solubility parameter. *Ind. Eng. Chem. Res.* **1969**, *8* (1), 2-11.

127. Barton, A. F. Solubility parameters. *Chem. Rev.* **1975**, *75* (6), 731-753.

128. Ghose, A. K.; Viswanadhan, V. N.; Wendoloski, J. J. Prediction of Hydrophobic (Lipophilic) Properties of Small Organic Molecules Using Fragmental Methods: An Analysis of ALOGP and CLOGP Methods. *J. Phys. Chem. A* **1998**, *102* (21), 3762-3772.

129. Venkatram, S.; Kim, C.; Chandrasekaran, A.; Ramprasad, R. Critical Assessment of the Hildebrand and Hansen Solubility Parameters for Polymers. *J. Chem. Inf. Model* **2019**, *59* (10), 4188-4194.

130. Xi, E.; Patel, A. J. The hydrophobic effect, and fluctuations: The long and the short of it. *Proc. Natl. Acad. Sci. U.S.A.* **2016**, *113* (17), 4549-4551.

131. Wu, X.; Lu, W.; Streacker, L. M.; Ashbaugh, H. S.; Ben-Amotz, D. Temperature-Dependent Hydrophobic Crossover Length Scale and Water Tetrahedral Order. *J. Phys. Chem. Lett.* **2018**, *9* (5), 1012-1017.

132. Athawale, M. V.; Goel, G.; Ghosh, T.; Truskett, T. M.; Garde, S. Effects of lengthscales and attractions on the collapse of hydrophobic polymers in water. *Proc. Natl. Acad. Sci. U.S.A.* **2007**, *104* (3), 733-738.

133. Long, J.; Hyder, M. N.; Huang, R. Y. M.; Chen, P. Thermodynamic modeling of contact angles on rough, heterogeneous surfaces. *Adv. Colloid Interface Sci.* **2005**, *118* (1), 173-190.

134. Guan, Y.; Ding, X.; Zhang, W.; Wan, G.; Peng, Y. Polytetrahydrofuran Amphiphilic Networks, 5. Synthesis and Swelling Behavior of Thermosensitive Poly(N-isopropylacrylamide)-l-polytetrahydrofuran Networks. *Macromol. Chem. Phys.* **2002**, *203* (5-6), 900-908.

135. Krokhin, O. V.; Spicer, V. Peptide Retention Standards and Hydrophobicity Indexes in Reversed-Phase High-Performance Liquid Chromatography of Peptides. *Anal. Chem.* **2009**, *81* (22), 9522-9530.

136. Reichardt, C. Solvatochromic dyes as solvent polarity indicators. *Chem. Rev.* **1994**, *94* (8), 2319-2358.

137. Hildebrand, J.; Scott, R. Solutions of nonelectrolytes. *Annu. Rev. Phys. Chem.* **1950**, *1* (1), 75-92.

138. Hansen, C. M. Hansen Solubility Parameters. **2007**.

139. Lipinski, C. A.; Lombardo, F.; Dominy, B. W.; Feeney, P. J. Experimental and computational approaches to estimate solubility and permeability in drug discovery and development settings. *Adv. Drug Del. Rev.* **1997**, *23* (1), 3-25.

140. Chandler, D. Interfaces and the driving force of hydrophobic assembly. *Nature* **2005**, *437* (7059), 640-647.

141. Lum, K.; Chandler, D.; Weeks, J. D. Hydrophobicity at Small and Large Length Scales. *J. Phys. Chem. B* **1999**, *103* (22), 4570-4577.

142. Yildirim, E.; Dakshinamoorthy, D.; Peretic, M. J.; Pasquinelli, M. A.; Mathers, R. T. Synthetic design of polyester electrolytes guided by hydrophobicity calculations. *Macromolecules* **2016**, *49* (20), 7868-7876.

143. Dharmaratne, N. U.; Jouaneh, T. M. M.; Kiesewetter, M. K.; Mathers, R. T. Quantitative measurements of polymer hydrophobicity based on functional group identity and oligomer length. *Macromolecules* **2018**, *51* (21), 8461-8468.

144. Min, K.; Cuiffi, J. D.; Mathers, R. T. Ranking environmental degradation trends of plastic marine debris based on physical properties and molecular structure. *Nat. Commun* **2020**, *11* (1), 727.

145. Varlas, S.; Foster, J. C.; Arkinstall, L. A.; Jones, J. R.; Keogh, R.; Mathers, R. T.; O'Reilly, R. K. Predicting Monomers for Use in Aqueous Ring-Opening Metathesis Polymerization-Induced Self-Assembly. *ACS Macro Lett.* **2019**, *8* (4), 466-472.

Chapter 2. Grafting Density Governs the Thermoresponsive Behavior of P(OEGMA-*co*-RMA) copolymers

2.1. Manuscript details and overview

Title: Grafting Density Governs the Thermoresponsive Behavior of P(OEGMA-*co*-RMA) Statistical Copolymers

Authors: **Irem Akar**,[†] Robert Keogh, [†,‡] Lewis D. Blackman, [‡] Jeffrey C. Foster,[*,†] Robert. T. Mathers[*,§] and Rachel K. O'Reilly[*,†]

Affiliations: [†]School of Chemistry, University of Birmingham, Edgbaston, Birmingham B15 2TT, United Kingdom

[‡]Department of Chemistry, University of Warwick, Gibbet Hill Road, Coventry CV4 7AL, United Kingdom

[§]Department of Chemistry, Pennsylvania State University, New Kensington Pennsylvania 15068, United States

Journal: ACS Macro Letters

Year: 2020

Volume: 9

Page numbers: 1149–1154

DOI: 10.1021/acsmacrolett.0c00461

Submitted: 18 June 2020 **Published:** 27 July 2020

Copyright statement: "*This is an open access article published under an ACS AuthorChoice License, which permits copying and redistribution of the article or any adaptations for non-commercial purposes*." Copyright 2020 American Chemical Society.

Permissions: This article and its supporting information are available on the ACS Publications website at https://pubs.acs.org/doi/full/10.1021/acsmacrolett.0c00461. Further permissions related to the material excerpted should be directed to the ACS Publications Support.

Co-author contributions: Dr Robert Keogh aided with the synthesis and characterization of the polymers for the project, in addition to providing technical and synthetic advice. Dr Lewis D. Blackman provided synthetic advice, Dr Jeffrey C. Foster provided technical and synthetic advice, performed the statistical analysis, and edited the manuscript. Prof. Robert T. Mathers performed computational calculation of hydrophobicity values. Prof. Rachel O'Reilly supervised the project, provided guidance, and edited the manuscript.

Overview: The objective of this chapter was to investigate the relationship between hydrophobicity and thermoresponsive behavior of copolymer brushes with the aim of developing a predictive tool. A specific thermoresponsive behavior known as lower critical solution temperature (LCST), and copolymerization is one of a few methods to tune the LCST behavior, where a thermoresponsive monomer is diluted with hydrophobic or hydrophilic comonomers to increase or decrease the LCST. However, the copolymerization method to tune the LCST remains a challenge due to limited knowledge with respect to range of monomers that can be copolymerized

to create polymers with LCST behavior or lack of understanding of the polymer solution behavior and its effect on the LCST.

A recent computational method was developed by our group which correlated polymer properties like solubility or self-assembly behavior to its hydrophobicity. We aimed to expand use of this method to explain LCST phenomena by correlating copolymer hydrophobicity to thermal transition temperatures (*i.e.* cloud point temperature, T_{CP}). To do this, we prepared a library of copolymers based on hydrophilic brushy oligo(ethylene glycol) monomethyl ether methacrylate (OEGMA) and various hydrophobic alkyl methacrylates (methyl, ethyl, *n*-butyl, hexyl, and lauryl methacrylate) *via* RAFT polymerization. The hydrophobic composition in each series was diversified with the aim of observing the effect of alkyl chain length and initial feed ratios. LCST behavior of the copolymers was determined using T_{CP} as a proxy for LCST. T_{CP} of the copolymers was measured by using UV-Vis and NanoDSC as complementary methods. On the other hand, copolymer hydrophobicity was determined by calculating a hydrophobicity parameter, the surface area normalized partition coefficients, LogP_{oct}/SA. Finally, T_{CP} of the copolymers were attempted to correlate their LogP_{oct}/SA. Even though the inverse relationship between these two parameters was observed for individual copolymer series, no general correlation could be drawn.

Further statistical study was done to investigate determinants of T_{CP} by employing different polymer parameters such as MW, polymer DP, polydispersity, and comonomer mol% and weight%. This study revealed that the mol% of the hydrophobic comonomers is the strongest influencer of the copolymer $T_{CP.}$ This result was validated by applying the same statistical study to the OEGMA based copolymers reported in the literature, which revealed a similar correlation between the T_{CP} and LogP_{oct}/SA.

The information gained from our experimental and literature data suggested that grafting density is the strongest determinant of T_{CP} for brushy OEGMA copolymers. We believe that this principle will allow chemists to design new functional thermoresponsive materials by simply altering the grafting density as the T_{CP} of copolymers is not dependent on comonomer chemistry.

This is an open access article published under a Creative Commons Attribution (CC-BY) License, which permits unrestricted use, distribution and reproduction in any medium, provided the author and source are cited.

ACS AUTHORCHOICE

ACS Macro Letters

pubs.acs.org/macroletters Letter

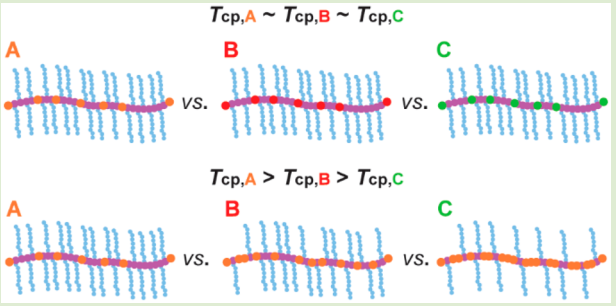
Grafting Density Governs the Thermoresponsive Behavior of P(OEGMA-*co*-RMA) Statistical Copolymers

Irem Akar, Robert Keogh, Lewis D. Blackman, Jeffrey C. Foster,* Robert T. Mathers,* and Rachel K. O'Reilly*

Cite This: *ACS Macro Lett.* 2020, 9, 1149–1154 Read Online

ACCESS | Metrics & More | Article Recommendations | Supporting Information

ABSTRACT: Thermoresponsive copolymers that exhibit a lower critical solution temperature (LCST) have been exploited to prepare stimuli-responsive materials for a broad range of applications. It is well understood that the LCST of such copolymers can be controlled by tuning molecular weight or through copolymerization of two known thermoresponsive monomers. However, no general methodology has been established to relate polymer properties to their temperature response in solution. Herein, we sought to develop a predictive relationship between polymer hydrophobicity and cloud point temperature (T_{CP}). A series of statistical copolymers were synthesized based on hydrophilic oligoethylene glycol monomethyl ether methacrylate (OEGMA) and hydrophobic alkyl methacrylate monomers and their hydrophobicity was compared using surface area-normalized partition coefficients (log P_{oct}/SA). However, while some insight was gained by comparing T_{CP} and hydrophobicity values, further statistical analysis on both experimental and literature data showed that the molar percentage of comonomer (i.e., grafting density) was the strongest influencer of T_{CP}, regardless of the comonomer used. The lack of dependence of T_{CP} on comonomer chemistry implies that a broad range of functional, thermoresponsive materials can be prepared based on OEGMA by simply tuning grafting density.

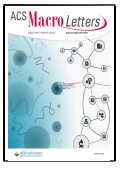


Downloaded via 176.41.231.36 on January 10, 2023 at 19:48:49 (UTC).
See https://pubs.acs.org/sharingguidelines for options on how to legitimately share published articles.

The motivation to design polymers to respond to environmental triggers such as light, ultrasound, pH, redox state, or temperature has led to significant advances in the field of stimuli-responsive materials.[1−5] These developments have underwritten their application as biosensors,[6] coating materials,[7] or drug delivery systems.[8] Temperature has been most widely studied because of the simplicity of its external application and the availability of methods for tuning polymer thermoresponsiveness.[9] Such thermoresponsive polymers typically display two distinct behaviors in solution, known as the upper critical solution temperature (UCST) and lower critical solution temperature (LCST), representing the critical points above and below which the polymer and solvent are completely miscible.[10] Polymers that exhibit an LCST transition are soluble below a critical temperature, above which they undergo a phase transition and demix as a result of increased entropy (for further details, see the following representative references).[8,11] The LCST transition is particularly attractive for biological applications due to the relatively low temperatures required to elicit response.[12]

There are several ways to control the LCST of a polymer solution and thus achieve a phase transition at a desired temperature.[13−18] The LCST can be tuned via changing polymer molecular weight (MW) or solution concentration or by varying the composition of a copolymer based on two or more monomers (i.e., P(oligoethylene glycol monomethyl ether methacrylate-*co*-diethylene glycol methacrylate), P(OEGMA-*co*-DEGMA), Figure 1).[19−22] For example, Gibson and co-workers studied the thermoresponsive behavior of a series of P(*N*-vinylpiperidone) homopolymers with molecular weights ranging from 4.5 to 83 kDa. The authors showed that the cloud point (T_{CP}) of P(*N*-vinylpiperidone) decreased from 99 to 67 °C with increasing polymer MW.[14] Lecommandoux and co-workers investigated the possibility of manipulating the LCST through copolymerization of 2-isopropyl-2-oxazoline (hydrophobic) with 2-methyl-2-oxazoline (hydrophilic). The T_{CP} of the resulting copolymer increased by 21 °C compared with the P(2-isopropyl-2-oxazoline) homopolymer due to an overall increase in hydrophilicity.[23] However, the scope of monomers known to yield LCST-responsive materials upon copolymerization is currently limited, complicating the design of new and functional polymers with bespoke transition temperatures.

Received: June 18, 2020
Accepted: July 22, 2020
Published: July 27, 2020



ACS Publications © 2020 American Chemical Society

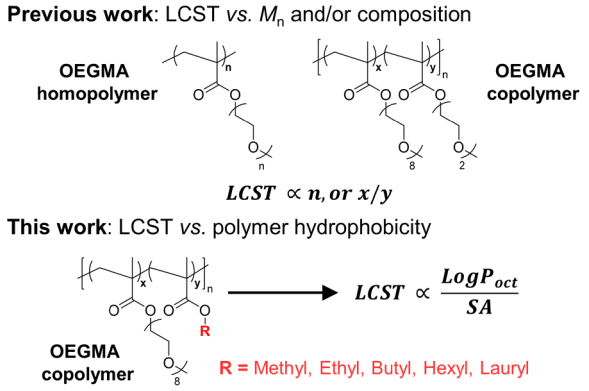


Figure 1. Previous studies have focused on the influence of MW or composition on LCST. Herein, we investigate how hydrophobicity influences thermoresponsive behavior.

We have had recent success correlating polymer properties such as solubility and self-assembly behavior to descriptors of their hydrophobicity. In particular, the classification of small molecule hydrophobicity using octanol−water partition coefficients (log P_{oct}) has proven exceptionally successful when leveraged to describe polymer phenomena. For example, we demonstrated that surface area-normalized log P_{oct} (log P_{oct}/SA) values provided predictive information to guide the selection of corona- and core-forming monomers for polymerization-induced self-assembly (PISA) using either reversible addition−fragmentation chain transfer (RAFT) polymerization or ring-opening metathesis polymerization (ROMP).[24,25] Log P_{oct}/SA was also used effectively as a tool to optimize solvent selection for crystallization-driven self-assembly (CDSA) of P(L-lactic acid) (PLLA)-based block copolymers.[26] In order to further benefit from the advantages of using this computational tool to dramatically reduce experimental workload, we postulated that it could be exploited to relate polymer chemical structure to T_{CP}.

Herein, we synthesized a series of copolymers of OEGMA and various alkyl methacrylates (RMA, R = methyl, ethyl, *n*-butyl, *n*-hexyl, and *n*-dodecyl (lauryl)) and studied their LCST response. Polymer cloud point temperature (T_{CP}), the temperature at which polymers undergo a solubility-to-insolubility transition,[14] was used as a proxy for the LCST. We then attempted to correlate T_{CP} to copolymer hydrophobicity via log P_{oct}/SA to predict T_{CP} of new polymers. Surprisingly, we found log P_{oct}/SA to be a secondary descriptor of T_{CP} for OEGMA copolymers compared to mol % of comonomer. Indeed, copolymer molar composition (which can be viewed through the lens of grafting density) correlated strongly for both copolymers synthesized in this study and for related copolymers identified from previous literature reports. These discoveries highlight the importance of copolymer topology in determining thermal properties and suggest a route to prepare a wide variety of functional, brush-like copolymers with precisely defined T_{CP} values.

In the vast majority of studies regarding the manipulation of the LCST through copolymerization, two monomers known to produce homopolymers with LCSTs are copolymerized to produce statistical copolymers possessing intermediate LCSTs (Figure 1). Luzon, Ramirez-Jiménez, Porsch, Bebis, and Lutz have all reported thermoresponsive copolymers based on OEGMA and DEGMA, where T_{CP} decreased as a linear function of the molar quantity of DEGMA.[20,27−30] While numerous studies have been carried out involving the copolymerization of these two monomers, no consensus has been reached regarding the mechanisms underlying the capability to tune the LCST through copolymerization. Compared with their homopolymers, copolymers of the same degree of polymerization (DP) containing two or more thermoresponsive monomers can have different MW, hydrophobicity, surface area, radius of gyration, and so on. It is unclear if a single factor dominates the LCST or a combination of multiple factors. Moreover, parameters that contribute to determining the LCST in one system may not be general for others.

To isolate influence of copolymer hydrophobicity upon T_{CP}, we prepared a series of copolymers of OEGMA and various alkyl methacrylates (RMA), varying the composition within each series by changing the hydrophobic molar composition in order to observe the effect of both alkyl chain length (hydrophobicity) and initial feed ratio. Alkyl methacrylates (e.g., MMA, *n*BMA, LMA) were selected as comonomers due to their commercial availability, compatibility with polymerization conditions, and simple hydrocarbon side chain structure. Overall copolymer MW and composition range (i.e., targeted hydrophobic mol %) were maintained as consistently as possible across each series.

The copolymers were prepared via reversible addition−fragmentation chain transfer (RAFT) polymerization in 1,4-dioxane for 6−8 h until targeted DPs were reached (Figure 2A). The final molar and mass composition of the purified copolymers were determined using ^{1}H NMR spectroscopy by relative integration of resonances corresponding to each monomer (Figures 2B and S16−S19). Kinetic analysis was conducted to confirm the statistical nature of the copolymerizations. As shown in Figure 2C (and Figures S12−S15), both OEGMA and RMA monomers were consumed at an approximately equal rate. Molecular weight distributions (MWDs) for the P(OEGMA-*co*-RMA) copolymers were determined using size-exclusion chromatography (SEC). As shown in Figure 2D (and Figures S12−S15), copolymers were obtained with narrow and symmetrical MWDs. Variations in number-average MW (M_n) and dispersity ($Đ_M$) values were determined by calculating coefficients of variance. Using this measure, M_n varied by only 17% across the entire data set, while $Đ_M$ varied by 5% with all values <1.40.

Turbidity measurements were conducted using UV−vis spectroscopy in order to measure the T_{CP} of the copolymers. Changes in the percentage transmittance were recorded at λ = 550 nm within the temperature range of 20 to 93 °C. Temperature points that corresponded to 50% transmittance values were taken as the T_{CP} of polymers (see Supporting Information for the detailed method). In general, T_{CP} decreased for P(OEGMA-*co*-RMA) copolymers with increasing RMA content (Figure 2E). This inverse relationship was further corroborated by microcalorimetry (μDSC), which measures changes in heat flow as a function of temperature for dilute liquid samples. For these data, the maximum point of the first derivative of the heating traces were chosen as the T_{CP} values. Figure 2F shows a similar decrease in T_{CP} as the hydrophobic content of the copolymers increased. Good agreement between the T_{CP} values obtained from both measurements confirmed their consistency. A similar analysis was performed for the other copolymer series (see Supporting Information).

https://dx.doi.org/10.1021/acsmacrolett.0c00461
ACS Macro Lett. 2020, 9, 1149−1154

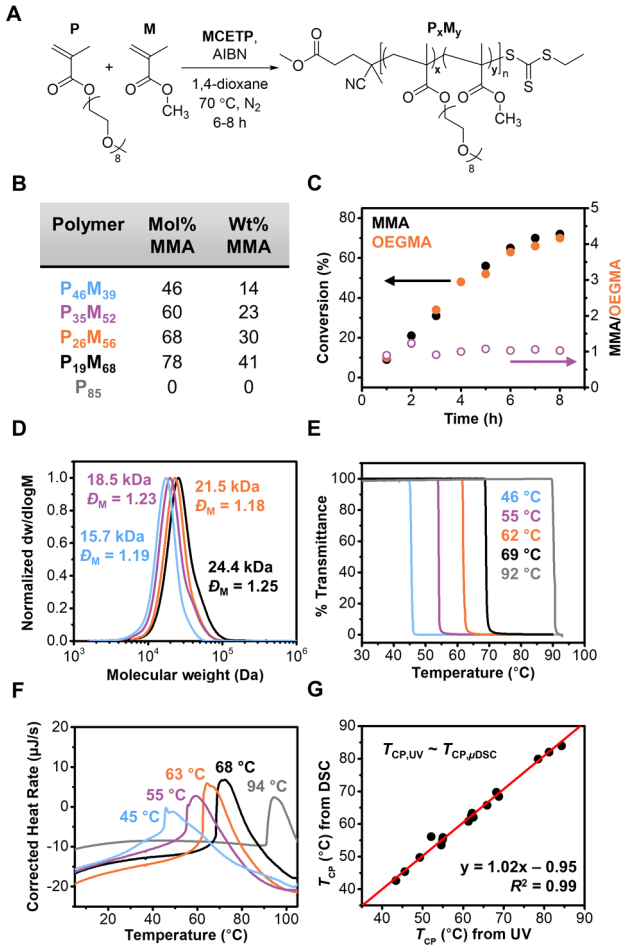


Figure 2. (A) Representative synthetic scheme for the preparation of P(OEGMA-*co*-RMA) statistical copolymers. MMA is used as the comonomer in this example. (B) Composition of P(OEGMA-*co*-MMA) copolymers, as determined by ^{1}H NMR spectroscopy. (C) Kinetics of monomer conversion during the synthesis of P(OEGMA-*co*-MMA) with an initial monomer molar feed ratio of 1:1 OEGMA/MMA. (D) Normalized SEC molecular weight distributions for the P(OEGMA-*co*-MMA) series (eluent: $CHCl_3$ + 0.5 v/v% NEt_3, PS standards). (E) Percent transmittance as a function of temperature for the P(OEGMA-*co*-MMA) copolymers dissolved in H_2O at 5 mg/mL as measured by UV−vis spectroscopy (λ = 550 nm, 20−93 °C, 1 °C min^{-1}). (F) μDSC thermograms for the P(OEGMA-*co*-MMA) copolymers (3 atm, 0−115 °C, 0.5 °C min^{-1}). (G) Comparison of T_{CP} values measured by UV−vis spectroscopy and μDSC. The solid red line represents a linear fit of the data. The colors in (D), (E), and (F) correspond to those assigned to the various copolymers in (B).

We next sought to understand the relationship between measured T_{CP} values and copolymer hydrophobicity.

Log P_{oct}, which describes the partitioning of a substance between octanol and water and reflects transfer free energy, was used as the means of quantifying and comparing hydrophobicity.[31−33] Toward this end, we calculated log P_{oct} values for short oligomers as proxies for the synthesized copolymers and normalized them with surface areas of optimized conformations using Molecular Dynamics (MD) simulations (see Supporting Information for the detailed model). We then attempted to relate these calculated log P_{oct}/SA values to measured T_{CP} values.

As shown in Figure 3A, log P_{oct}/SA increased with increasing RMA content, consistent with the established relationship

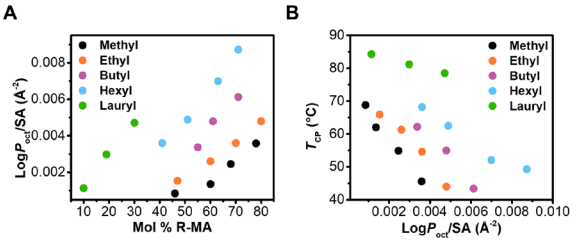


Figure 3. (A) Calculated log P_{oct}/SA values for various copolymer oligomers as a function of the mol % of hydrophobic comonomer. (B) Plot of T_{CP} as measured by UV−vis spectroscopy vs log P_{oct}/SA for the same copolymer series.

between hydrophobicity and log *P*. Comonomers with longer alkyl chains had a more dramatic impact on log P_{oct}/SA than those with shorter ones and thus produced relationships with relatively steeper slopes. Figure 3B shows the relationship between T_{CP} and log P_{oct}/SA. Here, inverse linear relationships were observed for each series, confirming our hypothesis that increased copolymer hydrophobicity, resulting from increasing the molar ratio of hydrophobic comonomer in the P(OEGMA-*co*-RMA) copolymers, acted to decrease T_{CP}. We also hypothesize log P_{oct}/SA values reflect localized degrees of hydrophobicity and the size of the oligomeric models represents a length scale that may not extend to longer range topological influences. As such, each series possessed a unique slope that was related to the alkyl chain length of the comonomer and thus no general correlation could be drawn between copolymer log P_{oct}/SA and T_{CP}.

The complexity of the LCST process was further reinforced by investigating the influence of hydrophobicity on the heat of phase separation (ΔH) calculated from the μDSC data.[34] As shown in Figure S22, weak correlations and lack of a general linear relationship were noted between log P_{oct}/SA or polymer composition and ΔH. These data indicate that hydrophobicity contributes to the LCST for statistical copolymers. However, they also imply that a picture of hydrophobicity based on transfer free energy (log *P*) and conformational insight (SA) only partially captures the LCST process for brush-like copolymers and that other factors must be considered.

The mixing of polymer molecules with H_2O, described by ΔG_{mix}, represents a balance of the enthalpically favorable binding of H_2O molecules ($\Delta H_{mix} > 0$) and their increased ordering upon binding ($\Delta S_{mix} > 0$). The LCST phenomenon is thus understood as a disruption in the balance of these contributors at higher temperatures, where the entropic term dominates.[10,35] Based on this argument and the fact that log *P* represents a transfer free energy term,[36] it was somewhat surprising that a general relationship could not be drawn between copolymer hydrophobicity and T_{CP}, as we anticipated ΔH_{mix} to be directly relatable to hydrophobicity. To better understand determinants of T_{CP}, we searched for relationships involving other polymer descriptors such as molar (mol % RMA) and mass (wt % RMA) composition, M_n, $Đ_M$, and DP.

Figure S1 shows a scatterplot matrix highlighting the intercorrelations between descriptors or correlations with the response variable T_{CP}. It should be noted that data from all of the copolymer series were combined prior to analysis. From these data, relationships were apparent between T_{CP} and each of the descriptors, with the molar and mass compositions exhibiting the strongest correlations. Intriguingly, this initial visualization seemed to imply that the identity (chemistry) of

https://dx.doi.org/10.1021/acsmacrolett.0c00461
ACS Macro Lett. 2020, 9, 1149−1154

the comonomer was less important in determining T_{CP} than was its quantity in the copolymers. Single and stepwise multivariable linear regression analyses were then applied to the collected data set to develop a quantitative structure−activity relationship (QSAR) model (see SI for full discussion). The model was trained on experimental data using stratified k-fold data sets. An initial optimized model based on two descriptors, the mol % and wt % RMA comonomer, was obtained using either R^2 or RMSE as the selection parameter. However, this model was deemed inappropriate due to concerns regarding the influence of collinearity between these parameters on model predictive power for future data sets. Instead, a simplified model using only the mol % of comonomer was adopted, allowing for a simple prediction of T_{CP} based on copolymer composition.

We then sought to validate this simple model against T_{CP} data for OEGMA copolymers in the literature. A total of 94 T_{CP} values for OEGMA copolymers with two different side chain lengths were extracted from about 20 reports.[37] These data were selected based on the following criteria: (1) they pertained to $OEGMA_{500/300}$ statistical copolymers; (2) they included T_{CP} measurements obtained via UV−vis spectroscopy on dilute polymer solutions (i.e., ≤5 mg mL^{-1}) in H_2O; (3) the comonomers were ideally simple in structure and/or commercially available; and (4) the comonomers did not possess ionizable groups that would introduce additional stimuli-responsiveness. Comonomers included diethylene glycol methyl ether methacrylate (DEGMA), methyl methacrylate (MMA), *N*-isopropylacrylamide, pentafluorostyrene (PFS), and others (Figure 4A). Again, the data was visualized

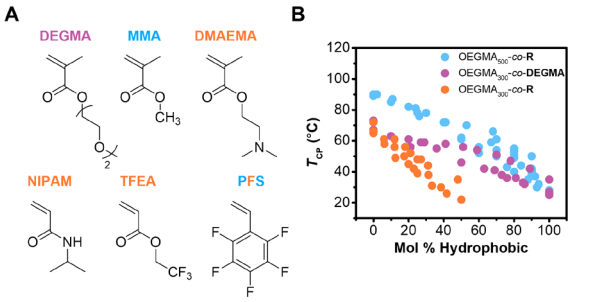


Figure 4. (A) Example comonomers present in P(OEGMA-*co*-R) copolymers for which T_{CP} values have been measured. (B) Plot of T_{CP} as a function of the molar quantity of comonomer constructed using data collected from literature sources.

using a scatterplot matrix (Figure S4), revealing a similarly strong correlation between T_{CP} and comonomer molar composition. As shown in Figure 4B, linear relationships could generally be drawn between T_{CP} and mol %, with two clusters similar in slope that corresponded to OEGMA copolymers with different OEG side chain lengths. $OEGMA_{300}$-*co*-DEGMA copolymers exhibited exceptional behavior, sharing slopes with both clusters depending on composition. Interestingly, the data collected from the literature for $OEGMA_{500}$ copolymers agreed strongly with our experimental observations (Figure 5A). The same model describing the relationship between T_{CP} and mol % was used to evaluate these literature data. As shown in Figure 5B, this model was reasonably successful in predicting the literature T_{CP} values. This further supported the hypothesis that comonomer chemistry plays a limited role in determining

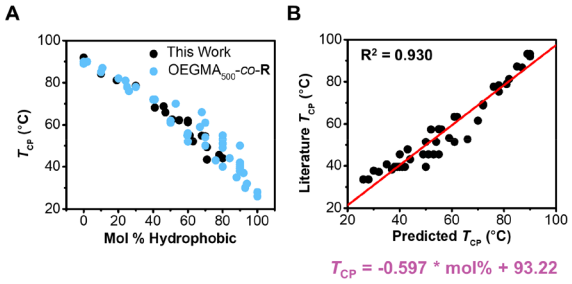


Figure 5. (A) Plot of T_{CP} vs the molar quantity of comonomer. Data from P($OEGMA_{500}$-*co*-R) copolymers obtained from literature sources is overlaid with experimental data from this report. (B) Comparison between literature T_{CP} values and those predicted from molar compositions. The solid red line represents a linear fit of these data.

T_{CP} for OEGMA copolymers. Given the "brushy" nature of poly(OEGMA), an increase in comonomer molar quantity can be viewed as a decrease in grafting density. A simple model relating T_{CP} to grafting density may be generally appropriate for other brush copolymers.

To conclude, we report the synthesis of a series of P(OEGMA-*co*-RMA) copolymers via copolymerization of OEGMA and different alkyl methacrylate monomers. LCST behavior of the brush-like copolymers was investigated by using complementary methods. We then attempted to relate T_{CP} to hydrophobicity based on a thermodynamic perspective (log *P*) and a structural parameter (SA); however, the multifaceted nature of T_{CP} complicated a predictive model. Instead, linear and stepwise regression analysis using a variety of predictors revealed that T_{CP} appeared to depend most significantly on the mol % of comonomer, suggesting that grafting density is the most important determinant of the LCST for OEGMA brush copolymers. Our analysis of both experimental and literature data implies that a wide variety of functional copolymers can be prepared using this guiding principle, as the identity of the comonomer in P(OEGMA-*co*-R) copolymers does not appear to influence T_{CP}.

■ ASSOCIATED CONTENT

Supporting Information

The Supporting Information is available free of charge at https://pubs.acs.org/doi/10.1021/acsmacrolett.0c00461.

Materials, characterization techniques, experimental procedures, and additional data (statistical analysis, SEC, ^{1}H NMR, μDSC, and UV−vis spectra) (PDF)

■ AUTHOR INFORMATION

Corresponding Authors

Robert T. Mathers − *Department of Chemistry, Pennsylvania State University, New Kensington, Pennsylvania 15068, United States;* orcid.org/0000-0002-0503-4571; Email: rtm11@psu.edu

Rachel K. O'Reilly − *School of Chemistry, University of Birmingham, Birmingham B15 2TT, United Kingdom;* orcid.org/0000-0002-1043-7172; Email: r.oreilly@bham.ac.uk

Jeffrey C. Foster − *School of Chemistry, University of Birmingham, Birmingham B15 2TT, United Kingdom;* Email: fosterjc@bham.ac.uk

https://dx.doi.org/10.1021/acsmacrolett.0c00461
ACS Macro Lett. 2020, 9, 1149−1154

Authors

Irem Akar − *School of Chemistry, University of Birmingham, Birmingham B15 2TT, United Kingdom*

Robert Keogh − *School of Chemistry, University of Birmingham, Birmingham B15 2TT, United Kingdom; Department of Chemistry, University of Warwick, Coventry CV4 7AL, United Kingdom*

Lewis D. Blackman − *Department of Chemistry, University of Warwick, Coventry CV4 7AL, United Kingdom;* orcid.org/0000-0002-6113-0584

Complete contact information is available at: https://pubs.acs.org/10.1021/acsmacrolett.0c00461

Author Contributions

The manuscript was written through contributions of all authors.

Notes

The authors declare no competing financial interest.

■ ACKNOWLEDGMENTS

This work is supported by the Ministry of Turkish Education EPSRC (EP/S00338X/1)), ERC Consolidator Grant (No. 615142), and the University of Birmingham.

■ REFERENCES

(1) Gibson, M. I.; O'Reilly, R. K. To aggregate, or not to aggregate? considerations in the design and application of polymeric thermally-responsive nanoparticles. *Chem. Soc. Rev.* **2013**, *42*, 7204−7213.

(2) Huo, M.; Yuan, J.; Tao, L.; Wei, Y. Redox-responsive polymers for drug delivery: from molecular design to applications. *Polym. Chem.* **2014**, *5*, 1519−1528.

(3) Manouras, T.; Vamvakaki, M. Field responsive materials: photo-, electro-, magnetic- and ultrasound-sensitive polymers. *Polym. Chem.* **2017**, *8*, 74−96.

(4) Dai, S.; Ravi, P.; Tam, K. C. pH-Responsive polymers: synthesis, properties and applications. *Soft Matter* **2008**, *4*, 435−449.

(5) Schumers, J.-M.; Fustin, C.-A.; Gohy, J.-F. Light-Responsive Block Copolymers. *Macromol. Rapid Commun.* **2010**, *31*, 1588−1607.

(6) Cabane, E.; Zhang, X.; Langowska, K.; Palivan, C. G.; Meier, W. Stimuli-Responsive Polymers and Their Applications in Nanomedicine. *Biointerphases* **2012**, *7*, 9.

(7) Zhai, L. Stimuli-responsive polymer films. *Chem. Soc. Rev.* **2013**, *42*, 7148−7160.

(8) Bawa, P.; Pillay, V.; Choonara, Y. E.; du Toit, L. C. Stimuli-responsive polymers and their applications in drug delivery. *Biomed. Mater.* **2009**, *4*, 022001.

(9) Hoogenboom, R. 2 - Temperature-responsive polymers: properties, synthesis and applications. In *Smart Polymers and their Applications*; Aguilar, M. R., San Román, J., Eds.; Woodhead Publishing, 2014; pp 15−44.

(10) Zhang, Q.; Weber, C.; Schubert, U. S.; Hoogenboom, R. Thermoresponsive polymers with lower critical solution temperature: from fundamental aspects and measuring techniques to recommended turbidimetry conditions. *Mater. Horiz.* **2017**, *4*, 109−116.

(11) Bromberg, L. E.; Ron, E. S. Temperature-responsive gels and thermogelling polymer matrices for protein and peptide delivery. *Adv. Drug Delivery Rev.* **1998**, *31*, 197−221.

(12) Roy, D.; Brooks, W. L. A.; Sumerlin, B. S. New directions in thermoresponsive polymers. *Chem. Soc. Rev.* **2013**, *42*, 7214−7243.

(13) Kempe, K.; Neuwirth, T.; Czaplewska, J.; Gottschaldt, M.; Hoogenboom, R.; Schubert, U. S. Poly(2-oxazoline) glycopolymers with tunable LCST behavior. *Polym. Chem.* **2011**, *2*, 1737−1743.

(14) Ieong, N. S.; Hasan, M.; Phillips, D. J.; Saaka, Y.; O'Reilly, R. K.; Gibson, M. I. Polymers with molecular weight dependent LCSTs are essential for cooperative behaviour. *Polym. Chem.* **2012**, *3*, 794−799.

(15) Glassner, M.; Lava, K.; de la Rosa, V. R.; Hoogenboom, R. Tuning the LCST of poly(2-cyclopropyl-2-oxazoline) via gradient copolymerization with 2-ethyl-2-oxazoline. *J. Polym. Sci., Part A: Polym. Chem.* **2014**, *52*, 3118−3122.

(16) Yu, G.; Zhou, J.; Chi, X. Pillar[10]arene-Based Size-Selective Host−Guest Complexation and Its Application in Tuning the LCST Behavior of a Thermoresponsive Polymer. *Macromol. Rapid Commun.* **2015**, *36*, 23−30.

(17) Keogh, R.; Blackman, L. D.; Foster, J. C.; Varlas, S.; O'Reilly, R. K. The Importance of Cooperativity in Polymer Blending: Toward Controlling the Thermoresponsive Behavior of Blended Block Copolymer Micelles. *Macromol. Rapid Commun.* **2020**, *41*, 1900599.

(18) Ortiz de Solorzano, I.; Bejagam, K. K.; An, Y.; Singh, S. K.; Deshmukh, S. A. Solvation dynamics of N-substituted acrylamide polymers and the importance for phase transition behavior. *Soft Matter* **2020**, *16*, 1582−1593.

(19) Hoogenboom, R.; Thijs, H. M. L.; Jochems, M. J. H. C.; van Lankvelt, B. M.; Fijten, M. W. M.; Schubert, U. S. Tuning the LCST of poly(2-oxazoline)s by varying composition and molecular weight: alternatives to poly(N-isopropylacrylamide)? *Chem. Commun.* **2008**, 5758−5760.

(20) Ramírez-Jiménez, A.; Montoya-Villegas, K. A.; Licea-Claverie, A.; Gónzalez-Ayón, M. A. Tunable Thermo-Responsive Copolymers from DEGMA and OEGMA Synthesized by RAFT Polymerization and the Effect of the Concentration and Saline Phosphate Buffer on its Phase Transition. *Polymers* **2019**, *11*, 1657.

(21) Uğuzdoğan, E.; Çamli, T.; Kabasakal, O. S.; Patir, S.; Öztürk, E.; Denkbaş, E. B.; Tuncel, A. A new temperature-sensitive polymer: Poly(ethoxypropylacrylamide). *Eur. Polym. J.* **2005**, *41*, 2142−2149.

(22) Ward, M. A.; Georgiou, T. K. Thermoresponsive triblock copolymers based on methacrylate monomers: effect of molecular weight and composition. *Soft Matter* **2012**, *8*, 2737−2745.

(23) Legros, C.; De Pauw-Gillet, M.-C.; Tam, K. C.; Taton, D.; Lecommandoux, S. Crystallisation-driven self-assembly of poly(2-isopropyl-2-oxazoline)-block-poly(2-methyl-2-oxazoline) above the LCST. *Soft Matter* **2015**, *11*, 3354−3359.

(24) Foster, J. C.; Varlas, S.; Couturaud, B.; Jones, J. R.; Keogh, R.; Mathers, R. T.; O'Reilly, R. K. Predicting Monomers for Use in Polymerization-Induced Self-Assembly. *Angew. Chem., Int. Ed.* **2018**, *57*, 15733−15737.

(25) Varlas, S.; Foster, J. C.; Arkinstall, L. A.; Jones, J. R.; Keogh, R.; Mathers, R. T.; O'Reilly, R. K. Predicting Monomers for Use in Aqueous Ring-Opening Metathesis Polymerization-Induced Self-Assembly. *ACS Macro Lett.* **2019**, *8*, 466−472.

(26) Inam, M.; Cambridge, G.; Pitto-Barry, A.; Laker, Z. P. L.; Wilson, N. R.; Mathers, R. T.; Dove, A. P.; O'Reilly, R. K. 1D vs. 2D shape selectivity in the crystallization-driven self-assembly of polylactide block copolymers. *Chem. Sci.* **2017**, *8*, 4223−4230.

(27) Bebis, K.; Jones, M. W.; Haddleton, D. M.; Gibson, M. I. Thermoresponsive behaviour of poly[(oligo(ethyleneglycol methacrylate)]s and their protein conjugates: importance of concentration and solvent system. *Polym. Chem.* **2011**, *2*, 975−982.

(28) Lutz, J.-F.; Akdemir, Ö.; Hoth, A. Point by Point Comparison of Two Thermosensitive Polymers Exhibiting a Similar LCST: Is the Age of Poly(NIPAM) Over? *J. Am. Chem. Soc.* **2006**, *128*, 13046−13047.

(29) Luzon, M.; Corrales, T. Thermal studies and chromium removal efficiency of thermoresponsive hyperbranched copolymers based on PEG-methacrylates. *J. Therm. Anal. Calorim.* **2014**, *116*, 401−409.

(30) Porsch, C.; Hansson, S.; Nordgren, N.; Malmström, E. Thermo-responsive cellulose-based architectures: tailoring LCST using poly(ethylene glycol) methacrylates. *Polym. Chem.* **2011**, *2*, 1114−1123.

(31) Leo, A.; Hansch, C.; Elkins, D. Partition coefficients and their uses. *Chem. Rev.* **1971**, *71*, 525−616.

(32) Yildirim, E.; Dakshinamoorthy, D.; Peretic, M. J.; Pasquinelli, M. A.; Mathers, R. T. Synthetic Design of Polyester Electrolytes

Guided by Hydrophobicity Calculations. *Macromolecules* **2016**, *49*, 7868−7876.
(33) He, Y.; Eloi, J.-C.; Harniman, R. L.; Richardson, R. M.; Whittell, G. R.; Mathers, R. T.; Dove, A. P.; O'Reilly, R. K.; Manners, I. Uniform Biodegradable Fiber-Like Micelles and Block Comicelles via "Living" Crystallization-Driven Self-Assembly of Poly(l-lactide) Block Copolymers: The Importance of Reducing Unimer Self-Nucleation via Hydrogen Bond Disruption. *J. Am. Chem. Soc.* **2019**, *141*, 19088−19098.
(34) Feil, H.; Bae, Y. H.; Feijen, J.; Kim, S. W. Effect of comonomer hydrophilicity and ionization on the lower critical solution temperature of N-isopropylacrylamide copolymers. *Macromolecules* **1993**, *26*, 2496−2500.
(35) Smith, G. D.; Bedrov, D. Roles of Enthalpy, Entropy, and Hydrogen Bonding in the Lower Critical Solution Temperature Behavior of Poly(ethylene oxide)/Water Solutions. *J. Phys. Chem. B* **2003**, *107*, 3095−3097.
(36) Bannan, C. C.; Calabró, G.; Kyu, D. Y.; Mobley, D. L. Calculating Partition Coefficients of Small Molecules in Octanol/Water and Cyclohexane/Water. *J. Chem. Theory Comput.* **2016**, *12*, 4015−4024.
(37) Tabulated data and their sources can be found in the Supporting Information.

https://dx.doi.org/10.1021/acsmacrolett.0c00461
ACS Macro Lett. 2020, 9, 1149−1154

2.2. Supporting Information

Supporting Information

"Grafting density governs the thermoresponsive behavior of P(OEGMA-*co*-RMA) statistical copolymers"

Irem Akar,[†] *Robert Keogh,*[†,‡] *Lewis D. Blackman,*[‡] *Jeffrey C. Foster,**[,†] *Robert T. Mathers,**[,§] *and Rachel K. O'Reilly**[,†]

[†]School of Chemistry, University of Birmingham, Edgbaston, Birmingham, B15 2TT, UK

[‡]Department of Chemistry, University of Warwick, Gibbet Hill Road, Coventry, CV4 7AL, UK

[§]Department of Chemistry, Pennsylvania State University, New Kensington, PA 15068, USA

*Corresponding Authors: fosterjc@bham.ac.uk (J.C.F.), rtm11@psu.edu (R.T.M.), and r.oreilly@bham.ac.uk (R.K.O.R.)

Materials and Methods

Materials

Methyl methacrylate (MMA, Sigma-Aldrich, 99%), ethyl methacrylate (EMA, Sigma-Aldrich, 99%), *n*-butyl methacrylate (BMA, Sigma-Aldrich, 99%), hexyl methacrylate (HMA, Sigma-Aldrich, 98%), lauryl methacrylate (LMA, Sigma-Aldrich, 96%), oligoethyleneglycol glycol methyl ether methacrylate (OEGMA, Sigma-Aldrich, M_n = 500 g mol^{-1}), and 1,4-dioxane (Sigma-Aldrich, 99.8%) were filtered through basic alumina prior to use. AIBN 2,2′-Azobis(2-methylpropionitrile) (AIBN) was received from Molekula, recrystallized from methanol and stored at 4 °C. Methyl 4-cyano-4-(((ethylthio)carbonothioyl) thio)pentanoate (MCETP) was prepared according to a previously described procedure.[1]

Characterization Techniques

NMR Spectroscopy. ^{1}H-NMR and ^{13}C-NMR spectra were recorded at 300 MHz on a Bruker DPX-300 spectrometer, using chloroform-*d* ($CDCl_3$) as the solvent. Chemical shifts of protons are reported as δ in parts per million (ppm) and are relative to solvent residual peaks.

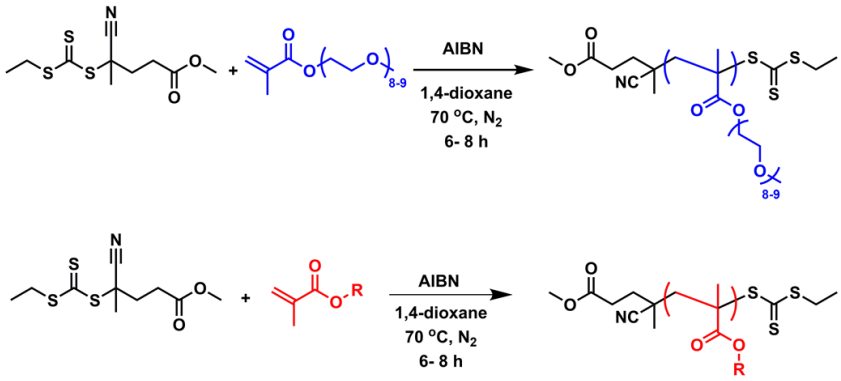
Size Exclusion Chromatography. Size exclusion chromatography (SEC) analysis was performed on a system composed of an Agilent 1260 Infinity II LC system equipped with an Agilent guard column (PLGel 5 μM, 50 × 7.5 mm) and two Agilent Mixed-C columns (PLGel 5 μM, 300 × 7.5 mm). The mobile phase used was $CHCl_3$ (HPLC grade) containing 0.5% v/v NEt_3 at 40 °C at flow rate of 1.0 mL min^{-1} (polymethyl methacrylate (PM) standards were used for calibration). Detection was conducted using a differential refractive index (RI) detector. Number-average molecular weights (M_n), weight-average molecular weights (M_w) and dispersities ($Đ_M = M_w/M_n$) were determined using the Agilent GPC/SEC software.

UV-Vis Spectroscopy. UV-Vis analysis was performed on a Thermo Scientific Evolution™ 350 spectrophotometer equipped with a Peltier heating and cooling system to record the LCST behaviour, temperature dependent transmittance spectra of polymers by heating the samples in solution from 20 °C to 93 °C at a rate of 1 °C min^{-1}. Samples were corrected against a background of DI water. Measurements were carried out using glass cuvettes with a path length of 10.00 mm.

Micro-Differential Scanning Calorimetry. Temperature *vs* heat rate spectra for $OEGMA_{500}$-*co*-RMA copolymer samples were recorded at a TA Instruments NanoDSC differential scanning calorimeter (μDSC) by heating the samples in solution from 0 °C to 115 °C at a rate of 0.5 °C min^{-1}. Samples were degassed for 15 min prior to injection of 600 μL into the instrument and corrected against a background of DI water. Collected data were processed using NanoAnalyze Software.

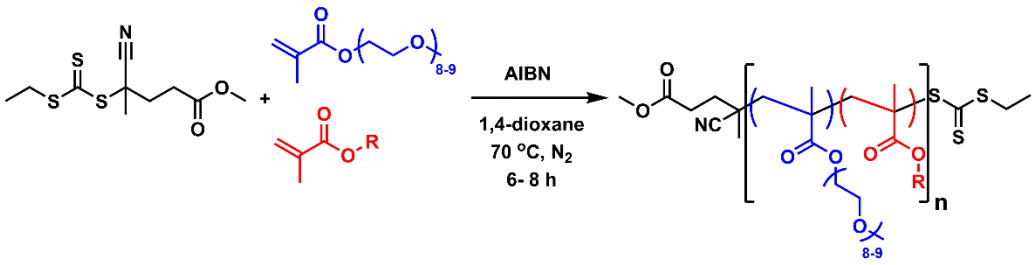
Synthetic Methods

Synthesis of P(OEGMA) and P(RMA) homopolymers



Homopolymerization of $OEGMA_{500}$ (M_n = 500 g mol^{-1}) or RMA monomers was conducted using AIBN as the initiator, MCETP as the RAFT agent, 1,3,5-Trioxane as an internal reference, and 1,4-dioxane as the solvent ([Monomer]/[1,3,5-Trioxane]/[MCETP]/[AIBN] = 120:20:1:0.1, monomer/1,4-dioxane = 1:1 by volume). A stock solution of 10 mg mL^{-1} AIBN was prepared in 1,4-dioxane and 60 µL of this solution (0.6 mg, 3.6 x 10^{-3} mmol, 0.1 eq) was added to a vial of MCETP (10 mg, 3.6 x 10^{-2} mmol, 1.0 eq), monomer (4.3 mmol, 120 eq), 1,3,5-Trioxane (65 mg, 7.2 x 10^{-1} mmol, 20 eq) and 1,4- dioxane and was stirred in an oven-dried ampoule containing a magnetic stir bar until all solids dissolved. The resulting solution was degassed using at least three freeze-pump-thaw cycles, back-filled with N_2, and placed in a preheated oil bath at 70 °C. Samples were taken periodically to determine monomer conversion using ^{1}H NMR spectroscopy. After 6-8 h, the polymerizations were quenched by submerging into liquid nitrogen and exposing the reaction solutions to air. Purification of P(RMA) homopolymers was achieved *via* precipitation into methanol three times while P(OEGMA) was purified *via* dialysis (6-8 kDa MWCO) against nanopure water followed by lyophilisation.

Synthesis of P($OEGMA_{500}$-*co*-RMA) copolymers



Copolymerization of RMA monomers with $OEGMA_{500}$ (M_n = 500 g mol^{-1}) was conducted using AIBN as the initiator, MCETP as the RAFT agent, 1,3,5-trioxane as an internal reference, and 1,4-dioxane as the

solvent. RMA content was varied between 50-90% for MMA, 50-80% for EMA, 50-80% for BMA, 40-70% for HMA and 10-40% for LMA, targeting the total DP of 80 to 85 with a molar ratio of [Monomer]/[1,3,5-Trioxane]/[MCETP]/[AIBN] = 120:20:1:0.1 in 1,4-dioxane (monomer/1,4-dioxane = 1:1 by volume). For the synthesis of a copolymer with 50% RMA: A stock solution of 10 mg mL^{-1} AIBN was prepared in 1,4-dioxane and 60 µL of the solution (0.6 mg, 3.6 x 10^{-3} mmol, 0.1 eq) was added to a vial containing MCETP (10 mg, 3.6 x 10^{-2} mmol, 1.0 eq), OEGMA (1.0 mL, 2.2 mmol, 60 eq), RMA monomer (2.2 mmol, 60 eq) and 1,3,5-Trioxane (65 mg, 7.2 x 10^{-1} mmol, 20 eq) in 1,4-dioxane and mixed in an oven-dried ampoule containing a magnetic stir bar until all solids dissolved. The resulting solution was degassed using at least three freeze-pump-thaw cycles, back-filled with N_2, and placed in a preheated oil bath at 70 °C. Samples were taken periodically to determine the overall and relative conversion of comonomers. Purification was achieved by dialysis (6-8 kDa MWCO) against nanopure water followed by lyophilisation.

Experimental Methods

Copolymerization kinetic studies. Kinetic experiments for one polymer from each series (50% RMA for P(OEGMA$_{500}$-*co*-MMA), P(OEGMA$_{500}$-*co*-EMA), P(OEGMA$_{500}$-*co*-BMA), P(OEGMA$_{500}$-*co*-HMA) and 30% RMA for P(OEGMA$_{500}$-*co*-LMA) were carried out in order to determine the conversion of each monomer at the same time intervals (i.e., 60, 120, 180, 240, 300, 360, 420 and 480 min). Samples were periodically taken from the polymerization mixtures under nitrogen and then diluted with $CDCl_3$ prior to ^{1}H NMR analysis. Integrations of monomer signals were compared to those internal standard resonances to determine monomer conversions.

Determination of T_{CP} by UV-Vis spectroscopy. Solutions of P(OEGMA) homopolymer or P(OEGMA$_{500}$-*co*-RMA) copolymer were prepared at 5 mg mL^{-1} in nanopure water. The temperature-dependent change in transmittance % was recorded at λ = 550 nm within the temperature range of 20 °C to 93 °C at a heating rate of 1 °C min^{-1}. Samples were run for two heating/cooling cycles and T_{CP} values taken as the temperature at which the sample transmittance had decreased to 50% on the second heating cycle.

Determination of T_{CP} by µDSC. Solutions of P(OEGMA) homopolymer or P(OEGMA$_{500}$-*co*-RMA) copolymer were prepared at 5 mg mL^{-1} in nanopure water. Samples and reference solvent (nanopure water) were degassed for 15 min prior to measurement by using the degassing unit of the instrument. Measurements were conducted within the temperature range of 0 °C to 115 °C under a constant pressure of 3 atm. Samples were run two for heating/cooling cycles, with heating and cooling rates for the first and second cycles of 2 °C min^{-1} and 0.5 °C min^{-1}, respectively. Data were processed using NanoAnalyze software and T_{CP} values were determined by taking the maximum of the first derivative of the corrected heat rate (µJ s^{-1}) *vs.* temperature (°C) plots of the second heating trace.

Determination of ΔH_{mix} by µDSC. Data obtained from μDSC as described above were normalized based on their peak maxima. Normalized ΔH values were then calculated *via* integration of the signal associated with the demixing transition using straight line baseline correction across the collected temperature range from ca. 5-100 °C.

Evaluation of Oligomer Hydrophobicity

LogP_{oct} Analysis. Octanol-water partition coefficients (LogP_{oct}) were calculated for monomers and oligomeric models in Materials Studio 2019,[2] using an atom-based approach (ALogP98 method)[3] for all molecular models containing C, H, N, and O atoms.

Surface Area Analysis. Octanol-water partition coefficients (LogP_{oct}) were normalized by solvent accessible surface area (SA) using Materials Studio 2019.[4-7] First, single oligomers were subjected to a Geometry Optimization procedure using the Forcite Molecular Dynamics (MD) module with a COMPASS II force field. The force field contains information on important parameters, like preferred bond lengths, bond angles, torsion angles, partial charges, and van der Waals radii that influence the conformation.[8] To minimize energy and determine a preferred conformation, these simulations ran until the energy of the oligomer decreased below predetermined convergence criteria (1×10^{-4} kcal mol^{-1} energy convergence, 0.005 kcal mol^{-1} /Å force convergence, and 5×10^{-5} Å displacement convergence). Second, these SA values represent the Connolly surface area created by an algorithm that rolls a ball over the surface of the oligomer. To ensure the SA values are meaningful in the context of octanol-water partition coefficients (LogP_{oct}), the probe had a 1.4 Å radius to match the size of a water molecule. Third, to monitor variations in surface area calculations as the n-mer size increased, oligomers were annealed for 25 cycles using a sinusoidal temperature ramp (300 – 700 K) to maximize variability in SA values. After averaging SA values for cycles 23-25, the standard deviation ranged from 0.2-1.2% with an average of 1.0%.

Models. Oligomeric models contained appropriate ratios of OEGMA and alkyl methacrylate units to mimic experimental conditions. In addition, models were proton terminated and contained OEGMA units randomly distributed throughout the oligomer. For example, MMA/OEGMA oligomers contained 3-10 OEGMA units with 9-20 MMA units for a total of 16-23 units such that the amount of MMA ranged from 47.4-87.0 mol %. EMA/OEGMA oligomers combined 4-9 OEGMA units and 8-14 EMA units for a total of 17-20 units with 47.1-76.5 mol % EMA. BMA/OEGMA oligomers contained 4-8 OEGMA units and 8-15 BMA units for a total of 16-22 units in order that the amount of BMA varied from 50-78.9 mol %. HMA/OEGMA oligomers contained 6-10 OEGMA units with 7-14 HMA units for a total of 16-20 monomer units to achieve 41.2-70.0 mol % HMA. The quantity of monomers in LMA/OEGMA oligomers ranged from 6-11 OEGMA units and 1-3 LMA units for a total of 9-14 units with 11.1-33.3 mol % LMA.

Data Analysis

Initial Screening of Descriptors

Correlations between polymer descriptors and T_{CP} were initially screened by visual inspection of the scatter plot matrix shown below in Figure S1. This scatterplot matrix was constructed using the R language environment (v 3.6.3) and the RStudio integrated development environment (v 1.2.5033). Experimental descriptors were the molar percentage of comonomer (Mol), the weight percentage of comonomer (Wt), copolymer M_n (MW), $Đ_M$ (D), and degree of polymerization (DP), and computational descriptors included LogP_{oct} (LP), polar surface area (SA), and surface area-normalized LogP_{oct} (LPSA). Both the molar percentage of comonomer (Mol) and the weight percentage (Wt) of comonomer appeared to be linearly related to the measured T_{CP} values (UV). In addition, there were several instances of collinearity that could be observed between descriptors such as between Mol and Wt or LP and LPSA. However, since the relationships between these descriptors were not expected change beyond the range of the training dataset and the aim of the model discussed below was the prediction of new cases, these descriptors were included in model development.

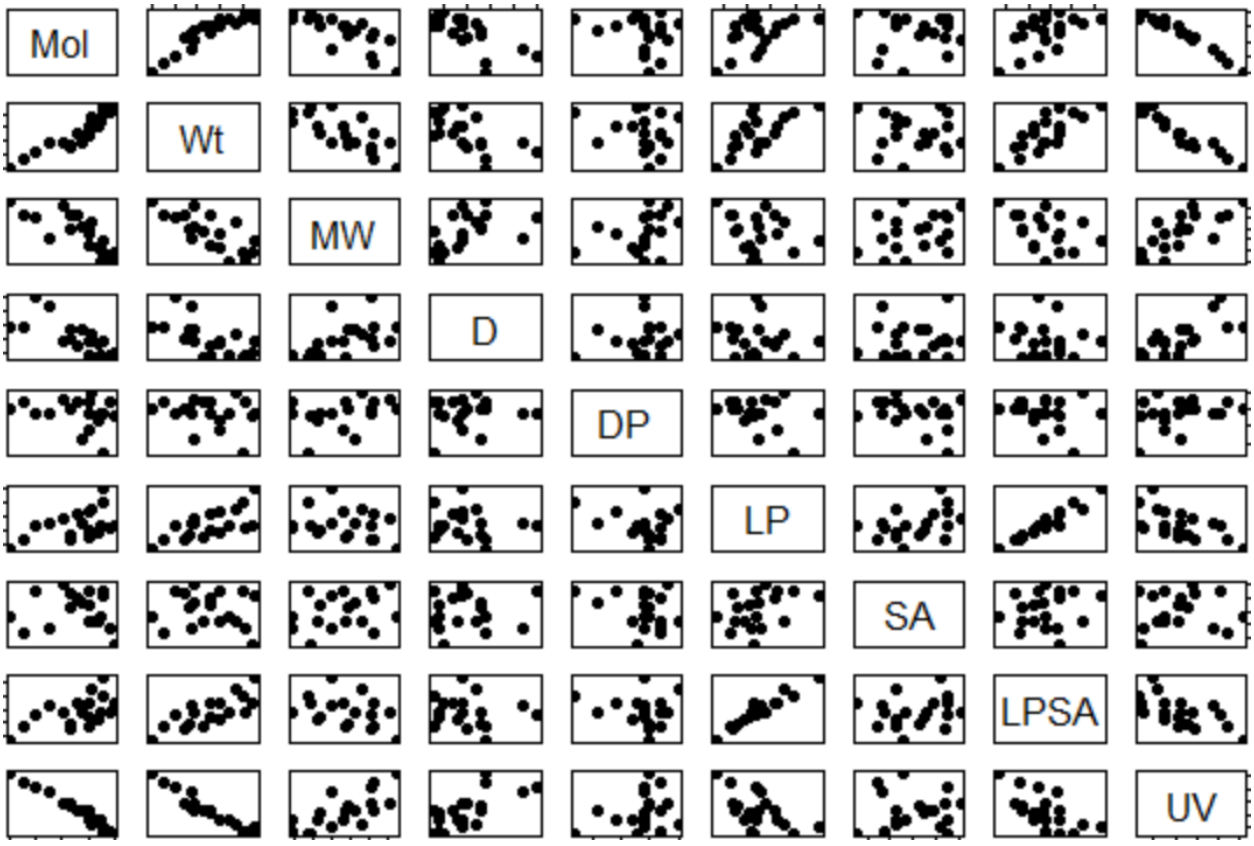


Figure S1. Scatterplot matrix of experimental data collected for P(OEGMA$_{500}$-*co*-RMA) copolymers.

These relationships were further investigated using a correlation plot (Figure S2, generated *via* the corrplot package). Here, positive correlations are displayed in blue and negative in red. The color intensity of the circles is proportional to the Pearson correlation coefficients, ρ, which describes the "degree of correlation" between the two variables as defined by the relationship

$$\rho_{x,y} = \frac{E[(X - \mu_x)(Y - \mu_y)]}{\sigma_x \sigma_y}$$

where σ_x and σ_x are the standard deviation of x and y, respectively, μ_x and μ_y are the means of x and y, respectively, and E is the expectation. Cells with significance test values of $p \leq 0.05$ are marked with an asterisk. This analysis suggested that several descriptors (Mol, Wt, MW, D, LP, and LPSA) were related to the response variable, UV, and were considered as potential model predictors. Non-significant parameters were excluded from the model development discussed below.

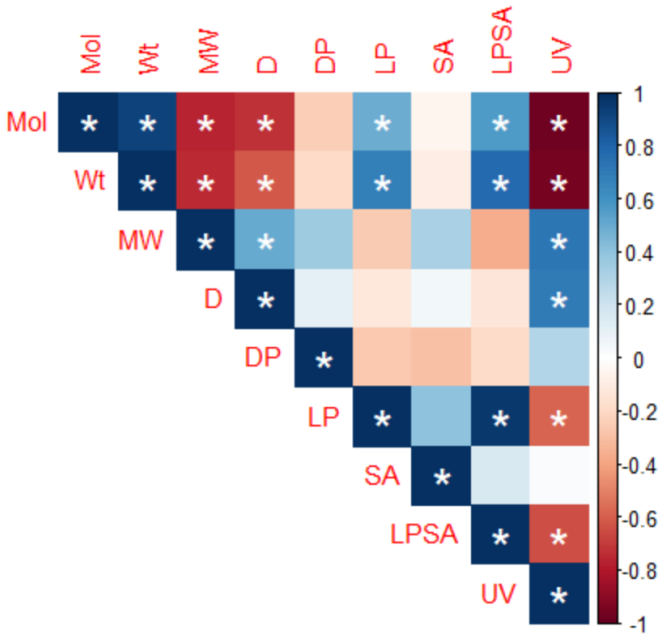


Figure S2. Correlation plot to understand relationships between experimental descriptors and the response variable, UV. Color intensity is related to the Pearson correlation coefficient, as indicated by the legend. An asterisk denotes a linear relationship with $p < 0.05$.

Predictive Model Development

A rigorous elimination/selection stepwise regression analysis was performed to construct a quantitative structure-activity relationship (QSAR) model from the experimental data. The model was trained on the 19 OEGMA copolymers using 4 experimental descriptors (Mol, Wt, MW, and D) and 2 computational descriptors (LP and LPSA) identified as significant in the analysis above. The models were validated *via* a 5-fold repeated resampling method wherein stratified k-fold datasets were used. This analysis was implemented using the R language environment (v 3.6.3) and the RStudio integrated development environment (v 1.2.5033). Algorithms for model training and cross-validation were implemented using the classification and regression training (CARET) package developed by Dr. Max Kuhn.[9]

Table S1 shows the results of the stepwise regression, expressed in terms of the fitness of each model as a function of the number of included descriptors. Based on these data, the optimum model includes 2 descriptors: Mol and Wt. Linear regression statistics for this model are provided in Table S2 and model validation using the training dataset is shown in Figure S3.

Table S1. Summary of linear regression with stepwise selection.

Number of descriptors	R^2	RMSE[a]
1	0.955	3.073
2	0.976	2.530
3	0.970	2.764
4	0.958	3.248
5	0.961	3.337
6	0.957	3.522

[a]Root-mean-squared error.

Table S2. Liner regression statistics for 2-descriptor model.

Coefficient	Estimate	Std. Error	t-value	p-value	Significance[a]
Intercept	92.34	1.42	65.01	$< 2 \times 10^{-16}$	***
Mol	-0.39	0.07	-6.02	1.8×10^{-5}	***
Wt	-0.39	0.11	-3.49	3.1×10^{-3}	**

[a]Significance codes: '***' $p \leq 0.001$; '**' $p \leq 0.01$; '*' $p \leq 0.05$.

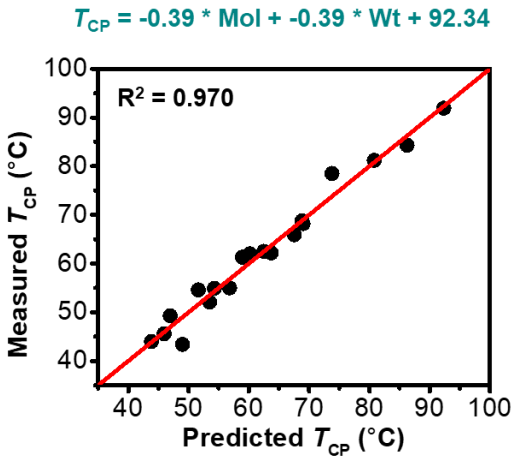


Figure S3. Validation of 2-descriptor model using training data. Measured T_{CP} values are plotted against those generated by the model (shown in teal) using experimentally determined Mol and Wt inputs. The solid red line represents a linear fit of the data.

Screening of Literature Descriptors

As before, correlations between descriptors and the response variable UV were screened using a scatter plot matrix. These data include a total of 44 unique entries from 10 literature reports (see below for a complete list of raw data and literature references). Data selection was restricted to P(OEGMA-*co*-R) containing OEGMA units with M_n ~ 500 g mol^{-1} where the apparent linear relationship between UV and the descriptors was most obvious (see Figure 4 in main text). Scatter plot and correlation matrices for these data are shown in Figures S4 and S5, respectively. As before, Mol and Wt were most strongly correlated to UV.

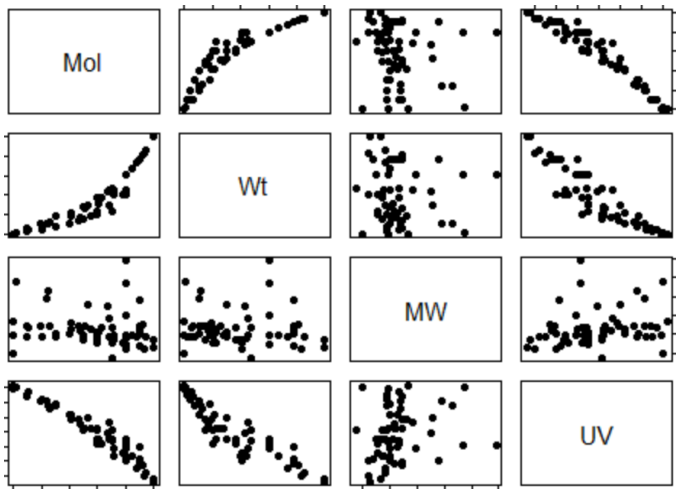


Figure S4. Scatterplot matrix of literature data for P(OEGMA$_{500}$-*co*-RMA) copolymers.

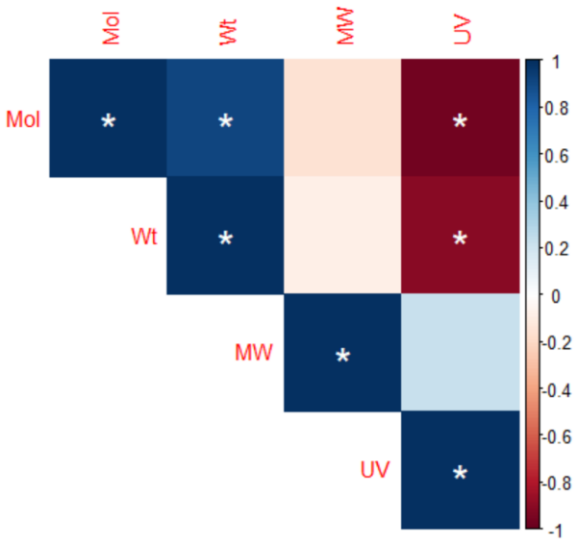


Figure S5. Correlation plot to understand relationships between literature descriptors and the response variable UV. Color intensity is related to the Pearson correlation coefficient, as indicated by the legend. An asterisk denotes a linear relationship with $p < 0.05$.

Model Validation with Literature (Test) Data

The 2-descriptor model was validated using a test dataset consisting of literature Mol, Wt, and UV values. Whilst the predicted values appear to be linearly correlated with literature UV data, R^2 and RMSE values (R^2 = 0.920, RMSE = 8.42) obtained from this prediction were comparatively worse than for the training dataset (R^2 = 0.976, RMSE = 2.53). This result was diagnostic of "overfitting" of the initial training dataset, likely the result of the strong intercorrelation between the Mol and Wt descriptors that differed between the experimental and literature datasets. Thus, a standard single variable linear regression model was employed in further analysis that related measured or literature UV values to Mol which yielded similar R^2 and RMSE for both the training and test (R^2 = 0.970, RMSE = 4.57) datasets. Linear regression statistics for this model using training (experimental) data are provided in Table S3.

Table S3. Linear regression statistics for simple single variable model.

Coefficient	Estimate	Std. Error	t-value	p-value	Significance[a]
Intercept	92.22	1.80	51.81	$< 2 \times 10^{-16}$	***
Mol	-0.598	0.03	-18.63	9.49×10^{-13}	***

[a]Significance codes: '***' $p \leq 0.001$; '**' $p \leq 0.01$; '*' $p \leq 0.05$.

Raw Literature Data and Citations

Copolymer	Mol	Wt	MW (kDa)	UV (°C)	DOI
OEGMA$_{500}$-*co*-DEGMA	0	0	10.0	90	10.1021/ma0517042
	67	44	35.0	59	
	80	60	29.7	49	
	84	67	19.9	44	
	90	77	24.3	39	
	92	81	24.8	37	
	94	86	18.3	32	
	100	100	16.7	28	
OEGMA$_{500}$-*co*-MAA	80	41	12.0	40	10.1002/pola.23018
	60	21	15.8	52	
	50	15	17.0	61	
	40	10	20.0	72	
	30	7	19.0	78	
	20	4	19.0	82	
	10	2	19.0	85	
	0	0	19.5	89	
OEGMA$_{500}$-*co*-DEGMA	100	100	13.0	26	10.1002/pola.24027
	90	77	14.0	42	
	80	60	15.0	55	
OEGMA$_{500}$-*co*-PFS	60	37	17.4	55	10.1002/pola.23872
	50	28	19.5	62	
	26	12	24.0	76	
	11	5	23.7	87	
OEGMA$_{500}$-*co*-DEGMA	90	77	37.8	41	10.1002/marc.201000713
	80	60	47.0	51	
	70	47	7.5	61	
OEGMA$_{500}$-*co*-DEGMA-*co*-VBK	93	83	12.0	30	10.1021/ma202648k
	88	74	18.5	35	
	90	77	23.1	50	
	70	47	23.4	54	
	68	45	28.7	66	
	53	30	35.9	70	
	41	21	22.9	72	
	25	11	43.2	78	
	24	11	39.2	81	
	2	1	47.7	90	
OEGMA$_{500}$-*co*-DEGMA-*co*-4-DMN	80	60	59.0	51	10.1039/C3TC31304B
OEGMA$_{500}$-*co*-DEGMA	90	77	22.0	38	10.1007/s00396-016-4006-4
OEGMA$_{500}$-*co*-DEGMA	90	77	20.1	40	10.1021/ma062925q
	80	60	19.5	53	
OEGMA$_{500}$-*co*-MMA	76	43	N/A	43	10.1021/ma030485m
	70	36	N/A	50	
	60	26	N/A	56	

	0	0	N/A	90	
OEGMA$_{300}$-*co*-DMAEMA	100	100	9.5	35	10.1021/ma062199r
	89	81	9.0	42	
	78	65	9.0	47	
	70	55	10.9	51	
	59	43	11.2	54	
	51	34	13.2	56	
	41	27	13.3	58	
	29	18	14.2	59	
	20	12	15.5	61	
	10	6	17.4	63	
	0	0	17.6	65	
OEGMA$_{300}$-*co*-DEGMA	100	100	13.3	25	10.3390/polym11101657
	86	79	18.6	32	
	76	66	20.6	36	
	69	58	21.4	41	
	50	39	23.0	46	
	21	14	26.7	56	
	0	0	11.8	67	
OEGMA$_{300}$-*co*-DEGMA	100	100	30.4	27	10.1039/C0PY00417K
	85	78	25.8	33	
	81	73	33.0	36	
	73	63	53.4	38	
	63	52	58.1	42	
	36	26	21.2	55	
	27	19	30.0	59	
	0	0	14.1	73	
OEGMA$_{300}$-*co*-MAEBA	50	28	13.7	22	10.1039/C0CC03856C
	33	21	13.0	31	
	25	17	13.8	39	
	13	9	12.2	49	
	6	5	15.8	58	
	0	0	17.7	66	
OEGMA$_{300}$-*co*-TFEA	20	11	39.7	45	10.1021/acs.macromol.5b00641
OEGMA$_{300}$-*co*-MAECA	0	0	12.8	72	10.1039/c3py01317k
	6	10	17.0	61	
	12	20	20.3	56	
	23	35	21.8	42	
OEGMA$_{300}$-*co*-SAMA	0	0	9.2	65	10.1039/C6RA00336B
	12	16	8.8	61	
	18	23	14.3	56	
	21	27	13.5	52	
	27	34	20.5	48	
	31	39	15.3	44	
OEGMA$_{300}$-*co*-PFS	0	0	69.0	65	10.1016/j.polymer.2017.01.080
	18	19	81.0	50	
	25	27	82.0	48	

	31	35	75.0	38	
	38	45	83.0	30	
	42	49	56.0	26	
OEGMA$_{300}$-*co*-NIPAM	48	26	39.1	35	10.1039/B105990B

Supplementary Characterization Data for p(OEGMA) and p(RMA) Homopolymers

Table S4. Molecular characteristics of P(RMA) homopolymers prepared *via* RAFT, as determined by ^{1}H NMR spectroscopy and SEC analyses.[a]

Homopolymer	Conversion (%)[b]	DP based on $M_{n,\,theo}$[c]	$M_{n,\,theo}$[c] (kDa)	$M_{n,\,SEC}$[d] (kDa)	$Đ_M$[d]
P(MMA)	60	72	7.5	13.6	1.13
P(BMA)	59	71	10.4	4.7	1.14
P(HMA)	68	82	14.2	12.4	1.13
P(LMA)	59	71	18.3	16.0	1.16
P(OEGMA)	71	85	42.8	27.0	1.29

[a] Conditions – [Monomer]/[1,3,5-Trioxane]/[MCETP]/[AIBN] = 120:20:10:0.1 in 1,4-dioxane (monomer/1,4-dioxane = 1:1 by volume).
[b] Determined by ^{1}H NMR spectroscopy ($CDCl_3$, 300 MHz).
[c] Calculated from monomer conversion.
[d] M_n and $Đ_M$ determined by SEC (in $CHCl_3$ + 0.5% NEt_3, calibrated against PMMA standards).

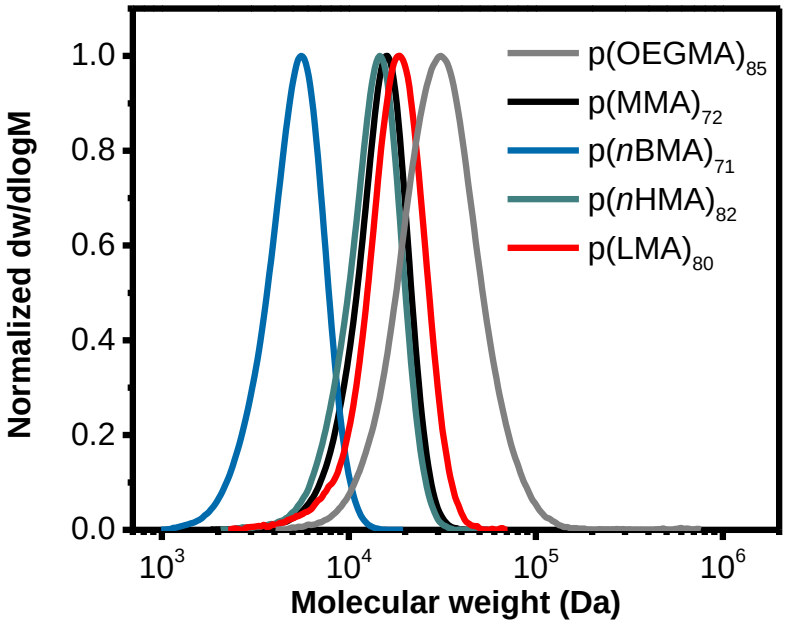


Figure S6. Normalized molecular weight distributions determined by SEC ($CHCl_3$ + 0.5% NEt_3 as the eluent and calibrated against PMMA standards) using an RI detector for P(OEGMA) and P(RMA) homopolymers.

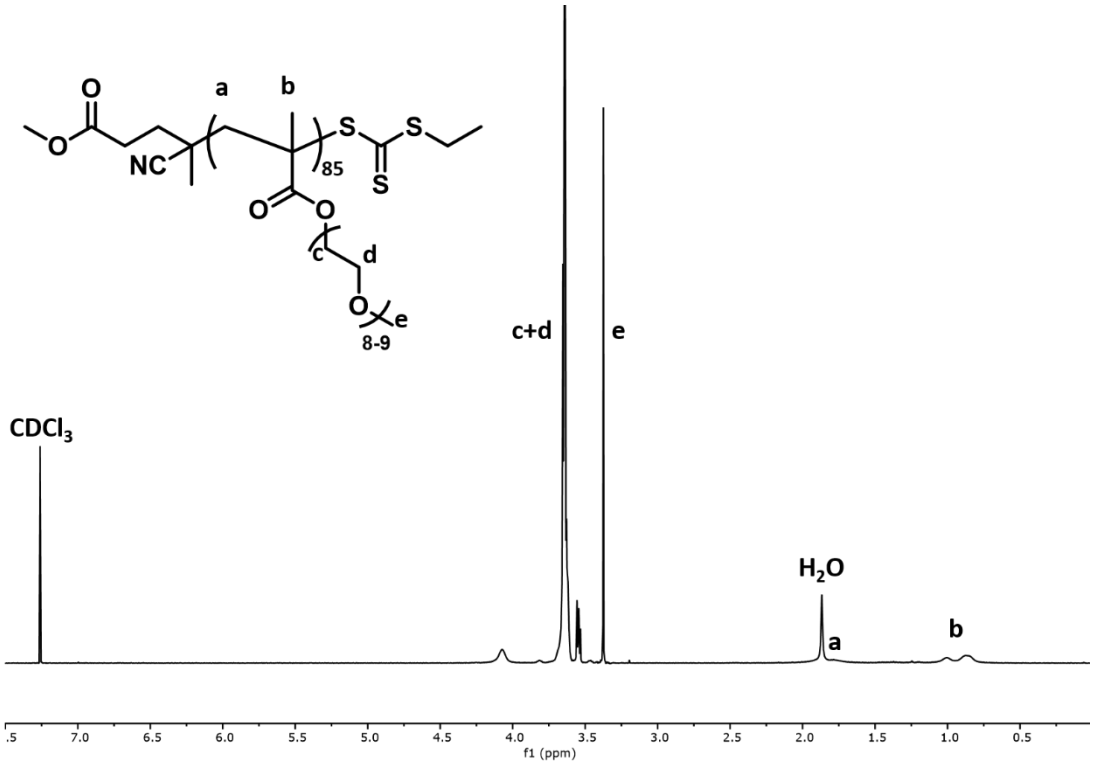


Figure S7. ^{1}H-NMR spectrum of $P(OEGMA)_{85}$ in $CDCl_3$ (300 MHz).

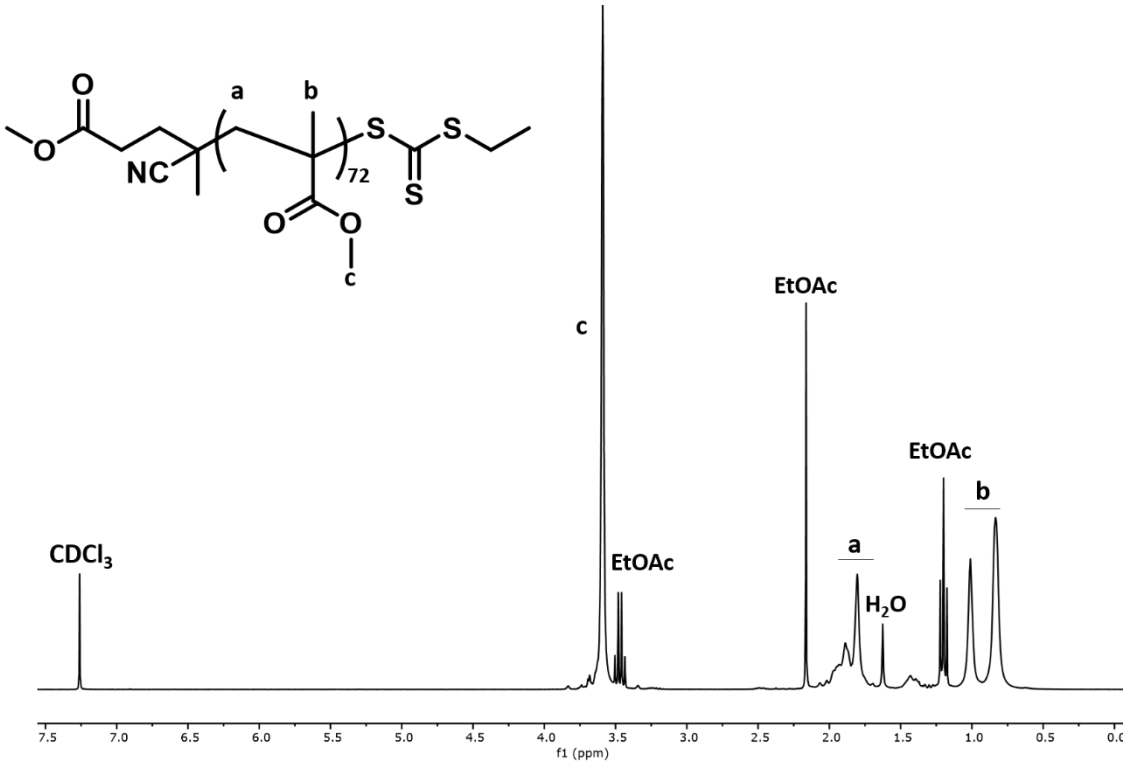


Figure S8. ^{1}H-NMR spectrum of $P(MMA)_{72}$ in $CDCl_3$ (300 MHz).

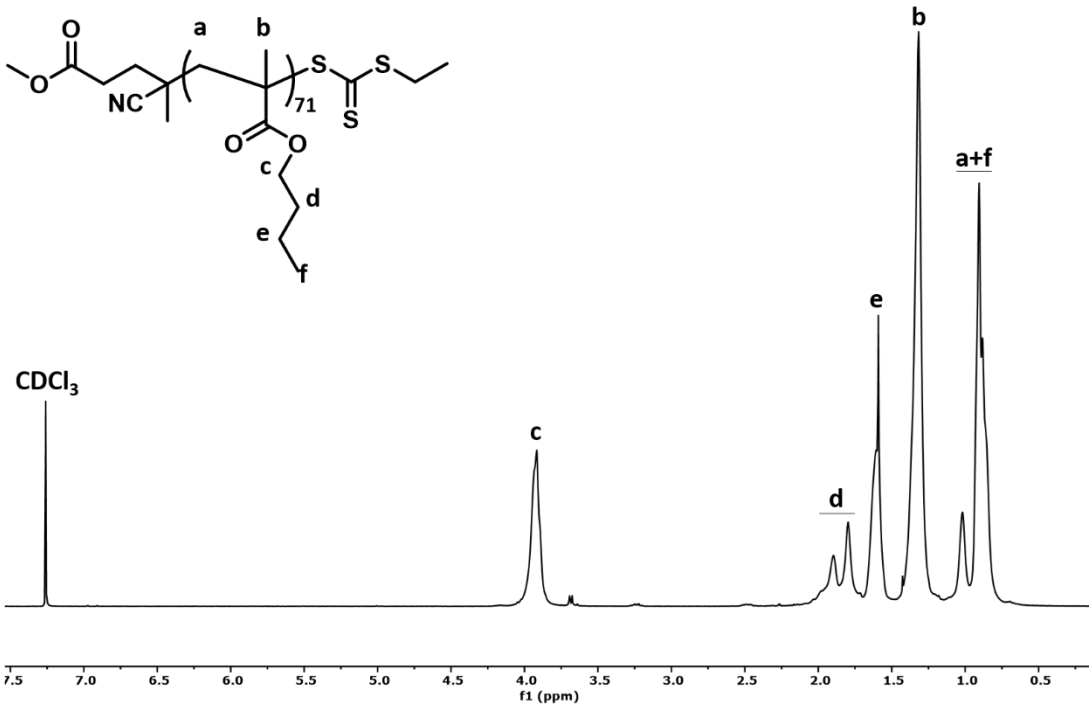


Figure S9. ^{1}H-NMR spectrum of $P(BMA)_{71}$ in $CDCl_3$ (300 MHz).

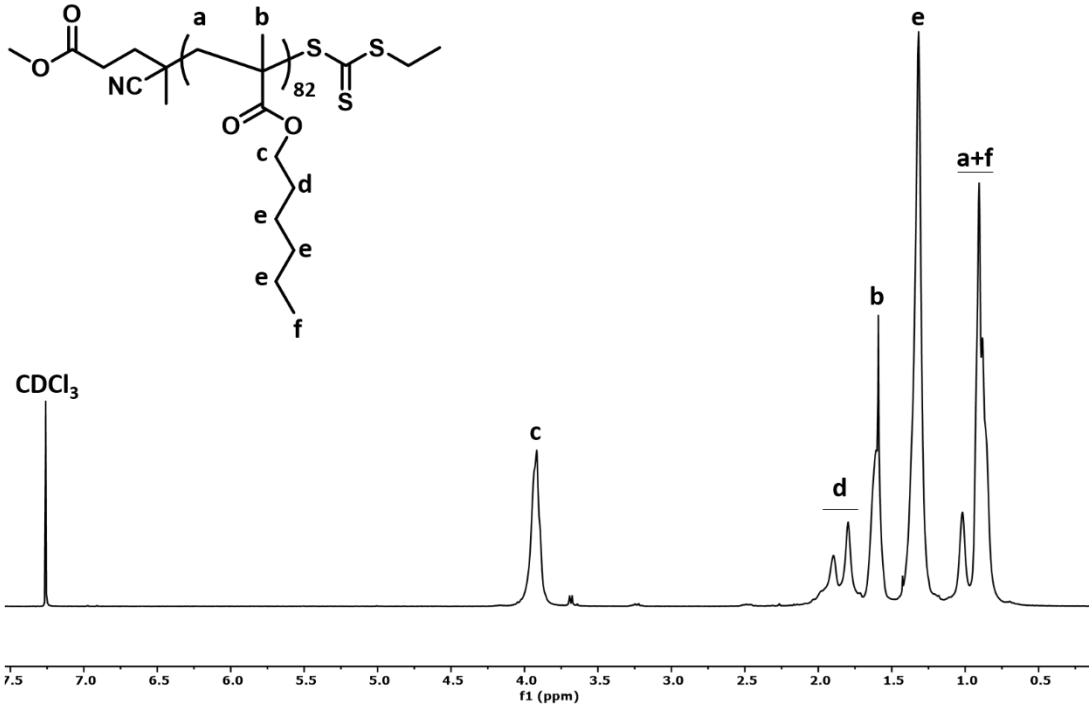


Figure S10. ^{1}H-NMR spectrum of $P(HMA)_{82}$ in $CDCl_3$ (300 MHz).

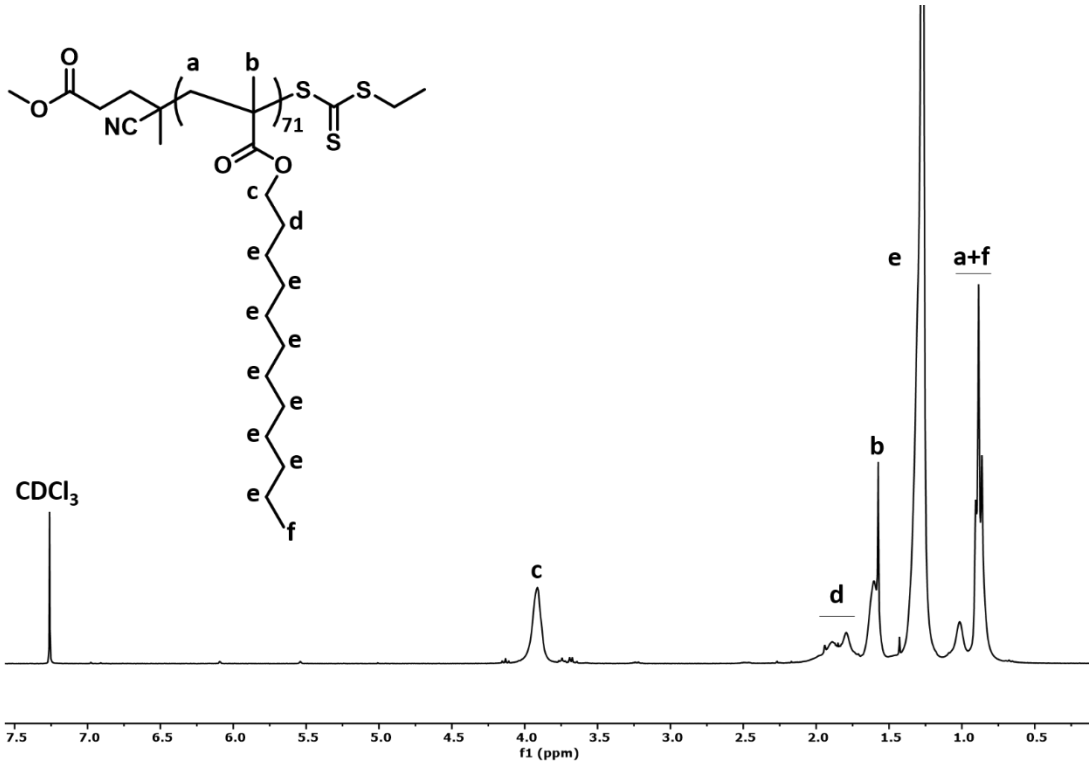


Figure S11. ^{1}H-NMR spectrum of $P(LMA)_{71}$ in $CDCl_3$ (300 MHz).

Supplementary Characterization Data for OEGMA$_{500}$-*co*-RMA Copolymers

Table S5. Molecular characteristics of P(OEGMA$_{500}$-*co*-RMA) copolymers prepared *via* RAFT, as determined by ^{1}H NMR spectroscopy and SEC analyses.[a]

Polymer	Target RMA Percentage	Final RMA Percentage[b]	DP[c]	$M_{n,\,NMR}$[c] (kDa)	$M_{n,\,SEC}$[d] (kDa)	$Đ_M$[e]
P(OEGMA$_{0.54}$-*co*-MMA$_{0.46}$)	50	46	85	27.2	24.4	1.25
P(OEGMA$_{0.4}$-*co*-MMA$_{0.6}$)	60	60	87	23.0	21.5	1.18
P(OEGMA$_{0.32}$-*co*-MMA$_{0.68}$)	70	68	82	18.9	18.5	1.23
P(OEGMA$_{0.22}$-*co*-MMA$_{0.78}$)	80	78	87	16.6	15.7	1.19
P(OEGMA$_{0.53}$-*co*-EMA$_{0.47}$)	50	47	85	27.3	21.8	1.28
P(OEGMA$_{0.4}$-*co*-EMA$_{0.6}$)	60	60	84	22.6	18.7	1.19
P(OEGMA$_{0.3}$-*co*-EMA$_{0.7}$)	70	70	84	19.5	15.7	1.19
P(OEGMA$_{0.2}$-*co*-EMA$_{0.8}$)	80	80	83	15.2	17.7	1.2
P(OEGMA$_{0.45}$-*co*-BMA$_{0.55}$)	50	55	76	26.1	22.4	1.28
P(OEGMA$_{0.39}$-*co*-BMA$_{0.61}$)	60	61	79	22.6	21.2	1.24
P(OEGMA$_{0.29}$-*co*-BMA$_{0.71}$)	70	71	72	18.0	17.4	1.18
P(OEGMA$_{0.20}$-*co*-BMA$_{0.80}$)	80	80	76	16.5	14.1	1.14
P(OEGMA$_{0.59}$-*co*-HMA$_{0.41}$)	40	41	88	32.4	26.4	1.24
P(OEGMA$_{0.49}$-*co*-HMA$_{0.51}$)	50	51	87	29.3	24.5	1.22
P(OEGMA$_{0.37}$-*co*-HMA$_{0.63}$)	60	63	90	26.5	23.3	1.27
P(OEGMA$_{0.29}$-*co*-HMA$_{0.71}$)	70	71	84	22.5	19.9	1.24
P(OEGMA$_{0.9}$-*co*-LMA$_{0.1}$)	10	10	87	40.6	24.6	1.29
P(OEGMA$_{0.81}$-*co*-LMA$_{0.19}$)	20	19	84	38.3	24.2	1.40
P(OEGMA$_{0.7}$-*co*-LMA$_{0.3}$)	30	30	84	36.1	20.0	1.37

[a] Conditions – [Monomer]/[1,3,5-Trioxane]/[MCETP]/[AIBN] = 120:20:1:0.1 in 1,4-dioxane (monomer/1,4-dioxane = 1 : 1 by volume).
[b] Determined by ^{1}H NMR spectroscopy ($CDCl_3$, 300 MHz).
[c] Calculated from monomer conversion.
[d] M_n and $Đ_M$ determined by SEC (in $CHCl_3$ + 0.5% NEt_3, calibrated against PM standards).

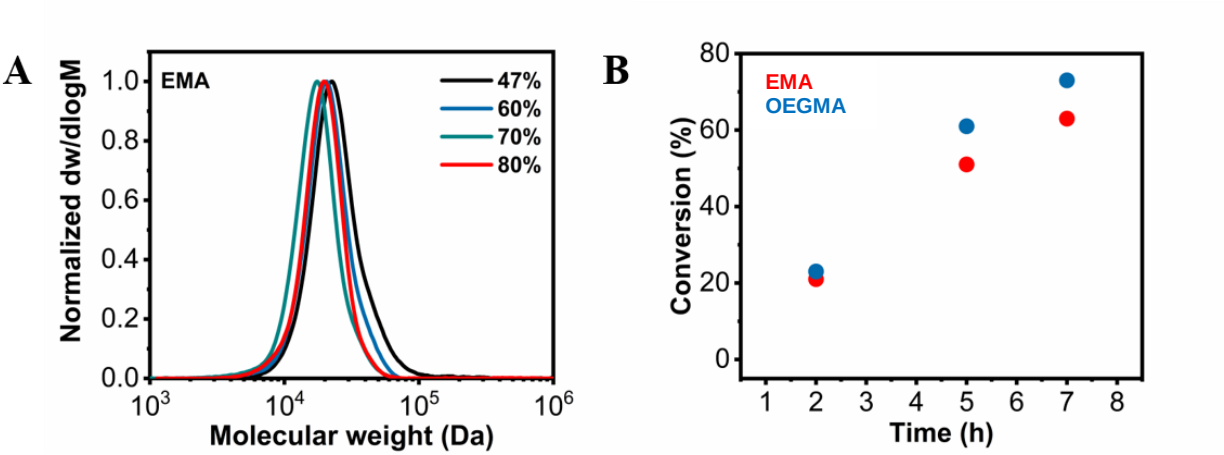


Figure S12. (A) Normalized molecular weight distributions for P(OEGMA-*co*-EMA) copolymers determined by SEC ($CHCl_3$ + 0.5% NEt_3 as the eluent and calibrated against PMMA standards) using an RI detector. The legend shows the molar percentage of EMA in the final copolymers. **(B)** Conversion of EMA and OEGMA monomers for the 47% EMA system determined by ^1H NMR spectroscopy ($CDCl_3$, 300 MHz).

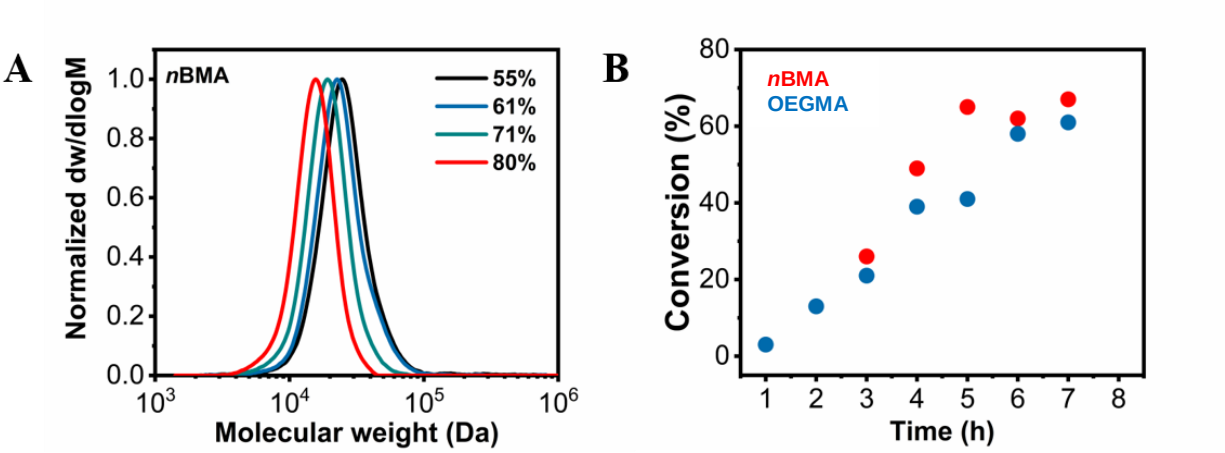


Figure S13. **(A)** Normalized molecular weight distributions for P(OEGMA-*co*-BMA) copolymers determined by SEC ($CHCl_3$ + 0.5% NEt_3 as the eluent and calibrated against PMMA standards) using an RI detector. The legend shows the molar percentage of BMA in the final copolymers. **(B)** Conversion of BMA and OEGMA monomers for the 55% BMA system determined by ^1H NMR spectroscopy ($CDCl_3$, 300 MHz).

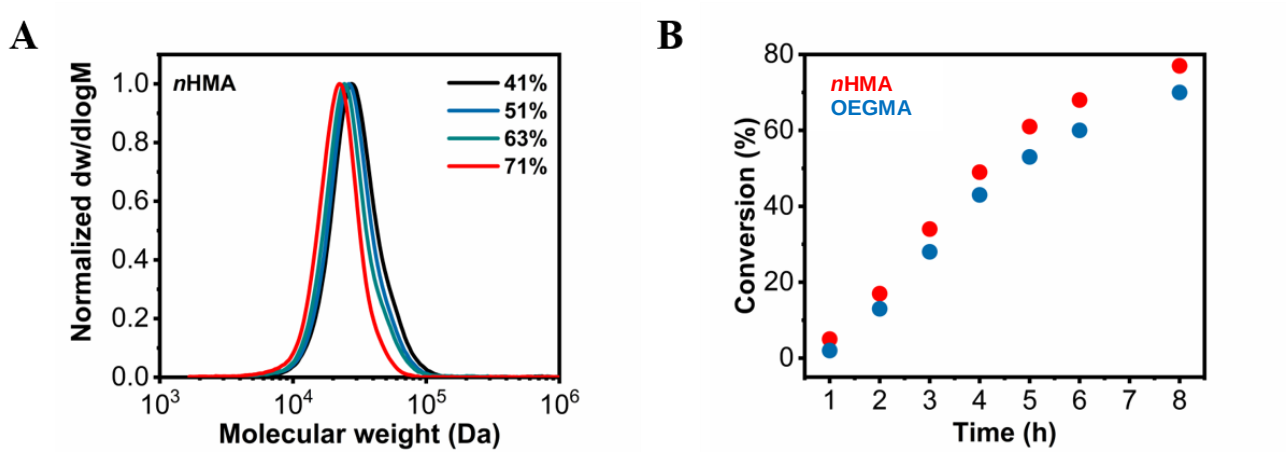


Figure S14. (A) Normalized molecular weight distributions for P(OEGMA-*co*-HMA) copolymers determined by SEC ($CHCl_3$ + 0.5% NEt_3 as the eluent and calibrated against PMMA standards) using an RI detector. The legend shows the molar percentage of HMA in the final copolymers. **(B)** Conversion of HMA and OEGMA monomers for the 51% HMA system determined by ^1H NMR spectroscopy ($CDCl_3$, 300 MHz).

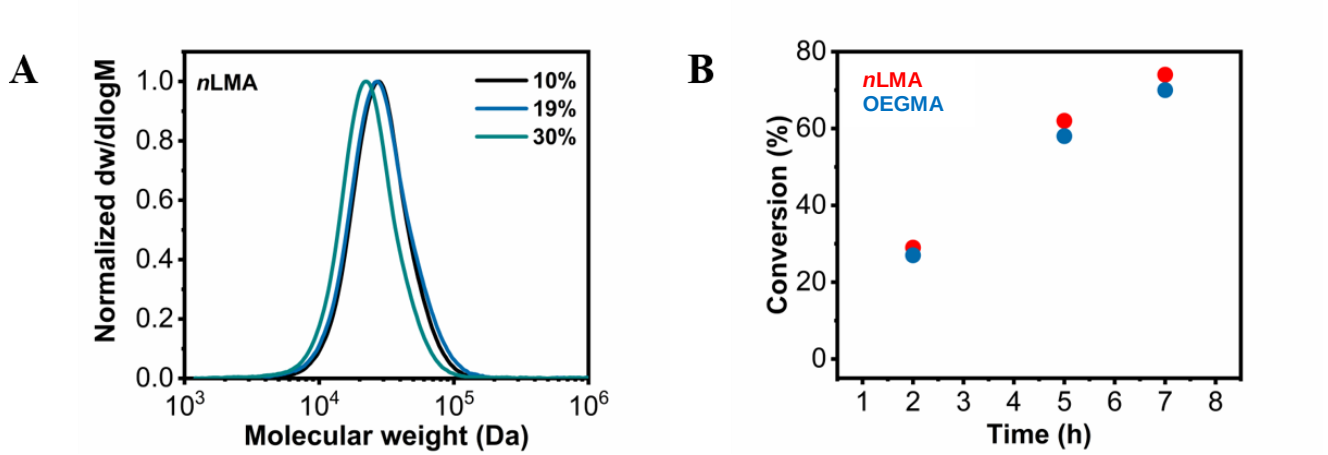


Figure S15. (A) Normalized molecular weight distributions for P(OEGMA-*co*-LMA) copolymers determined by SEC ($CHCl_3$ + 0.5% NEt_3 as the eluent and calibrated against PMMA standards) using an RI detector. The legend shows the molar percentage of LMA in the final copolymers. **(B)** Conversion of LMA and OEGMA monomers for the 30% LMA system determined by ^1H NMR spectroscopy ($CDCl_3$, 300 MHz).

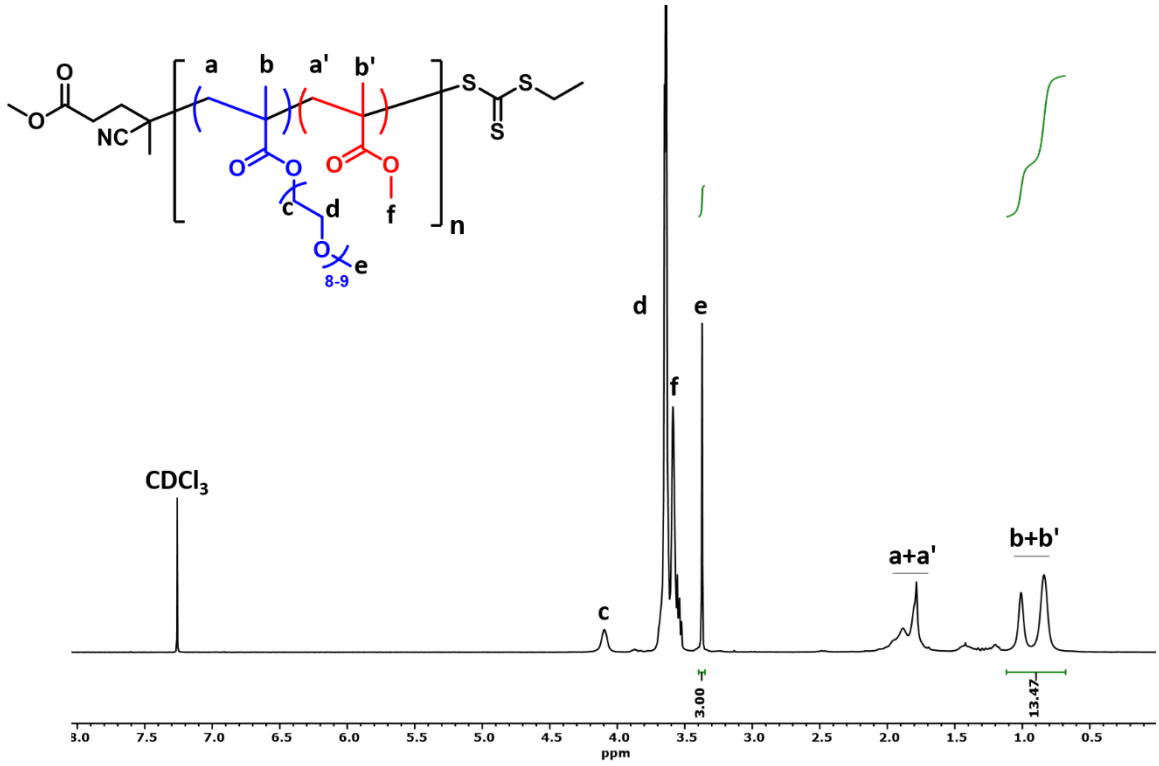


Figure S16. ^{1}H-NMR spectrum of P(OEGMA-*co*-MMA)$_{85}$ in $CDCl_3$ (300 MHz).

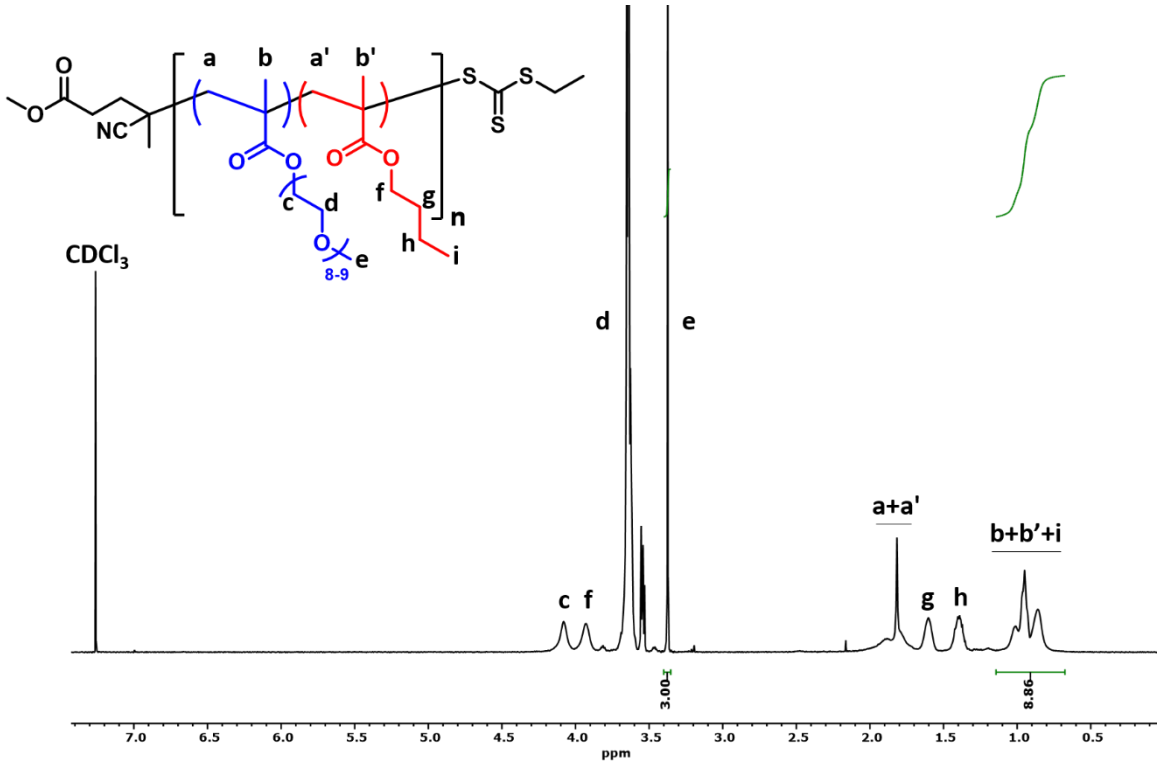


Figure S17. ^{1}H-NMR spectrum of P(OEGMA-*co*-BMA)$_{76}$ in $CDCl_3$ (300 MHz).

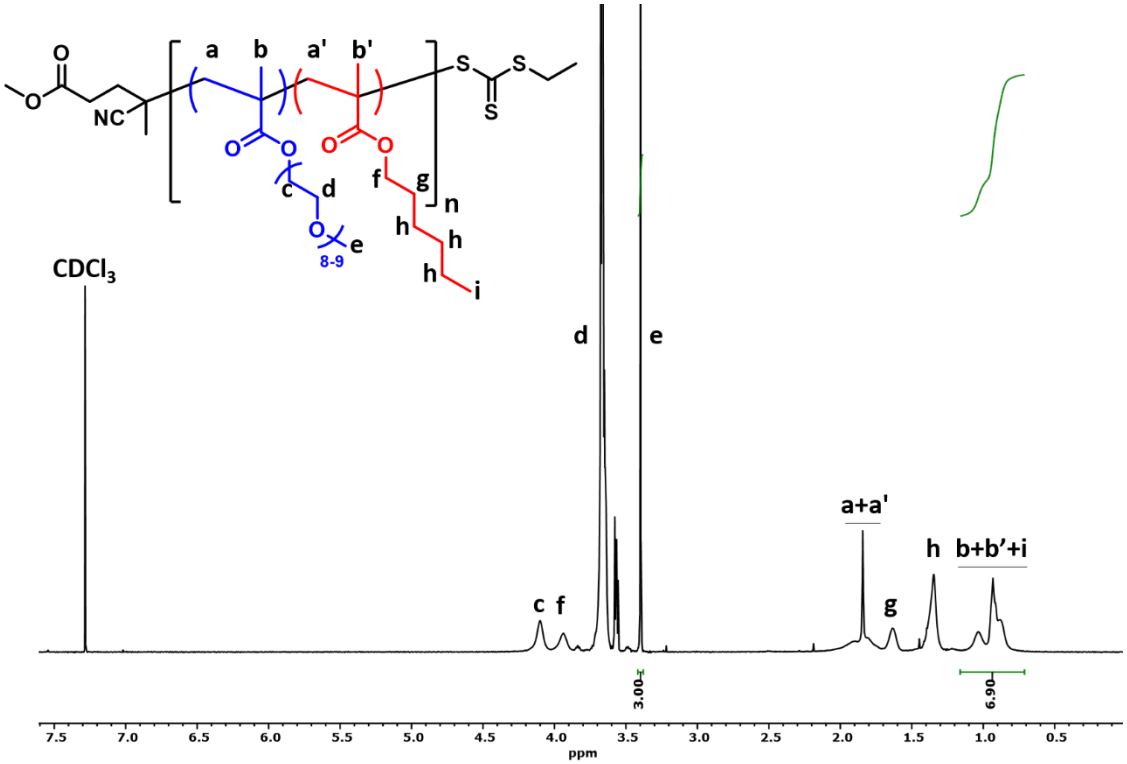


Figure S18. ^{1}H-NMR spectrum of P(OEGMA-*co*-HMA)$_{87}$ in $CDCl_3$ (300 MHz).

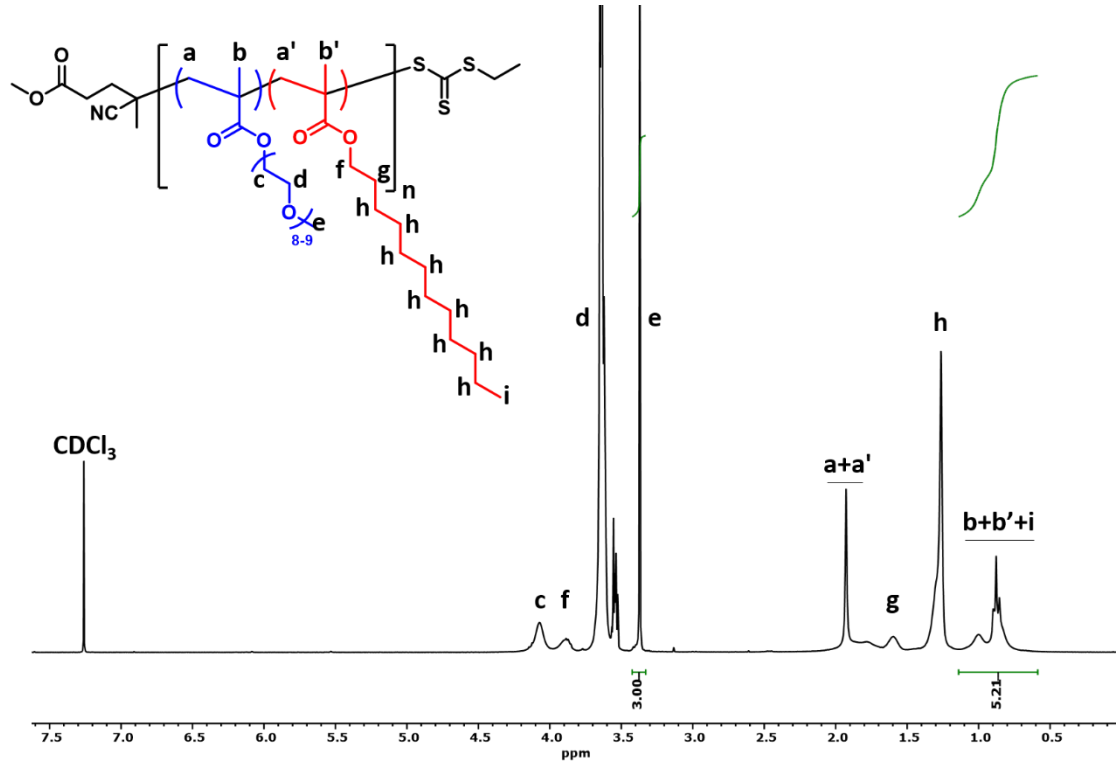


Figure S19. ^{1}H-NMR spectrum of P(OEGMA-*co*-LMA)$_{84}$ in $CDCl_3$ (300 MHz).

Table S6. T_{CP} of P(OEGMA$_{500}$-*co*-RMA) copolymers determined by UV-Vis spectrometry.

Polymer[a]	T_{CP} from UV-Vis (°C)[b]	Polymer[a]	T_{CP} from UV-Vis (°C)[b]
P(OEGMA$_{0.53}$-*co*-EMA$_{0.47}$)	66	**p(OEGMA$_{0.59}$-*co*-HMA$_{0.41}$)**	68
P(OEGMA$_{0.4}$-*co*-EMA$_{0.6}$)	61	**p(OEGMA$_{0.49}$-*co*-HMA$_{0.51}$)**	63
P(OEGMA$_{0.3}$-*co*-EMA$_{0.7}$)	55	**p(OEGMA$_{0.37}$-*co*-HMA$_{0.63}$)**	52
P(OEGMA$_{0.2}$-*co*-EMA$_{0.8}$)	44	**p(OEGMA$_{0.29}$-*co*-HMA$_{0.71}$)**	49
P(OEGMA$_{0.45}$-*co*-BMA$_{0.55}$)	62	**p(OEGMA$_{0.9}$-*co*-LMA$_{0.1}$)**	84
P(OEGMA$_{0.39}$-*co*-BMA$_{0.61}$)	55	**p(OEGMA$_{0.81}$-*co*-LMA$_{0.19}$)**	81
P(OEGMA$_{0.29}$-*co*-BMA$_{0.71}$)	43	**p(OEGMA$_{0.7}$-*co*-LMA$_{0.3}$)**	79

[a] Aqueous solution of copolymers were prepared at 5 mg mL^{-1} in nanopure water.
[b] Data obtained from the second heating of the samples within the temperature range of 20 °C to 93 °C at a heating rate of 1 °C min^{-1}.

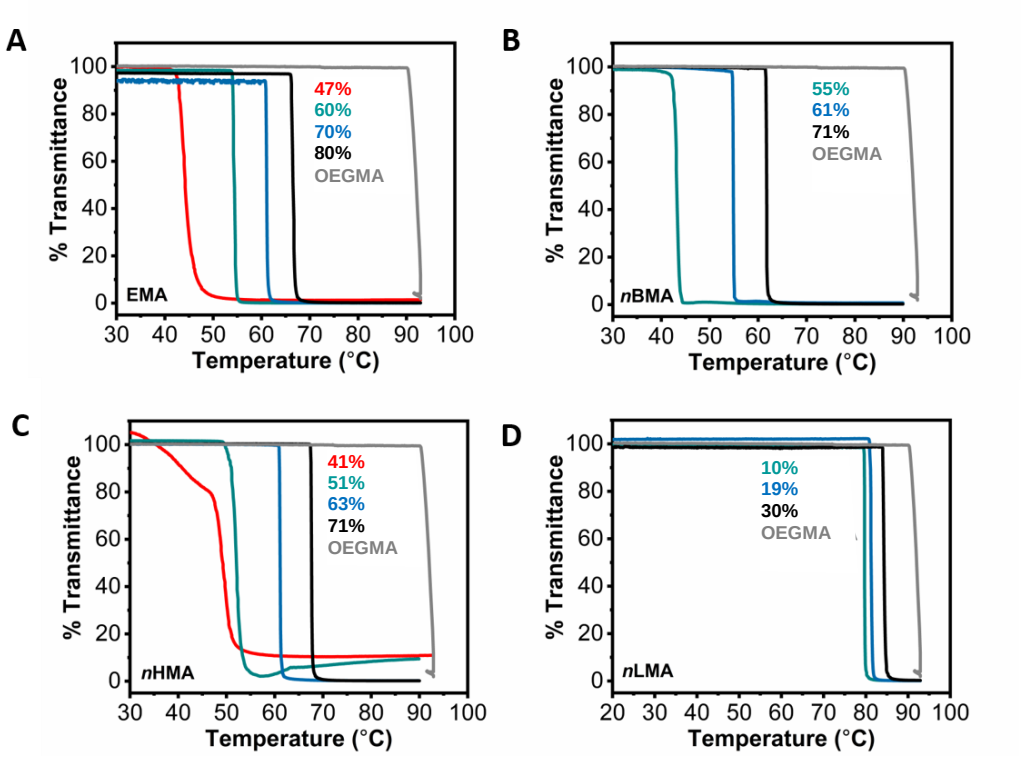


Figure S20. Turbidimetry analysis for P(OEGMA$_{500}$-*co*-RMA) copolymers determined by UV-Vis spectrometry (20 °C to 93 °C, 1 °C min^{-1}, recorded at λ = 550 nm) at 5 mg ml^{-1}.

Table S7. T_{CP} of P(OEGMA$_{500}$-*co*-RMA) copolymers determined by µDSC.

Polymer[a]	T_{CP} from µDSC (°C)[b]	Polymer[a]	T_{CP} from µDSC (°C) [b]
P(OEGMA$_{0.53}$-*co*-EMA$_{0.47}$)	66	**P(OEGMA$_{0.59}$-*co*-HMA$_{0.41}$)**	70
P(OEGMA$_{0.4}$-*co*-EMA$_{0.6}$)	61	**P(OEGMA$_{0.49}$-*co*-HMA$_{0.51}$)**	62
P(OEGMA$_{0.3}$-*co*-EMA$_{0.7}$)	54	**P(OEGMA$_{0.37}$-*co*-HMA$_{0.63}$)[c]**	56
P(OEGMA$_{0.2}$-*co*-EMA$_{0.8}$)	*d*	**P(OEGMA$_{0.29}$-*co*-HMA$_{0.71}$)**	50
P(OEGMA$_{0.45}$-*co*-BMA$_{0.55}$)	63	**P(OEGMA$_{0.9}$-*co*-LMA$_{0.1}$)**	84
P(OEGMA$_{0.39}$-*co*-BMA$_{0.61}$)	56	**P(OEGMA$_{0.81}$-*co*-LMA$_{0.19}$)**	82
P(OEGMA$_{0.29}$-*co*-BMA$_{0.71}$)	43	**P(OEGMA$_{0.7}$-*co*-LMA$_{0.3}$)**	80

[a] Aqueous solution of copolymers were prepared at 5 mg mL^{-1} in nanopure water.
[b] Data obtained by taking the first derivative of second heating of the samples within the temperature range of 0 °C to 115 °C at a heating rate of 0.5 °C min^{-1}.
[c] First derivative of second heating of P(OEGMA$_{0.37}$-*co*-nHMA$_{0.63}$) polymer did not give a peak. Therefore, T_{CP} data for this polymer was determined directly from the heating trace.
[d] Not determined.

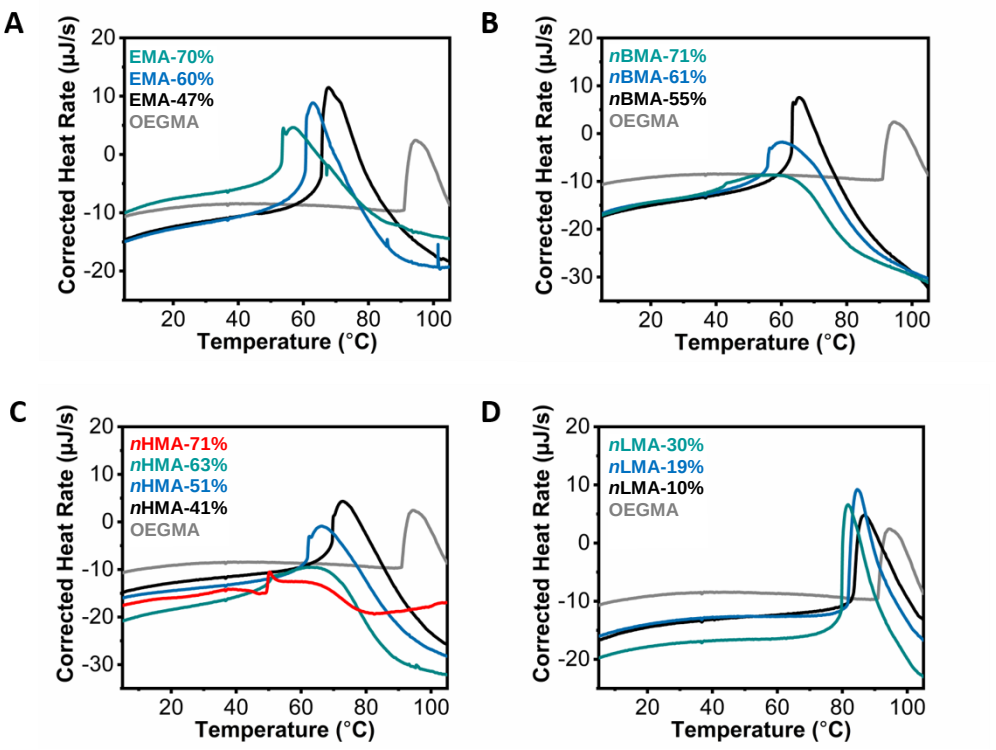


Figure S21. Turbidimetry analysis for P(OEGMA$_{500}$-*co*-RMA) copolymers determined by µDSC (0 °C to 115 °C, 0.5 °C min^{-1}) at 5 mg ml^{-1}.

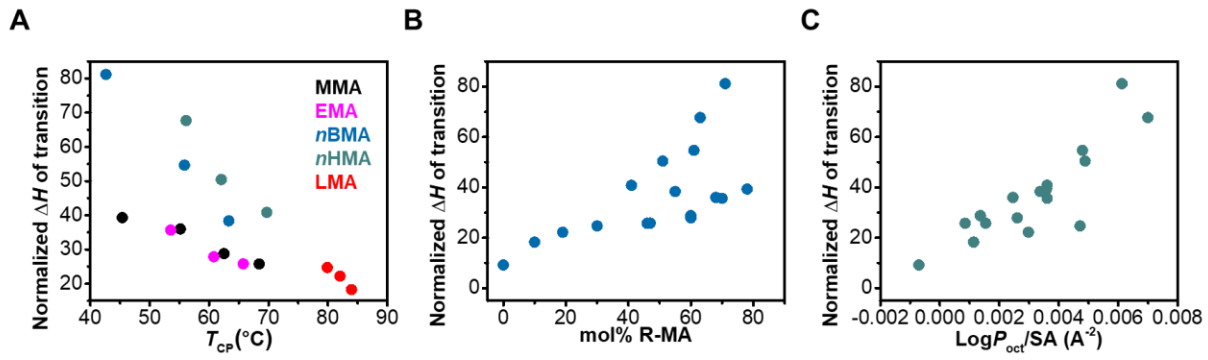


Figure S22. Normalized enthalpies of LCST phase transitions for the various P(OEGMA$_{500}$-*co*-RMA) copolymers as a function of T_{CP} (A), molar composition (B), or hydrophobicity (C) as determined by µDSC (0 °C to 115 °C, 0.5 °C min-1) at 5 mg ml^{-1}.

References

1. Blackman, L. D.; Gibson, M. I.; O'Reilly, R. K., Probing the causes of thermal hysteresis using tunable Nagg micelles with linear and brush-like thermoresponsive coronas. *Polym. Chem.* **2017,** *8* (1), 233-244.
2. *Materials Studio 2019*, Accelrys Software Inc.: San Diego, 2019.
3. Ghose, A. K.; Viswanadhan, V. N.; Wendoloski, J. J., Prediction of Hydrophobic (Lipophilic) Properties of Small Organic Molecules Using Fragmental Methods: An Analysis of ALOGP and CLOGP Methods. *J. Phys. Chem. A* **1998,** *102* (21), 3762-3772.
4. Min, K.; Cuiffi, J. D.; Mathers, R. T., Ranking environmental degradation trends of plastic marine debris based on physical properties and molecular structure. *Nat. Commun.* **2020,** *11* (1), 727.
5. Varlas, S.; Foster, J. C.; Arkinstall, L. A.; Jones, J. R.; Keogh, R.; Mathers, R. T.; O'Reilly, R. K., Predicting Monomers for Use in Aqueous Ring-Opening Metathesis Polymerization-Induced Self-Assembly. *ACS Macro Letters* **2019,** *8* (4), 466-472.
6. Foster, J. C.; Varlas, S.; Couturaud, B.; Jones, J. R.; Keogh, R.; Mathers, R. T.; O'Reilly, R. K., Predicting Monomers for use in Polymerization Induced Self-Assembly. *Angew. Chem. Int. Ed.* **2018,** *57* (48), 15733-15737.
7. Dharmaratne, N. U.; Jouaneh, T. M. M.; Kiesewetter, M. K.; Mathers, R. T., Quantitative Measurements of Polymer Hydrophobicity Based on Functional Group Identity and Oligomer Length. *Macromolecules* **2018**.
8. Sun, H.; Jin, Z.; Yang, C. W.; Akkermans, R. L. C.; Robertson, S. H.; Spenley, N. A.; Miller, S.; Todd, S. M., COMPASS II: extended coverage for polymer and drug-like molecule databases. *J. Mol. Model.* **2016,** *22* (2).
9. Kuhn, M., Building Predictive Models in R Using the caret Package. *J. Stat. Softw.* **2008,** *28* (5), 26.

Chapter 3. LogP_{oct}/SA Predicts the Thermoresponsive Behavior of P(DMA-*co*-RA) Statistical Copolymers

3.1. Manuscript details and overview

Title: LogP_{oct}/SA Predicts the Thermoresponsive Behavior of P(DMA-*co*-RA) Statistical Copolymers

Authors: **Irem Akar**,[†] Jeffrey C. Foster,[†] Xiyue Leng,[†] Amanda Pearce,[†] Robert. T. Mathers[*,§] and Rachel K. O'Reilly[*,†]

Affiliations: [†]School of Chemistry, University of Birmingham, Edgbaston, Birmingham B15 2TT, United Kingdom

[§]Department of Chemistry, Pennsylvania State University, New Kensington Pennsylvania 15068, United States

Journal: ACS Macro Letters

Year: 2022

Volume: 11

Page numbers: 498-503

DOI: 10.1021/acsmacrolett. 1c00776

Submitted: 10 December 2021

Published: 22 March 2022

Copyright statement: "*This is an open access article published under an ACS AuthorChoice License, which permits copying and redistribution of the article or any adaptations for non-commercial purposes*." Copyright 2022 American Chemical Society.

Permissions: This article and its supporting information are available on the ACS Publications website at https://pubs.acs.org/doi/full/10.1021/acsmacrolett.1c00776. Further permissions related to the material excerpted should be directed to the ACS Publications Support.

Co-author contributions: Dr Jeffrey C. Foster provided synthetic and technical advice. Ms. Xiyue Leng provided aid with the synthesis of polymers. Dr Amanda K. Pearce provided synthetic and technical advice in addition to editing the manuscript. Prof. Robert T. Mathers provided advice on the computational calculations. Prof. Rachel O'Reilly supervised the project, provided guidance, and edited the manuscript.

Overview: In this Chapter, based on the information gained from the previous chapter, we sought to establish correlations between polymer hydrophobicity and LCST behavior when using non-brushy monomers. Using series of polymers based on *N, N*-dimethylacrylamide (DMA) and various alkyl acrylates (*n*-butyl, benzyl, tetrahydrofurfuryl and *tert*-butyl acrylate), a library of copolymers were synthesized by varying the mol% of the alkyl acrylates in each copolymer series. Similarly to our previous study, thermoresponsive behavior of the copolymers were determined by measuring their T_{CP}, and hydrophobicity was determined by calculating the LogP_{oct}/SA by using a computational tool. We were able to demonstrate a good correlation between T_{CP} and LogP_{oct}/SA for P(DMA-*co*-RA) copolymers. In order to validate this finding, T_{CP} of a new non-brushy copolymer, P(DMA-*co*-MMA), was predicted prior to synthesis.

Of particular importance, this study shows and validates a method to predict the T_{CP} of thermoresponsive copolymers derived from monomers which produce nonresponsive homopolymers (DMA and alkyl acrylates). In such cases, conventional methods like the Flory-

Fox equation cannot be used for predicting their thermal behavior, and thus this study provides an invaluable predictive tool for designing new thermoresponsive polymers.

We believe that our study holds great potential as a guiding principle, as it shows that copolymer LCST behavior can be tuned *via* changing hydrophobic composition of non-brushy copolymers in a manner that is predictable using computational tools. Overall, this provides a significant advance and guidance for generating design rules for functional polymers with precisely defined LCST.

ACS Macro Letters

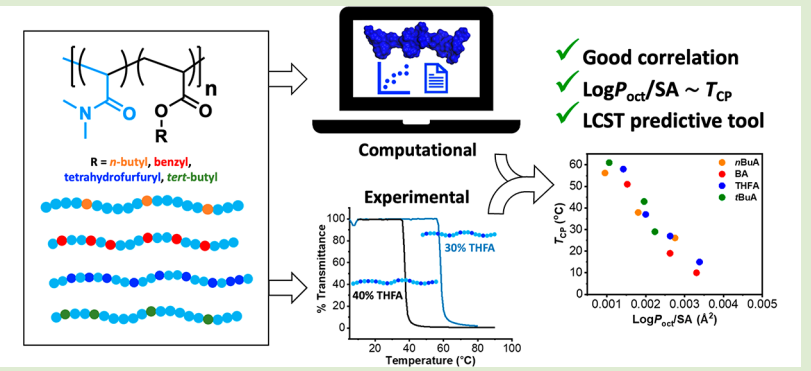
pubs.acs.org/macroletters Letter

Log P_{oct}/SA Predicts the Thermoresponsive Behavior of P(DMA-*co*-RA) Statistical Copolymers

Irem Akar, Jeffrey C. Foster, Xiyue Leng, Amanda K. Pearce, Robert T. Mathers,* and Rachel K. O'Reilly*

Cite This: *ACS Macro Lett.* 2022, 11, 498−503 Read Online

ACCESS | Metrics & More | Article Recommendations | Supporting Information



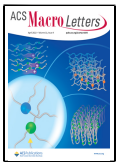
ABSTRACT: Polymers that exhibit a lower critical solution temperature (LCST) have been of great interest for various biological applications such as drug or gene delivery, controlled release systems, and biosensing. Tuning the LCST behavior through control over polymer composition (e.g., upon copolymerization of monomers with different hydrophobicity) is a widely used method, as the phase transition is greatly affected by the hydrophilic/hydrophobic balance of the copolymers. However, the lack of a general method that relates copolymer hydrophobicity to their temperature response leads to exhaustive experiments when seeking to obtain polymers with desired properties. This is particularly challenging when the target copolymers are comprised of monomers that individually form nonresponsive homopolymers, that is, only when copolymerized do they display thermoresponsive behavior. In this study, we sought to develop a predictive relationship between polymer hydrophobicity and cloud point temperature (T_{CP}). A series of statistical copolymers were synthesized based on hydrophilic *N*,*N*-dimethyl acrylamide (DMA) and hydrophobic alkyl acrylate monomers, and their hydrophobicity was compared using surface area-normalized octanol/water partition coefficients (Log P_{oct}/SA). Interestingly, a correlation between the Log P_{oct}/SA of the copolymers and their T_{CP}s was observed for the P(DMA-*co*-RA) copolymers, which allowed T_{CP} prediction of a demonstrative copolymer P(DMA-*co*-MMA). These results highlight the strong potential of this computational tool to improve the rational design of copolymers with desired temperature responses prior to synthesis.

Downloaded via 92.45.251.68 on January 22, 2023 at 23:02:37 (UTC).
See https://pubs.acs.org/sharingguidelines for options on how to legitimately share published articles.

"Smart" polymers that change their physical or chemical structures upon exposure to external stimuli such as light, pH, redox state, ultrasound, and temperature have been used extensively in a range of applications from biosensors to drug delivery systems.[1−5] Among these stimuli, temperature has been the most widely studied on account of its easy external applicability and the abundance of methods to tune thermoresponsive behavior within the desired range.[6] Thermoresponsive polymers display either a lower critical solution temperature (LCST) or an upper critical solution temperature (UCST) behavior in water, where they undergo structural changes and thus changes in their solubility upon heating up above or cooling down below a specific temperature, respectively.[3,7] In general, LCST-based systems are more preferable than UCST-based systems, particularly for biological applications, because of the high-temperature requirements of the latter.[8,9] In an LCST-based system, polymers are soluble below their LCST on account of strong interactions between polymer chains and the solvent (water); however, upon heating above a specific temperature, they undergo a phase transition where they become immiscible as a consequence of the weakening of the polymer−solvent interactions.[10]

It is desirable to be able to tune polymer LCST temperatures in order to suit the requirements of a particular application.

Received: December 10, 2021
Accepted: February 7, 2022
Published: March 22, 2022



ACS Publications

© 2022 The Authors. Published by American Chemical Society

Several methods have been studied toward this, such as changing the polymer molecular weight, hydrophobicity, or solution concentration.[11−16] In particular, tuning polymer hydrophobicity is an interesting strategy, as changes to overall hydrophobicity can readily modulate polymer−solvent interactions.[17] For example, Sumerlin and Vogt reported a method to decrease poly(*N*-isopropylacrylamide) (PNIPAM) LCST by moving from a linear to branched architecture, which increased polymer hydrophobicity through an increase in hydrophobic end groups. They confirmed that the hydrophobic end groups had the greatest impact on polymer LCST (rather than branching) by showing that polymer LCSTs increased significantly upon removal of the end groups.[18] Another route to tune polymer hydrophobicity is via copolymerization of a high LCST monomer with monomers of lower LCST.[19−24] For example, Lutz and Hoth reported copolymers of oligoethylene glycol monomethyl ether methacrylate (OEGMA) and diethylene glycol methacrylate (DEGMA) where they showed that the cloud point temperature (T_{CP}) of the copolymers decreased from 90 to 28 °C as the molar quantity of DEGMA increased.[25] Additionally, previous work has shown linear correlations of T_{CP} to hydrophobic mole fraction for copolymers of *N*-isopropylacrylamide (NiPA) and *N*-isopropylmethacrylamide (NiPMA) and poly(ethylene glycol) monomethyl ether methacrylate (PEGMA) and methyl methacrylate (MMA);[26,27] however, nonlinear T_{CP} behavior has also been reported.[28] These inconsistencies could be due to differences in experimentation, chain end effects, or the type of polymerization employed. Thus, despite some work in the field to date, there are still fundamental gaps in our understanding of how LCST behavior can be tuned using copolymerization, such as isolating the effect of polymer structure and specific monomer chemistry. Specifically, the ability to generate overall design rules for achieving desired thermoresponsive behavior would contribute essential knowledge toward the design of copolymers for many given applications.

Hydrophobicity is one of the most important phenomena that has been investigated to explain polymer behavior in bulk or solution; however, the influence of polymer hydrophobicity on solution behavior from a theoretical perspective is relatively underexplored.[29] In medicinal chemistry, hydrophobicity of small molecules can be quantified via octanol−water partition coefficient (Log P_{oct}) calculations, which describes the partitioning of a substance between octanol and water.[30,31] Inspired by this, Mathers and co-workers sought to adapt this method to computationally predict the hydrophobicity of macromolecules, developing a surface-area-normalized method (Log P_{oct}/SA). Subsequent studies have shown that the addition of the surface area normalization improves the predictive power for polymers compared to standard small molecule methods.[32−36]

In our previous study we were interested in correlating the polymer hydrophobicity to its LCST behavior by investigating the relationship between the Log P_{oct}/SA of a series of statistical copolymers of hydrophilic OEGMA with different hydrophobic methacrylate comonomers (Figure 1A). We aimed to determine a correlation between a polymer hydrophobicity and its T_{CP}, thereby reducing the experimental workload by predicting the T_{CP} of new copolymers prior to synthesis. However, we found that the strongest influence of the copolymer T_{CP} was the hydrophobic comonomer mol %, that is, the grafting density rather than the chemical identity of

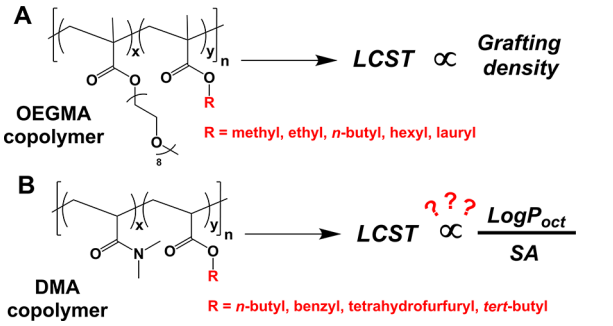


Figure 1. Our studies on how hydrophobicity influences thermoresponsive behavior of (A) brushy polymers and (B) nonbrushy polymers.

the comonomers, as the brushy nature of the OEGMA dominated the phase transition.[21] This finding inspired us to investigate whether a correlation could be found between polymer hydrophobicity and the T_{CP} when using nonbrushy monomers; thus, providing a route to uniquely tune polymer LCST behavior using specific monomer chemistry (Figure 1B).

With the goal of realizing this, we selected hydrophilic *N*,*N*-dimethyl acrylamide (DMA) as our nonbrushy monomer of interest, due to its simple chain structure and commercial availability, and alkyl acrylates such as *n*-butyl acrylate (*n*BuA), benzyl acrylate (BA), tetrahydrofurfuryl acrylate (THFA), and *tert*-butyl acrylate (*t*BuA) for the hydrophobic component on account of their commercial availability and compatibility with polymerization conditions. Interestingly, to the best of our knowledge, no literature studies report DMA homopolymers displaying LCST behaviors under the dilute conditions that are typically employed during T_{CP} measurements (ca. 1−10 mg mL^{-1} polymer), with only one study by Fischer et al. reporting a DMA homopolymer with a very high T_{CP} at a solution concentration of 20 mg mL^{-1}.[37] Thus, our aim was two-fold: to not only establish correlations for polymer hydrophobicity and T_{CP}, but to investigate the intriguing LCST behavior of this largely nonthermoresponsive monomer at lower concentrations and temperature windows.

To this end, we initially synthesized a library of copolymers based on DMA and various hydrophobic alkyl acrylates (RA, R = *n*-butyl, benzyl, tetrahydrofurfuryl, and *tert*-butyl) in order to observe the effect of monomer chemistry and copolymer composition and studied their LCST response. T_{CP} was used as a proxy of the LCST behavior as it is a macroscopic effect that can be detected easily via dynamic light scattering,[38] differential scanning calorimetry,[39] microdifferential scanning calorimetry,[21] and UV−vis spectroscopy.[21] Then, we attempted to correlate the T_{CP} of the copolymers to their hydrophobicity, which was determined by calculating the Log P_{oct}/SA of oligomeric models representative of the final copolymers. Overall, copolymer MW and the targeted hydrophobic mol % were maintained as consistently as possible across each series. The copolymers were prepared via reversible addition−fragmentation chain transfer (RAFT) polymerization in 1,4-dioxane for 4 h until targeted DPs were reached (Figure 2A). The final molar composition of the purified copolymers was determined using ^{1}H NMR spectroscopy by relative integration of resonances corresponding to each monomer (Figures 2B and S1−S4). Kinetic analysis showed that both DMA and RA monomers were consumed at

https://doi.org/10.1021/acsmacrolett.1c00776
ACS Macro Lett. 2022, 11, 498−503

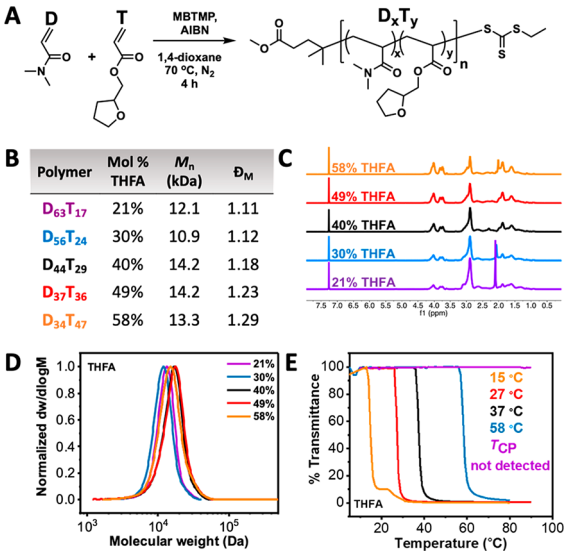


Figure 2. (A) Synthetic scheme for the preparation of P(DMA-*co*-RA) statistical copolymers. THFA is used as the comonomer in this example. (B) Molar composition (determined by ^{1}H NMR spectroscopy), number-average MW (M_n), and dispersity ($Đ_M$; determined by SEC) of P(DMA-*co*-THFA) copolymers. (C) ^{1}H NMR spectra of P(DMA-*co*-THFA) copolymers in $CDCl_3$ (300 MHz). (D) Normalized SEC molecular weight distributions for the P(DMA-*co*-THFA) series (eluent: $CHCl_3$ + 0.5 v/v% NEt_3, PMMA standards). (E) Percent transmittance as a function of temperature for the P(DMA-*co*-THFA) copolymers dissolved in H_2O at 10 mg/mL as measured by UV−vis spectroscopy (λ = 550 nm, 0−90 °C, 1 °C min^{-1}).

an approximately equal rate, confirming the statistical nature of the copolymerizations (Figures S5−S8). Molecular weight distributions (MWDs) for the P(DMA-*co*-RA) copolymers were determined using size-exclusion chromatography (SEC). Copolymers were obtained with narrow and symmetrical MWDs (Figures 2D and S6−S8). Variations in number-average MW (M_n) and dispersity ($Đ_M$) values were determined by calculating the coefficients of variance. Using this measure, M_n varied by only 2% across the entire data set, while $Đ_M$ varied by 0.04% with all values <1.36. Turbidity measurements were conducted using UV−vis spectroscopy in order to measure the T_{CP} of the copolymers. Changes in the percentage transmittance were recorded at λ = 550 nm within the temperature range of 0 to 90 °C. Temperature points that correspond to 50% transmittance values were taken as the T_{CP} of polymers (see Supporting Information for a detailed method). In general, an inverse relationship was observed between the T_{CP} of P(DMA-*co*-RA) copolymers and the RA content (Figures 2E and S9).

Log P_{oct} values of short oligomer models that represent each P(DMA-*co*-RA) copolymer were calculated (at T = 298 K) for quantifying hydrophobicity. Then, the Log P_{oct} value of each representative model was normalized by surface area using Molecular Dynamics (MD) simulations (see Supporting Information for a detailed model). Normalizing a thermodynamic parameter (i.e., Log P_{oct}) with a structural parameter (i.e., SA) facilitates comparison of architectural differences resulting from monomer size and functionality as well as oligomer length.[36,40,41] Furthermore, this strategy conforms to the Lum−Chandler−Weeks theory, which states that above a critical length scale, hydrophobicity scales with surface area rather than volume.[29,42] Consequently, Log P_{oct}/SA values provide a general method for correlating hydrophobicity to T_{CP} that accommodates models with enough repeating units to represent the actual polymer. Figure 3A shows the repeating

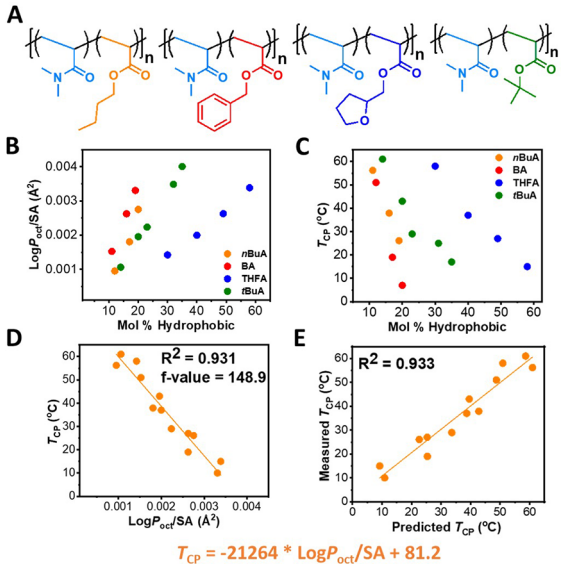


Figure 3. (A) Chemical structures of the repeating units for the P(DMA-*co*-*n*BuA), P(DMA-*co*-BA), P(DMA-*co*-THFA), and P(DMA-*co*-*t*BuA) copolymers, respectively. (B) Calculated Log P_{oct}/SA values for P(DMA-*co*-RA) copolymer oligomers as a function of the mol % of the hydrophobic comonomer. (C) Plot of T_{CP} as measured by UV−vis spectroscopy vs the mol % of hydrophobic comonomer. (D) Plot of T_{CP} as measured by UV−vis spectroscopy vs the calculated Log P_{oct}/SA values for P(DMA-*co*-RA) copolymer oligomers. The solid line represents a linear fit of these data. (E) Comparison between measured T_{CP} values of P(DMA-*co*-RA) copolymers and those predicted from their Log P_{oct}/SA. The solid line represents a linear fit of these data. The equation was generated using the linear fit of the data in the plot of Figure 3D.

units for each of the P(DMA-*co*-RA) copolymers that were used to build oligomer models to calculate the Log P_{oct}/SA values. The length of the oligomer models varied between 17 and 27 units and the models were built based on the hydrophobic mol % that each copolymer contains (see Supporting Information for detailed model). Log P_{oct}/SA increased as the hydrophobic mol % in the copolymers increased, confirming the relationship between hydrophobicity and Log P_{oct} (Figure 3B).[36] Comonomers *n*BuA, BA, and *t*BuA produced copolymers with similar slopes, while P(DMA-*co*-THFA) copolymers differed from the others. The ether oxygen in the tetrahydrofuran ring of THFA had a significant influence on Log P_{oct}/SA values. Importantly, this data demonstrates that the comonomer chemistry plays an important role in overall hydrophobicity of P(DMA-*co*-RA) copolymers. Figure 3C shows the inverse linear relationships between the hydrophobic mol % and T_{CP} of the copolymers for each series. Linear regression data for each series is shown in Table S3. This clearly illustrates that the increase in the hydrophobic comonomer content results in an increase in the overall copolymer hydrophobicity, causing the copolymer T_{CP} to decrease. Motivated by this, we next plotted the calculated Log P_{oct}/SA values against the measured T_{CP}s in order to see if any correlation could be built. Figure 3D shows the inverse relationship between the Log P_{oct}/SA (polymer hydro-

https://doi.org/10.1021/acsmacrolett.1c00776
ACS Macro Lett. 2022, 11, 498−503

phobicity) and the T_{CP} of P(DMA-*co*-RA) copolymers with each series possessing a similar slope. This indicates that copolymer hydrophobicity can be directly correlated to its T_{CP} for these nonbrushy copolymers, unlike the OEGMA-based brushy copolymers we studied in our previous work. Of importance, the data shown in Figure 3D was fitted using linear, exponential, and polynomial fits. We found that the prediction capability of the linear fit was superior to the polynomial fit and very similar to the exponential fit in terms of the similarity of the measured and calculated T_{CP} of the P(DMA-*co*-RA) copolymers. Therefore, we chose the linear fit for the T_{CP} prediction due to its greater simplicity. Comparison of the measured and predicted T_{CP} for P(DMA-*co*-RA) copolymers showed a reasonably strong correlation, suggesting that this tool could be used for predicting the T_{CP} of new nonbrushy copolymers (Figure 3E). Thus, we suggest that the experimental T_{CP} of new copolymers can be reliably predicted using this computational method.

It is important to note the significance of these findings in the context of facilitating the targeted design of new copolymers based on monomers known to produce non-responsive homopolymers. In such cases, conventional methods like the Flory−Fox equation, which determines the thermal properties of polymers based on both weight fraction and thermoresponse of the two homopolymers, cannot be used. Therefore, the predictive tool developed in this work significantly increases ease of access to new thermoresponsive copolymers with varied chemistries and tunable on-demand temperature responses.

Finally, to prove this hypothesis, we chose to design a new copolymer of DMA and the well-known hydrophobic monomer methyl methacrylate (MMA), which was one of the hydrophobic comonomers used in our previous work.

Log P_{oct}/SA of the P(DMA-*co*-MMA) copolymer with 31% hydrophobic mol % was calculated prior to synthesis, giving a predicted T_{CP} of 41 °C when using the equation generated based on the relationship between Log P_{oct}/SA and measured T_{CP}. Following the polymer synthesis, the measured T_{CP} of the copolymer was determined as 42 °C using UV−vis spectroscopy. This confirmed that the T_{CP} of new copolymers could be predicted using this guidance with only minor deviations from the targeted T_{CP}. Interestingly, unlike the P(DMA-*co*-RA) polymerizations, the copolymerization of DMA and MMA yielded a copolymer with a gradient topology (Figure S10). Based on the fact that Log P_{oct}/SA could still predict T_{CP} for this copolymer, it was hypothesized that the exact copolymer sequence may not be a critical determinant of thermoresponsiveness. Further investigation is warranted to test this hypothesis.

To conclude, we report the synthesis of a series of thermoresponsive P(DMA-*co*-RA) copolymers via copolymerization of DMA and different alkyl acrylate monomers and the investigation of their LCST behavior by measuring the copolymer T_{CP}s using UV−vis spectroscopy. Analysis of our experimental data using computational modeling of Log P_{oct}/SA revealed that the thermoresponsive behavior of nonbrushy P(DMA-*co*-RA) copolymers could be related to their hydrophobicity. We validated this method by predicting the T_{CP} of a P(DMA-*co*-MMA), which showed good correlation with the experimentally measured T_{CP} (1 °C difference from targeted T_{CP}). Overall, this study demonstrates the strength of the Log P_{oct}/SA computational modeling tool for the prediction of copolymer interactions in solution. We envisage this to be particularly powerful in the study of thermoresponsive copolymers comprised of monomers that produce non-responsive homopolymers, thus, widening access to new monomer chemistries that can be used in the rational design of polymers with thermoresponsive behavior.

■ ASSOCIATED CONTENT

Supporting Information

The Supporting Information is available free of charge at https://pubs.acs.org/doi/10.1021/acsmacrolett.1c00776.

Materials, characterization techniques, experimental procedures, and additional data (SEC, ^{1}H NMR, and UV−vis spectra) (PDF)

■ AUTHOR INFORMATION

Corresponding Authors

Robert T. Mathers − *Department of Chemistry, Pennsylvania State University, New Kensington, Pennsylvania 15068, United States;* orcid.org/0000-0002-0503-4571; Email: rtm11@psu.edu

Rachel K. O'Reilly − *School of Chemistry, University of Birmingham, Edgbaston, Birmingham B15 2TT, United Kingdom;* orcid.org/0000-0002-1043-7172; Email: r.oreilly@bham.ac.uk

Authors

Irem Akar − *School of Chemistry, University of Birmingham, Edgbaston, Birmingham B15 2TT, United Kingdom*

Jeffrey C. Foster − *School of Chemistry, University of Birmingham, Edgbaston, Birmingham B15 2TT, United Kingdom;* orcid.org/0000-0002-9097-8680

Xiyue Leng − *School of Chemistry, University of Birmingham, Edgbaston, Birmingham B15 2TT, United Kingdom*

Amanda K. Pearce − *School of Chemistry, University of Birmingham, Edgbaston, Birmingham B15 2TT, United Kingdom;* orcid.org/0000-0003-3372-7380

Complete contact information is available at: https://pubs.acs.org/10.1021/acsmacrolett.1c00776

Author Contributions

The manuscript was written through contributions of all authors.

Notes

The authors declare no competing financial interest.

■ ACKNOWLEDGMENTS

This work is supported by the Turkish Ministry of National Education, the Engineering and Physical Sciences Research Council, EPSRC, (EP/S00338X/1), and the University of Birmingham.

■ REFERENCES

(1) Dai, S.; Ravi, P.; Tam, K. C. pH-Responsive polymers: synthesis, properties and applications. *Soft Matter* **2008**, *4* (3), 435−449.

(2) Gibson, M. I.; O'Reilly, R. K. To aggregate, or not to aggregate? considerations in the design and application of polymeric thermally-responsive nanoparticles. *Chem. Soc. Rev.* **2013**, *42* (17), 7204−7213.

(3) Jochum, F. D.; Theato, P. Temperature- and light-responsive smart polymer materials. *Chem. Soc. Rev.* **2013**, *42* (17), 7468−7483.

(4) Zhang, A.; Jung, K.; Li, A.; Liu, J.; Boyer, C. Recent advances in stimuli-responsive polymer systems for remotely controlled drug release. *Prog. Polym. Sci.* **2019**, *99*, 101164.

(5) Zhang, X.; Han, L.; Liu, M.; Wang, K.; Tao, L.; Wan, Q.; Wei, Y. Recent progress and advances in redox-responsive polymers as controlled delivery nanoplatforms. *Mater. Chem. Front.* **2017**, *1* (5), 807−822.
(6) Roy, D.; Brooks, W. L. A.; Sumerlin, B. S. New directions in thermoresponsive polymers. *Chem. Soc. Rev.* **2013**, *42* (17), 7214−7243.
(7) Zhang, Q.; Hoogenboom, R. Polymers with upper critical solution temperature behavior in alcohol/water solvent mixtures. *Prog. Polym. Sci.* **2015**, *48*, 122−142.
(8) Vanparijs, N.; Nuhn, L.; De Geest, B. G. Transiently thermoresponsive polymers and their applications in biomedicine. *Chem. Soc. Rev.* **2017**, *46* (4), 1193−1239.
(9) Doberenz, F.; Zeng, K.; Willems, C.; Zhang, K.; Groth, T. Thermoresponsive polymers and their biomedical application in tissue engineering - a review. *J. Mater. Chem. B* **2020**, *8* (4), 607−628.
(10) Zhang, Q.; Weber, C.; Schubert, U. S.; Hoogenboom, R. Thermoresponsive polymers with lower critical solution temperature: from fundamental aspects and measuring techniques to recommended turbidimetry conditions. *Mater. Horiz.* **2017**, *4* (2), 109−116.
(11) Ieong, N. S.; Hasan, M.; Phillips, D. J.; Saaka, Y.; O'Reilly, R. K.; Gibson, M. I. Polymers with molecular weight dependent LCSTs are essential for cooperative behaviour. *Polym. Chem.* **2012**, *3* (3), 794−799.
(12) Liu, Z.; Guo, Y.; Inomata, K. LCST-type phase behavior of poly(2-chloroethyl vinyl ether-alt-maleic anhydride) in n-butyl acetate. *Polym. J.* **2011**, *43* (8), 676−682.
(13) Keogh, R.; Blackman, L. D.; Foster, J. C.; Varlas, S.; O'Reilly, R. K. The Importance of Cooperativity in Polymer Blending: Toward Controlling the Thermoresponsive Behavior of Blended Block Copolymer Micelles. *Macromol. Rapid Commun.* **2020**, *41* (6), 1900599.
(14) Miclotte, M. P. J.; Lawrenson, S. B.; Varlas, S.; Rashid, B.; Chapman, E.; O'Reilly, R. K. Tuning the Cloud-Point and Flocculation Temperature of Poly(2-(diethylamino)ethyl methacrylate)-Based Nanoparticles via a Postpolymerization Betainization Approach. *ACS Polym. Au* **2021**, *1* (1), 47−58.
(15) Ramírez-Jiménez, A.; Montoya-Villegas, K. A.; Licea-Claverie, A.; Gónzalez-Ayón, M. A. Tunable Thermo-Responsive Copolymers from DEGMA and OEGMA Synthesized by RAFT Polymerization and the Effect of the Concentration and Saline Phosphate Buffer on Its Phase Transition. *Polymer* **2019**, *11* (10), 1657.
(16) Van Guyse, J. F. R.; Bera, D.; Hoogenboom, R. Adamantane Functionalized Poly(2-oxazoline)s with Broadly Tunable LCST-Behavior by Molecular Recognition. *Polymer* **2021**, *13* (3), 374.
(17) Eggenhuisen, T. M.; Becer, C. R.; Fijten, M. W. M.; Eckardt, R.; Hoogenboom, R.; Schubert, U. S. Libraries of Statistical Hydroxypropyl Acrylate Containing Copolymers with LCST Properties Prepared by NMP. *Macromolecules.* **2008**, *41* (14), 5132−5140.
(18) Vogt, A. P.; Sumerlin, B. S. Tuning the Temperature Response of Branched Poly(N-isopropylacrylamide) Prepared by RAFT Polymerization. *Macromolecules.* **2008**, *41* (20), 7368−7373.
(19) Smith, A. A. A.; Maikawa, C. L.; Lopez Hernandez, H.; Appel, E. A. Controlling properties of thermogels by tuning critical solution behaviour of ternary copolymers. *Polym. Chem.* **2021**, *12* (13), 1918−1923.
(20) Luzon, M.; Boyer, C.; Peinado, C.; Corrales, T.; Whittaker, M.; Tao, L.; Davis, T. P. Water-soluble, thermoresponsive, hyperbranched copolymers based on PEG-methacrylates: Synthesis, characterization, and LCST behavior. *J. Polym. Sci. A: Polym. Chem.* **2010**, *48* (13), 2783−2792.
(21) Akar, I.; Keogh, R.; Blackman, L. D.; Foster, J. C.; Mathers, R. T.; O'Reilly, R. K. Grafting Density Governs the Thermoresponsive Behavior of P(OEGMA-co-RMA) Statistical Copolymers. *ACS Macro Lett.* **2020**, *9* (8), 1149−1154.
(22) Fournier, D.; Hoogenboom, R.; Thijs, H. M. L.; Paulus, R. M.; Schubert, U. S. Tunable pH- and Temperature-Sensitive Copolymer Libraries by Reversible Addition-Fragmentation Chain Transfer Copolymerizations of Methacrylates. *Macromolecules* **2007**, *40* (4), 915−920.
(23) Bebis, K.; Jones, M. W.; Haddleton, D. M.; Gibson, M. I. Thermoresponsive behaviour of poly[(oligo(ethyleneglycol methacrylate)]s and their protein conjugates: importance of concentration and solvent system. *Polym. Chem.* **2011**, *2* (4), 975−982.
(24) Porsch, C.; Hansson, S.; Nordgren, N.; Malmström, E. Thermo-responsive cellulose-based architectures: tailoring LCST using poly(ethylene glycol) methacrylates. *Polym. Chem.* **2011**, *2* (5), 1114−1123.
(25) Lutz, J.-F.; Hoth, A. Preparation of Ideal PEG Analogues with a Tunable Thermosensitivity by Controlled Radical Copolymerization of 2-(2-Methoxyethoxy)ethyl Methacrylate and Oligo(ethylene glycol) Methacrylate. *Macromolecules* **2006**, *39* (2), 893−896.
(26) Kokufuta, M. K.; Sato, S.; Kokufuta, E. LCST behavior of copolymers of N-isopropylacrylamide and N-isopropylmethacrylamide in water. *Colloid Polym. Sci.* **2012**, *290* (16), 1671−1681.
(27) Kumbhakar, K.; Saha, B.; De, P.; Biswas, R. Cloud Point Driven Dynamics in Aqueous Solutions of Thermoresponsive Copolymers: Are They Akin to Criticality Driven Solution Dynamics? *J. Phys. Chem. B* **2019**, *123* (51), 11042−11054.
(28) Liu, H. Y.; Zhu, X. X. Lower critical solution temperatures of N-substituted acrylamide copolymers in aqueous solutions. *Polymer* **1999**, *40* (25), 6985−6990.
(29) Foster, J. C.; Akar, I.; Grocott, M. C.; Pearce, A. K.; Mathers, R. T.; O'Reilly, R. K. 100th Anniversary of Macromolecular Science Viewpoint: The Role of Hydrophobicity in Polymer Phenomena. *ACS Macro Lett.* **2020**, *9* (11), 1700−1707.
(30) Padmanabhan, J.; Parthasarathi, R.; Subramanian, V.; Chattaraj, P. K. QSPR models for polychlorinated biphenyls: n-Octanol/water partition coefficient. *Bioorg. Med. Chem.* **2006**, *14* (4), 1021−1028.
(31) Bannan, C. C.; Calabró, G.; Kyu, D. Y.; Mobley, D. L. Calculating Partition Coefficients of Small Molecules in Octanol/Water and Cyclohexane/Water. *J. Chem. Theory Comput.* **2016**, *12* (8), 4015−4024.
(32) Foster, J. C.; Varlas, S.; Couturaud, B.; Jones, J. R.; Keogh, R.; Mathers, R. T.; O'Reilly, R. K. Predicting Monomers for Use in Polymerization-Induced Self-Assembly. *Angew. Chem. Int.l Ed.* **2018**, *57* (48), 15733−15737.
(33) Varlas, S.; Foster, J. C.; Arkinstall, L. A.; Jones, J. R.; Keogh, R.; Mathers, R. T.; O'Reilly, R. K. Predicting Monomers for Use in Aqueous Ring-Opening Metathesis Polymerization-Induced Self-Assembly. *ACS Macro Lett.* **2019**, *8* (4), 466−472.
(34) Inam, M.; Cambridge, G.; Pitto-Barry, A.; Laker, Z. P. L.; Wilson, N. R.; Mathers, R. T.; Dove, A. P.; O'Reilly, R. K. 1D vs. 2D shape selectivity in the crystallization-driven self-assembly of polylactide block copolymers. *Chem. Sci.* **2017**, *8* (6), 4223−4230.
(35) He, Y.; Eloi, J.-C.; Harniman, R. L.; Richardson, R. M.; Whittell, G. R.; Mathers, R. T.; Dove, A. P.; O'Reilly, R. K.; Manners, I. Uniform Biodegradable Fiber-Like Micelles and Block Comicelles via "Living" Crystallization-Driven Self-Assembly of Poly(l-lactide) Block Copolymers: The Importance of Reducing Unimer Self-Nucleation via Hydrogen Bond Disruption. *J. Am. Chem. Soc.* **2019**, *141* (48), 19088−19098.
(36) Magenau, A. J. D.; Richards, J. A.; Pasquinelli, M. A.; Savin, D. A.; Mathers, R. T. Systematic Insights from Medicinal Chemistry To Discern the Nature of Polymer Hydrophobicity. *Macromolecules* **2015**, *48* (19), 7230−7236.
(37) Fischer, F.; Zufferey, D.; Tahoces, R. Lower critical solution temperature in superheated water: the highest in the poly(N, N-dialkylacrylamide) series. *Polym. Int.* **2011**, *60* (8), 1259−1262.
(38) Lerch, A.; Käfer, F.; Prévost, S.; Agarwal, S.; Karg, M. Structural Insights into Polymethacrylamide-Based LCST Polymers in Solution: A Small-Angle Neutron Scattering Study. *Macromolecules* **2021**, *54* (16), 7632−7641.
(39) Tsui, H.-W.; Wang, J.-H.; Hsu, Y.-H.; Chen, L.-J. Study of heat of micellization and phase separation for Pluronic aqueous solutions

https://doi.org/10.1021/acsmacrolett.1c00776
ACS Macro Lett. 2022, 11, 498−503

by using a high sensitivity differential scanning calorimetry. *Colloid Polym. Sci.* **2010**, *288* (18), 1687−1696.
(40) Dharmaratne, N. U.; Jouaneh, T. M. M.; Kiesewetter, M. K.; Mathers, R. T. Quantitative Measurements of Polymer Hydrophobicity Based on Functional Group Identity and Oligomer Length. *Macromolecules* **2018**, *51* (21), 8461−8468.
(41) Yildirim, E.; Dakshinamoorthy, D.; Peretic, M. J.; Pasquinelli, M. A.; Mathers, R. T. Synthetic Design of Polyester Electrolytes Guided by Hydrophobicity Calculations. *Macromolecules* **2016**, *49* (20), 7868−7876.
(42) Chandler, D. Interfaces and the driving force of hydrophobic assembly. *Nature* **2005**, *437* (7059), 640−647.

Recommended by ACS

Combined Simulation and Experimental Study of Polyampholyte Solution Properties: Effects of Charge Ratio, Hydrophobic Groups, and Polymer Concentration

Wengang Zhang, Jack F. Douglas, *et al.*

JULY 14, 2022
MACROMOLECULES

READ

Ionic Compatibilization of Polymers

Glenn H. Fredrickson, Rachel A. Segalman, *et al.*

JULY 22, 2022
ACS POLYMERS AU

READ

How Dispersity from Step-Growth Polymerization Affects Polymer Dynamics from Coarse-Grained Molecular Simulations

Wengang Zhang, Francis W. Starr, *et al.*

NOVEMBER 09, 2022
MACROMOLECULES

READ

Unclonable Features via Electrospraying of Bulk Polymers

Abidin Esidir, M. Serdar Onses, *et al.*

JUNE 30, 2022
ACS APPLIED POLYMER MATERIALS

READ

Get More Suggestions >

https://doi.org/10.1021/acsmacrolett.1c00776
ACS Macro Lett. 2022, 11, 498−503

3.2. Supporting Information

Supporting Information

"LogP_{oct}/SA predicts thermoresponsive behavior of P(DMA-*co*-RA) statistical copolymers"

Irem Akar,† Jeffrey C. Foster,† Xiyue Leng,† Amanda K. Pearce, † Robert T. Mathers,,§ and Rachel K. O'Reilly*,†*

[†]School of Chemistry, University of Birmingham, Edgbaston, Birmingham, B15 2TT, UK

[§]Department of Chemistry, Pennsylvania State University, New Kensington, PA 15068, USA

*Corresponding Authors: rtm11@psu.edu (R.T.M.), and r.oreilly@bham.ac.uk (R.K.O.R.)

Materials and Methods

Materials

Benzyl acrylate (BA, Alfa-Aesar, 97%), *n*-butyl acrylate (*n*BA, Sigma-Aldrich, 99%), tetrahydrofurfuryl acrylate (THFA, Sigma-Aldrich), *tert*-butyl acrylate (*t*BA, Sigma-Aldrich, 98%), *N,N*-dimethyl acrylamide (DMA, Sigma-Aldrich, 99%), methyl methacrylate (MMA, Sigma-Aldrich, 99%), and 1,4-dioxane (Sigma-Aldrich, 99.8%) were filtered through basic alumina prior to use. 2,2′-Azobis(2-methylpropionitrile) (AIBN) was received from Molekula, recrystallized from methanol and stored at 4 °C. Methyl 2-(butylthio-carbonothioylthio)-2-methylpropanoate (MBTMP) was prepared according to a previously described procedure.[1]

Characterization Techniques

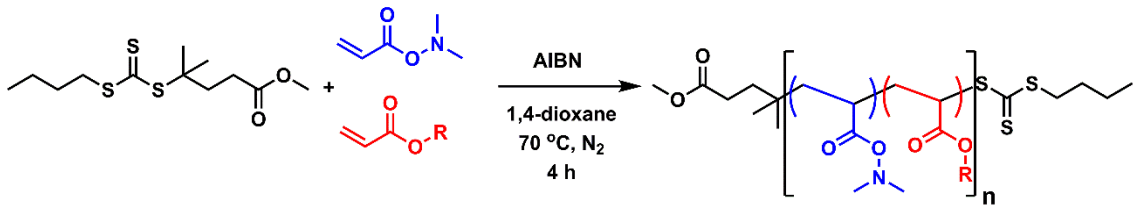
NMR Spectroscopy. ^{1}H-NMR and ^{13}C-NMR spectra were recorded at 300 MHz on a Bruker DPX-300 spectrometer, using chloroform-*d* ($CDCl_3$) as the solvent. Chemical shifts of protons are reported as δ in parts per million (ppm) and are relative to solvent residual peaks.

Size Exclusion Chromatography. Size exclusion chromatography (SEC) analysis was performed on a system composed of an Agilent 1260 Infinity II LC system equipped with an Agilent guard column (PLGel 5 μM, 50 × 7.5 mm) and two Agilent Mixed-C columns (PLGel 5 μM, 300 × 7.5 mm). The mobile phase used was $CHCl_3$ (HPLC grade) containing 0.5% v/v NEt_3 at 40 °C at flow rate of 1.0 mL min^{-1} (polymethyl methacrylate (PM) standards were used for calibration). Detection was conducted using a differential refractive index (RI) detector. Number-average molecular weights (M_n), weight-average molecular weights (M_w) and dispersities ($Đ_M = M_w/M_n$) were determined using the Agilent GPC/SEC software.

UV-Vis Spectroscopy. UV-Vis analysis was performed on an Agilent Cary 3500 UV-Vis Spectrophotometer to record the LCST behavior and temperature dependent transmittance spectra of polymers by heating the samples in solution from 0 °C to 90 °C at a rate of 1 °C min^{-1}. Samples were corrected against a background of DI water. Measurements were carried out using glass cuvettes with a path length of 10.00 mm.

Synthetic Methods

Synthesis of P(DMA-*co*-RA) copolymers



Copolymerization of RA monomers with DMA was conducted using AIBN as the initiator, MBTMP as the RAFT agent, 1,3,5-trioxane as an internal reference, and 1,4-dioxane as the solvent. RA content was varied between 10-20% for *n*BuA, 10-20% for BA, 30-60% for THFA, and 15-25% for *t*BuA, targeting the total DP of 80 to 85 with a molar ratio of [Monomer]/[1,3,5-Trioxane]/[MCETP]/[AIBN] = 85:20:1:0.1 in 1,4-dioxane (monomer/1,4-dioxane = 1:2 by volume). For the synthesis of a copolymer with 20% RA: a stock solution of 10 mg mL^{-1} AIBN was prepared in 1,4-dioxane and 62 µL of this solution (0.6 mg, 3.8 x 10^{-3} mmol, 0.1 eq) was added to a vial of MBTMP (10 mg, 3.8 x 10^{-2} mmol, 1.0 eq), RA monomer (0.6 mmol, 17 eq), DMA (0.26 mL, 2.6 mmol, 68 eq), and 1,3,5-trioxane (68 mg, 7.5 x 10^{-1} mmol, 20 eq) in 1,4-dioxane and mixed in an oven-dried ampoule containing a magnetic stir bar until all solids dissolved. The resulting solution was degassed using at least three freeze-pump-thaw cycles, back-filled with N_2, and placed in a preheated oil bath at 70 °C. Samples were taken periodically to determine the overall and relative conversion of comonomers. Purification was achieved by dialysis (6-8 kDa MWCO) against nanopure water followed by lyophilisation.

Experimental Methods

Copolymerization kinetic studies. Kinetic experiments for one polymer from each series (10% *n*BuA for P(DMA-*co*-*n*BuA), 20% BA P(DMA-*co*-BA), 30% THFA P(DMA-*co*-THFA), and 23% *t*BuA for P(DMA-*co*-*t*BuA) were carried out in order to determine the conversion of each monomer at the same time intervals (i.e., 60, 90, 120, 150, and 180 min). Samples were periodically taken from the polymerization mixtures under nitrogen and then diluted with $CDCl_3$ prior to ^1H NMR analysis. Integrations of monomer signals were compared to those internal standard resonances to determine monomer conversions.

Determination of T_{CP} by UV-Vis spectroscopy. Solutions of P(DMA-*co*-RA) copolymers were prepared at 10 mg mL^{-1} in nanopure water. The temperature-dependent change in transmittance % was recorded at λ = 550 nm within the temperature range of 0 °C to 90 °C at a heating rate of 1 °C min^{-1}. Samples were run for two heating/cooling cycles and T_{CP} values taken as the temperature at which the sample transmittance had decreased to 50% on the second heating cycle.

Evaluation of Oligomer Hydrophobicity

LogP_{oct} Analysis. Octanol-water partition coefficients (LogP_{oct}) were calculated for monomers and oligomeric models in Materials Studio 2020,[2] using an atom-based approach (ALogP98 method)[3] for all molecular models containing C, H, N, and O atoms.

Surface Area Analysis. Octanol-water partition coefficients (LogP_{oct}) were normalized by solvent accessible surface area (SA) using Materials Studio 2020.[4-7] First, single oligomers were subjected to a Geometry Optimization procedure using the Forcite Molecular Dynamics (MD) module with a COMPASS II force field. The force field contains information on important parameters, like preferred bond lengths, bond angles, torsion angles, partial charges, and van der Waals radii that influence the conformation.[8] To minimize energy and determine a preferred conformation, these simulations ran until the energy of the oligomer decreased below predetermined convergence criteria (1×10^{-4} kcal mol^{-1} energy convergence, 0.005 kcal mol^{-1} /Å force convergence, and 5×10^{-5} Å displacement convergence). Second, these SA values represent the Connolly surface area created by an algorithm that rolls a ball over the surface of the oligomer. To ensure the SA values are meaningful in the context of octanol-water partition coefficients (LogP_{oct}), the probe had a 1.4 Å radius to match the size of a water molecule. Third, to monitor variations in surface area calculations as the n-mer size increased, oligomers were annealed for 200 cycles using a sinusoidal temperature ramp (300 – 700 K) to maximize variability in SA values. After averaging SA values for cycles 100, 150 and 200, the standard deviation ranged from 0.4-2.7% with an average of 1.2%.

Models. Oligomeric models contained appropriate ratios of DMA and alkyl acrylate units to mimic experimental conditions. In addition, models were proton terminated and contained DMA units randomly distributed throughout the oligomer. For example, *n*BuA/DMA oligomers contained 16-17 DMA units with 2-4 *n*BuA units for a total of 19-20 units such that the amount of *n*BuA ranged from 10.7-19.3 mol %. The quantity of monomers in BA/DMA oligomers ranged from 15-19 DMA units and 2-5 BA units for a total of 17-24 units with 11.8-20.8 mol % BA. THFA/DMA oligomers contained 8-16 DMA units with 4-13 THFA units for a total of 19-27 monomer units to achieve 20.0-57.9 mol % THFA. *t*BuA/DMA oligomers combined 16-18 DMA units with 3-5 *t*BuA units for a total of 20-22 units such that the amount of *t*BuA ranged from 14.3-22.7 mol %.

Supplementary Characterization Data for DMA-*co*-RA Copolymers

Table S1. Molecular characteristics of P(DMA-*co*-RA) copolymers prepared *via* RAFT, as determined by ^{1}H NMR spectroscopy and SEC analyses.[a]

Polymer	Target RA Percentage	Final RA Percentage[b]	DP[c]	$M_{n,\,NMR}$[c] (kDa)	$M_{n,\,SEC}$[d] (kDa)	$Đ_M$[e]
P(DMA-*co*-*n*BuA)	10	11	84	8.9	10.5	1.10
	15	15	84	9.0	10.7	1.15
	20	19	83	9.0	12.1	1.11
P(DMA-*co*-BA)	10	12	84	9.2	9.6	1.21
	15	17	82	9.3	10.4	1.13
	20	20	83	9.6	11.0	1.13
P(DMA-*co*-THFA)	20	21	80	9.0	12.1	1.12
	30	30	80	9.6	10.9	1.12
	40	40	73	9.2	14.2	1.18
	50	49	73	9.6	14.2	1.23
	60	58	81	11.0	13.3	1.29
P(DMA-*co*-*t*BuA)	15	14	83	8.8	13.4	1.35
	20	20	83	9.0	10.4	1.09
	25	23	83	9.0	11.4	1.10
P(DMA-*co*-MMA)	30	31	81	8.3	12.9	1.93

[a] Conditions – [Monomer]/[1,3,5-Trioxane]/[MBTMP]/[AIBN] = 85:20:1:0.1 in 1,4-dioxane (monomer/1,4-dioxane = 1 : 2 by volume).
[b] Determined by ^{1}H NMR spectroscopy ($CDCl_3$, 300 MHz).
[c] Calculated from monomer conversion.
[d] M_n and $Đ_M$ determined by SEC (in $CHCl_3$ + 0.5% NEt_3, calibrated against PMMA standards).

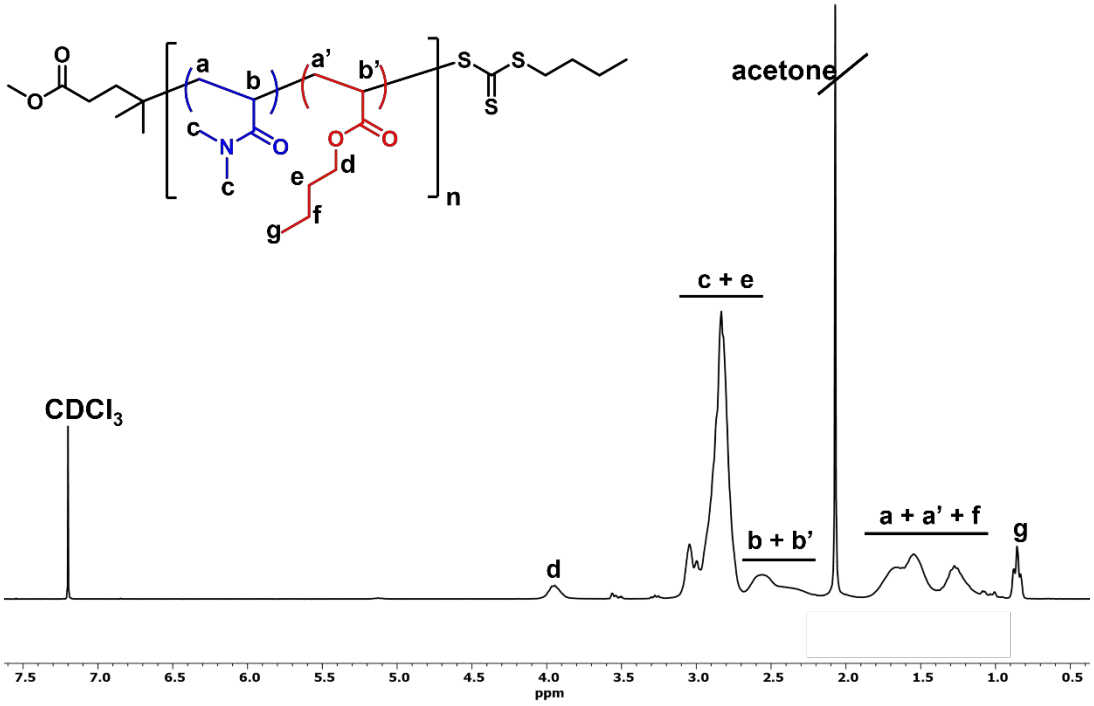


Figure S1. ^{1}H-NMR spectrum of P(DMA-*co*-*n*BuA)$_{84}$ in $CDCl_3$ (300 MHz).

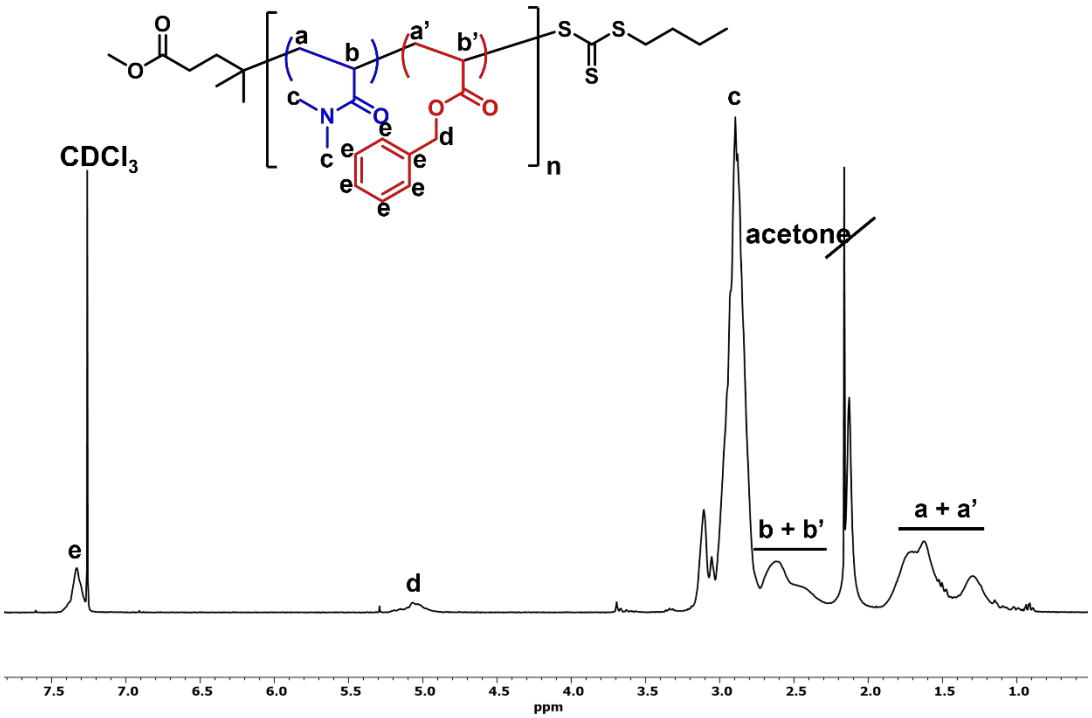


Figure S2. ^{1}H-NMR spectrum of P(DMA-*co*-BA)$_{82}$ in $CDCl_3$ (300 MHz).

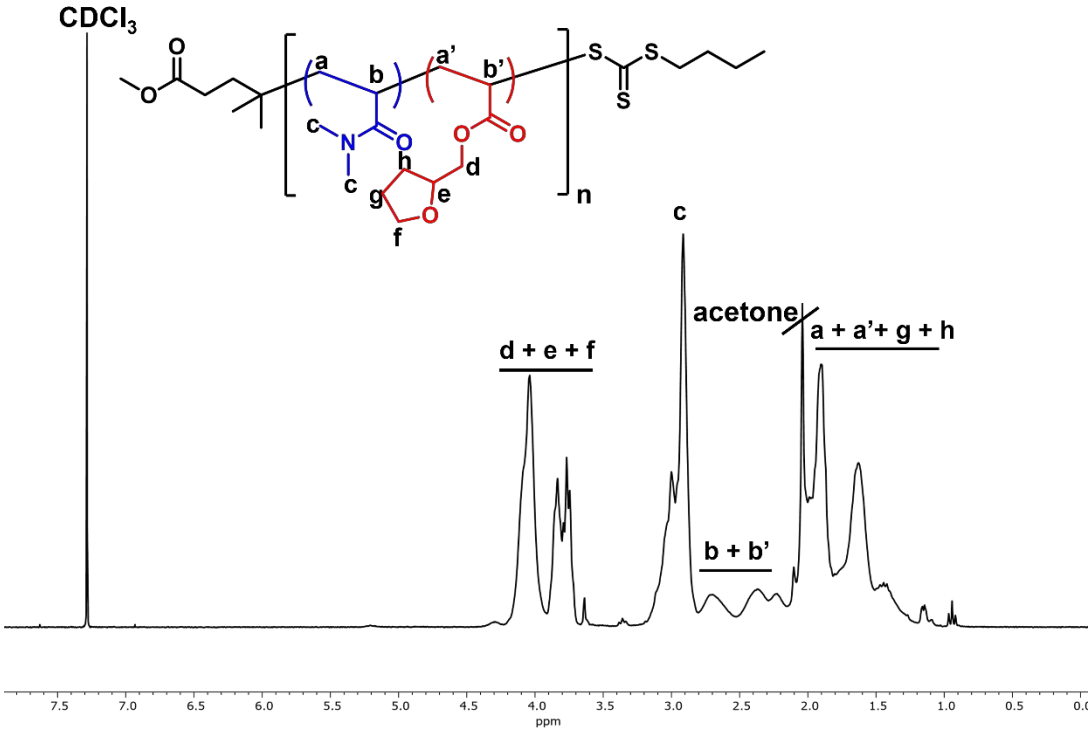


Figure S3. ^{1}H-NMR spectrum of P(DMA-*co*-THFA)$_{81}$ in $CDCl_3$ (300 MHz).

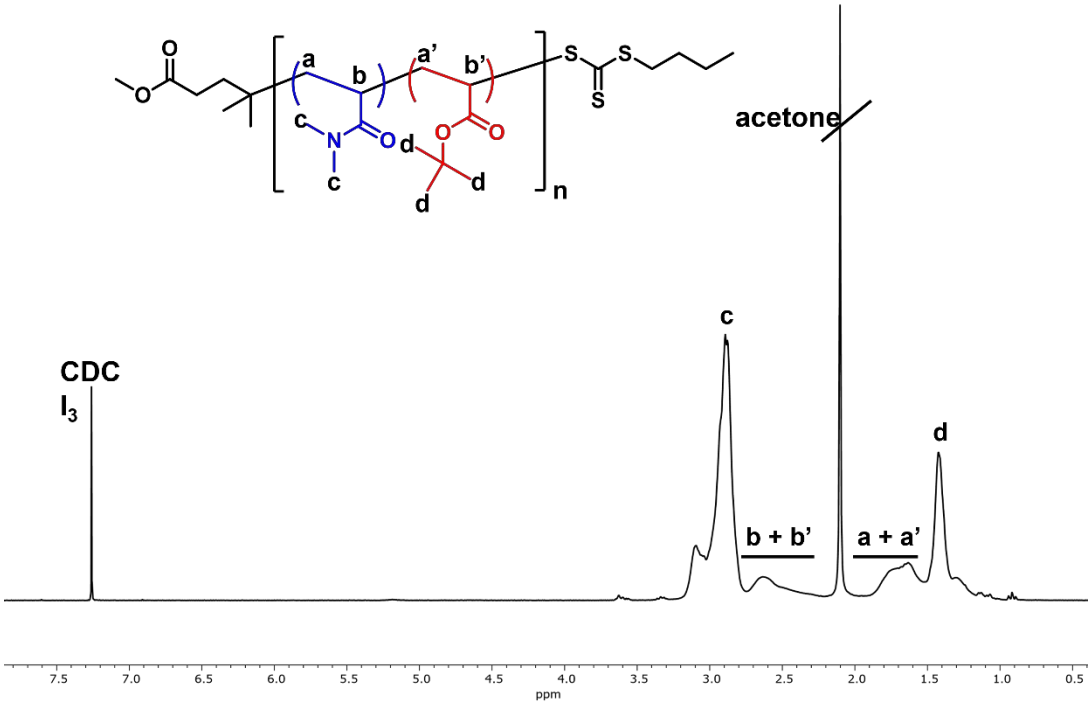


Figure S4. ^{1}H-NMR spectrum of P(DMA-*co*-*t*BuA)$_{84}$ in $CDCl_3$ (300 MHz).

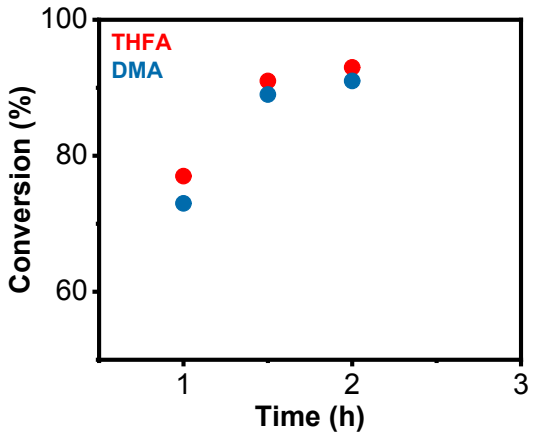


Figure S5. Conversion of THFA and DMA monomers for the 30% THFA system determined by ^{1}H NMR spectroscopy ($CDCl_3$, 300 MHz).

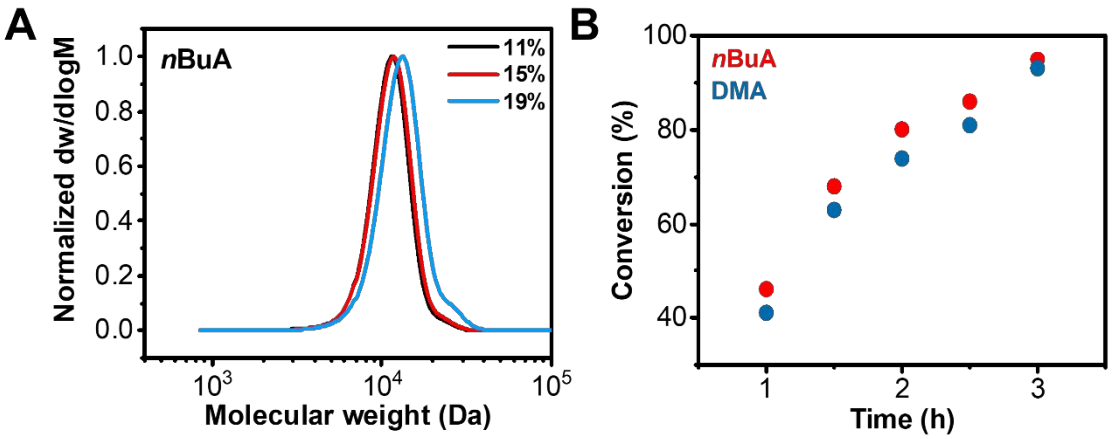


Figure S6. **(A)** Normalized molecular weight distributions for P(DMA-*co*-*n*BuA) copolymers determined by SEC ($CHCl_3$ + 0.5% NEt_3 as the eluent and calibrated against PMMA standards) using an RI detector. The legend shows the molar percentage of *n*BuA in the final copolymers. **(B)** Conversion of *n*BuA and DMA monomers for the 10% *n*BuA system determined by ^{1}H NMR spectroscopy ($CDCl_3$, 300 MHz).

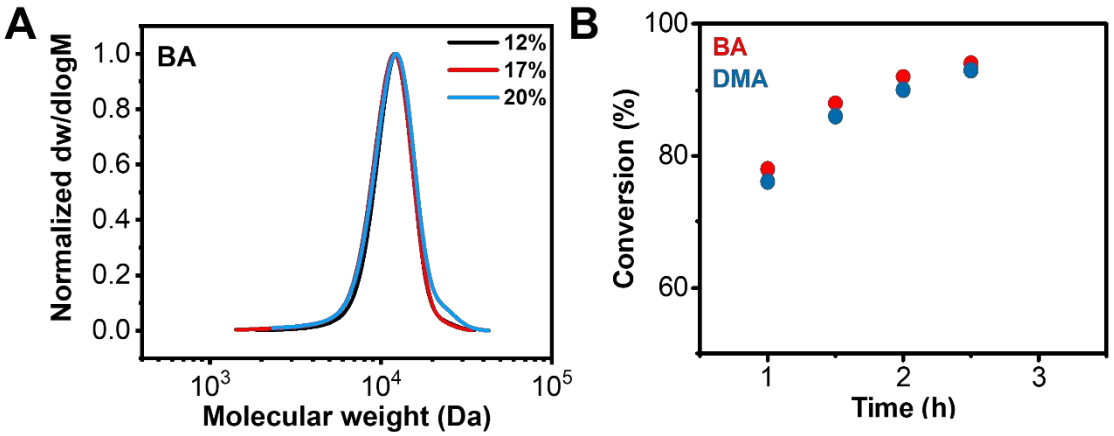


Figure S7. (A) Normalized molecular weight distributions for P(DMA-*co*-BA) copolymers determined by SEC ($CHCl_3$ + 0.5% NEt_3 as the eluent and calibrated against PMMA standards) using an RI detector. The legend shows the molar percentage of BA in the final copolymers. **(B)** Conversion of BA and DMA monomers for the 20% BA system determined by ^1H NMR spectroscopy ($CDCl_3$, 300 MHz).

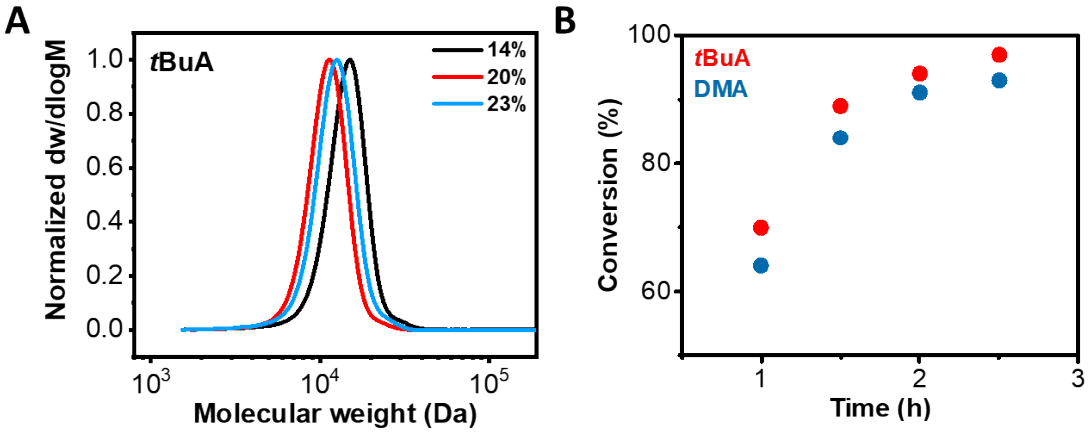


Figure S8. (A) Normalized molecular weight distributions for P(DMA-*co*-*t*BuA) copolymers determined by SEC ($CHCl_3$ + 0.5% NEt_3 as the eluent and calibrated against PMMA standards) using an RI detector. The legend shows the molar percentage of *t*BuA in the final copolymers. **(B)** Conversion of *t*BuA and DMA monomers for the 23% *t*BuA system determined by ^1H NMR spectroscopy ($CDCl_3$, 300 MHz).

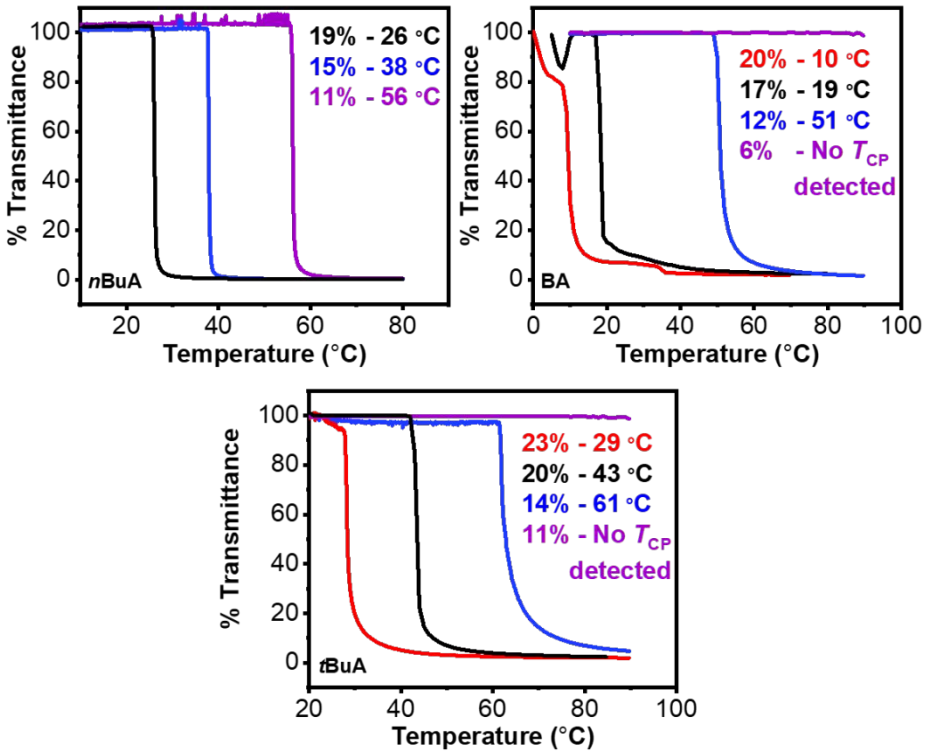


Figure S9. Turbidimetry analysis for P(DMA-*co*-RA) copolymers determined by UV-Vis spectrometry (0 °C to 93 °C, 1 °C min^{-1}, recorded at λ = 550 nm) at 10 mg ml^{-1}.

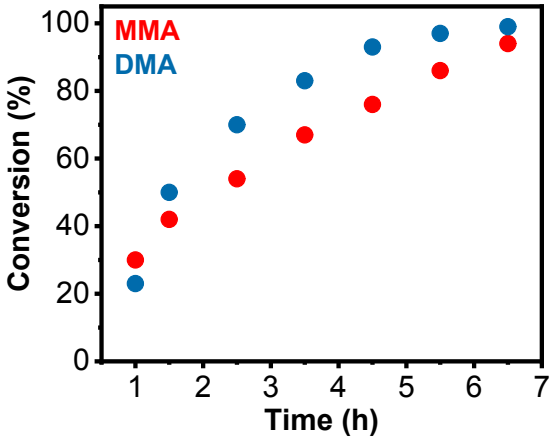


Figure S10. Conversion of MMA and DMA monomers for the 31% MMA system determined by ^{1}H NMR spectroscopy ($CDCl_3$, 300 MHz).

Table S2. T_{CP} of P(DMA-*co*-RA) copolymers determined by UV-Vis spectrometry.

Polymer[a]	T_{CP} from UV-Vis (°C)[b]	Polymer[a]	T_{CP} from UV-Vis (°C)[b]
P(DMA$_{0.89}$-*co*-*n*BuA$_{0.11}$)	56	**P(DMA$_{0.79}$-co-THFA$_{0.21}$)**	*soluble*
P(DMA$_{0.85}$-*co*-*n*BuA$_{0.15}$)	38	**P(DMA$_{0.70}$-co-THFA$_{0.30}$)**	58
P(DMA$_{0.81}$-*co*-*n*BuA$_{0.19}$)	26	**P(DMA$_{0.60}$-co-THFA$_{0.40}$)**	37
P(DMA$_{0.94}$-*co*-BA$_{0.06}$)	*soluble*	**P(DMA$_{0.51}$-co-THFA$_{0.49}$)**	27
P(DMA$_{0.88}$-*co*-BA$_{0.12}$)	51	**P(DMA$_{0.42}$-co-THFA$_{0.58}$)**	15
P(DMA$_{0.83}$-*co*-BA$_{0.17}$)	19	**P(DMA$_{0.86}$-co-*t*BuA$_{0.14}$)**	61
P(DMA$_{0.80}$-*co*-BA$_{0.20}$)	10	**P(DMA$_{0.80}$-co-*t*BuA$_{0.20}$)**	43
		P(DMA$_{0.77}$-co-*t*BuA$_{0.23}$)	29

[a] Aqueous solution of copolymers were prepared at 10 mg mL^{-1} in nanopure water.
[b] Data obtained from the second heating of the samples within the temperature range of 0 °C to 90 °C at a heating rate of 1 °C min^{-1}.

Table S3. Linear regression data for the P(DMA-*co*-RA) copolymers.

Polymer	Intercept	Slope
P(DMA-*co*-*n*BuA)	98	-3.8
P(DMA-*co*-BA)	117	-5.6
P(DMA-*co*-THFA)	101	-1.5
P(DMA-*co*-*t*BuA)	83	-1.9

References

1. Wang, X.; Shi, Y.; Graff, R. W.; Cao, X.; Gao, H., Synthesis of Hyperbranched Polymers with High Molecular Weight in the Homopolymerization of Polymerizable Trithiocarbonate Transfer Agent without Thermal Initiator. *Macromolecules* **2016,** *49* (17), 6471-6479.
2. *Materials Studio 2020*, Accelrys Software Inc.: San Diego, 2020.
3. Ghose, A. K.; Viswanadhan, V. N.; Wendoloski, J. J., Prediction of Hydrophobic (Lipophilic) Properties of Small Organic Molecules Using Fragmental Methods: An Analysis of ALOGP and CLOGP Methods. *J. Phys. Chem. A* **1998,** *102* (21), 3762-3772.
4. Min, K.; Cuiffi, J. D.; Mathers, R. T., Ranking environmental degradation trends of plastic marine debris based on physical properties and molecular structure. *Nat. Commun.* **2020,** *11* (1), 727.
5. Varlas, S.; Foster, J. C.; Arkinstall, L. A.; Jones, J. R.; Keogh, R.; Mathers, R. T.; O'Reilly, R. K., Predicting Monomers for Use in Aqueous Ring-Opening Metathesis Polymerization-Induced Self-Assembly. *ACS Macro Lett.* **2019,** *8* (4), 466-472.

6. Foster, J. C.; Varlas, S.; Couturaud, B.; Jones, J. R.; Keogh, R.; Mathers, R. T.; O'Reilly, R. K., Predicting Monomers for use in Polymerization Induced Self-Assembly. *Angew. Chem. Int. Ed.* **2018,** *57* (48), 15733-15737.
7. Dharmaratne, N. U.; Jouaneh, T. M. M.; Kiesewetter, M. K.; Mathers, R. T., Quantitative Measurements of Polymer Hydrophobicity Based on Functional Group Identity and Oligomer Length. *Macromolecules* **2018**.
8. Sun, H.; Jin, Z.; Yang, C. W.; Akkermans, R. L. C.; Robertson, S. H.; Spenley, N. A.; Miller, S.; Todd, S. M., COMPASS II: extended coverage for polymer and drug-like molecule databases. *J. Mol. Model.* **2016,** *22* (2).

Chapter 4. Preparation of Functional Nanoparticles of P(DMA-*co*-HA) Copolymers *via* Polymerization-Induced Thermal Self-Assembly

4.1. Manuscript details and overview

Title: Preparation of Functional Nanoparticles of P(DMA-*co*-HA) Copolymers via Polymerization-Induced Thermal Self-Assembly

Authors: **Irem Akar**,[†] Amanda Pearce,[†] Calum Ferguson[†,§] and Rachel K. O'Reilly[*,†]

Affiliations: [†]School of Chemistry, University of Birmingham, Edgbaston, Birmingham B15 2TT, United Kingdom

[§] Max Planck Institute for Polymer Research, Ackermannweg 10, 55128 Mainz, Germany

Manuscript Prepared

Co-author contributions: Dr Amanda K. Pearce provided technical and synthetic advice. Dr. Calum Ferguson provided technical and synthetic advice. Prof. Rachel O'Reilly supervised the project, provided guidance, and edited the manuscript.

Overview: In this Chapter, PITSA is employed as a methodology for the fabrication of azide functionalized DMA-based thermoresponsive nanoparticles. In our previous study we investigated the thermoresponsive behavior of copolymers of DMA and alkyl acrylate which produce nonresponsive homopolymers but provide thermoresponsive polymers when copolymerized together. Based on this, we wanted to explore the self-assembly behavior of the DMA-based copolymers.

First, we synthesized a simple system by using a PEG-CTA and chain extended it with DMA and hexyl acrylate *via* PITSA. Formation of nanoparticles was confirmed *via* DLS measurements at 50 °C followed by disassembling of the particles as the temperature decreases. After confirming the successful synthesis of nanoparticles, azidopropyl methacrylate and acrylic acid monomers were introduced to the system enabling functionalization through azide units and crosslinking through acrylic acid units to prevent disassembly at room temperature. Crosslinking of nanoparticles were confirmed *via* DLS measurements which remained stable at room temperature. Then, crosslinked particles were functionalized through the azide units with short $(WR)_3$ antibacterial peptides synthesized on an automated solid-phase peptide synthesizer.

In this contribution, we were interested in developing functional nanoparticles by combining the advantages of PISA with the thermoresponsive polymers. We have shown that functional thermoresponsive systems can be designed by using alternative monomers to the widely-used thermoresponsive monomers in the literature such as NIPAM, and believe that this study will provide insight into diversifying thermoresponsive systems used for therapeutic applications.

Preparation of functional nanoparticles of P(DMA-*co*-HA) copolymers *via* Polymerization-Induced Thermal Self-Assembly

*Irem Akar, Amanda K. Pearce, Calum T. J. Ferguson, and Rachel K. O'Reilly**

Irem Akar., Dr. Amanda K. Pearce, Prof. Rachel K. O'Reilly
School of Chemistry, University of Birmingham, Edgbaston, Birmingham, B15 2TT, UK
E-mail: r.oreilly@bham.ac.uk

Dr. Calum T. J. Ferguson
Max Planck Institute for Polymer Research, Ackermannweg 10, 55128 Mainz, Germany

Keywords: thermoresponsive polymers, polymerization-induced thermal self-assembly, nanoparticles

ABSTRACT: Self-assembled polymeric nanoparticles have been of great interest for various biological applications such as drug delivery, catalysis, and biosensing. In this regard, polymerization-induced self-assembly (PISA) has been widely explored as a more efficient technique than conventional self-assembly methods as it can be conducted in one pot and does not require harsh conditions. Recently, a method known as polymerization-induced thermal self-assembly (PITSA) has emerged, exploiting the inherent phase transition behavior of thermoresponsive polymers at a critical temperature point to generate thermoresponsive nanoparticles *in situ.* However, the narrow range of monomers suitable for PITSA limits the design of diverse thermoresponsive nanoparticles, and therefore this process has not yet been explored to its fullest capacity. In this study, we demonstrate the preparation of thermoresponsive nanoparticles based on hydrophilic *N,N*-dimethyl acrylamide (DMA) and hydrophobic hexyl acrylate (HA) monomers. This is particularly interesting as these monomers produce non-responsive homopolymers but display thermoresponsive behavior when copolymerized. The nanoparticles obtained were crosslinked to enable their characterization at room temperature, and further functionalized with a short synthetic antibacterial peptide $(WR)_3$ to demonstrate proof-of-concept potential as antimicrobial agents. Overall, this work expands the library of monomers amenable to PITSA for the production of thermoresponsive nanoparticles, contributing to the design of new functional nanoparticles for therapeutic purposes.

1. Introduction

Self-assembled polymeric nanoparticles have garnered increasing attention over the past decades as these nanoparticles have been used for wide range of applications such as drug delivery vehicles, sensors, catalysts, and coating materials.[1-5] Having the ability to modify their structure by tuning their compositions and/or functionalize them with small molecules renders them powerful tools for therapeutic applications.[6] Recent advances in controlled radical polymerizations have further aided the preparation of self-assembled polymeric nanoparticles, enabling their engineering by precisely controlling the different constituents in polymer structures.[7, 8] This in turn influences the size, shape, and morphology of the final nanoparticles, facilitating the preparation of diverse self-assembled polymeric systems.[9]

Conventional self-assembly methods such as solvent switch, direct dissolution and thin-film rehydration have been widely used for the formation of nanoparticles.[10] However, there are several drawbacks, including time consuming multi-step procedures such as synthesis and purification of polymers prior to self-assembly, and the requirement

of dilute polymerization solutions for self-assembly to occur.[8] More recently, the advent of polymerization-induced self-assembly (PISA) has addressed many of these challenges. PISA is a one-pot reaction that can be conducted under mild conditions and in organic solvents and water, can be performed at high solids content (up to 50% w/w) and does not require the use of surfactants. In an aqueous system, a water-soluble macro-chain-transfer agent is chain extended with water miscible monomers which becomes progressively more hydrophobic as the polymerization proceeds. This leads to the water-immiscible chains to self-assemble forming nanoparticles.[8, 11, 12]

"Smart" polymers that can change their properties upon exposure to external stimuli have been proven to be great tools for therapeutic applications.[13] Here, polymers can be functionalized by incorporating certain moieties that respond to external stimuli such as light, pH, redox and temperature.[13-17] If formulated into nanoparticles, upon applying the stimuli, polymer chains can undergo a physical or chemical change affecting the resulting nanoparticle structure.[18] Temperature has been the most widely studied among these stimuli as it is easily applicable externally, and is tunable *via* many methods within the desired range to create the required thermoresponse.[17] Thermoresponsive polymers display unique behavior in water known as lower critical solution temperature (LCST) or upper critical solution temperature (UCST), whereby a phase transition occurs above or below a certain temperature point for LCST and UCST behavior, respectively.[19] Since the transition happens at high temperatures in case of UCST, LCST polymers are preferable for biological applications, as the physiological temperature range can be targeted easily with LCST polymers.[20] The strong interactions between polymer chains and solvent allow polymers to be soluble below their LCST. The phase transition then occurs upon heating above a certain temperature leading to the polymer chains becoming immiscible as the polymer-solvent interactions weaken.[21, 22]

The ability to tune the LCST behavior is another advantage that makes thermoresponsive polymers attractive for many applications. A variety of methods have been reported to achieve this, such as changing polymer solution concentration, molecular weight, and hydrophobicity.[23-25] Tuning polymer hydrophobicity is particularly interesting, as this can readily alter polymer-solvent interactions.[26] There are several ways to tune the polymer hydrophobicity, such as altering the polymer structure or using copolymerization. Kempe and coworkers reported that overall polymer hydrophobicity of graft copolymers could be increased by increasing the length of the side chains, thereby decreasing polymer LCST.[27] Several groups including Lutz, Hoth, Kostjuk, and ourselves, have previously reported that polymer LCST could be controlled by copolymerizing with a high LCST monomer with monomers of lower LCST.[28-30] Recent reports by our group have also shown that the thermoresponsive behavior of amphiphilic copolymers can be tuned by diversifying the hydrophobicity of comonomers in case of both brushy and linear copolymers.[31] In the case of linear polymers, it was also shown that the thermoresponsive behavior of the polymers could be correlated to their hydrophobicity.[32]

The abundance of methods for tuning polymer thermoresponsiveness, as well as their facile production *via* controlled radical polymerization techniques, has led to these polymers being widely investigated. A recent technique that combines the advantages of thermoresponsive polymers with the versatility of PISA has been denoted as polymerization-induced thermal self-assembly (PITSA), and was first reported by Sumerlin and coworkers.[33] During PITSA, polymer chains self-assemble once they reach critical length, upon which they become hydrophobic, then proceed to follow the same mechanism as PISA. The entropic changes in the system contribute to the self-assembly process as this drives the phase transition of polymer chains once the system reaches a critical temperature.[33, 34] For example, Sumerlin and coworkers reported PITSA of a well-known thermoresponsive monomer *N*-isopropylacrylamide (NIPAM) using a hydrophilic chain transfer agent of *N, N*-dimethylacrylamide (DMA). Here, they reported the evolution of morphologies from micelles to micelle/worm mixture, to worms and finally to vesicles as the NIPAM polymerizes.[33]

Inspired by this work, we wanted to investigate whether we could expand the library of available monomers for the production of thermoresponsive nanoparticles *via* PITSA to be able to more exten-

sively utilize the advantage of inherent phase transition behavior of thermoresponsive polymers. Our previous study reports the production of thermoresponsive polymers by copolymerizing non-responsive *N*,*N*-dimethyl acrylamide (DMA) and alkyl acrylates. In particular, we sought to validate that this behavior would translate into a self-assembly process during PITSA, as this would provide an insight for the design of new thermoresponsive nanoparticles using monomers that produce non-responsive homopolymers. With this goal, we selected hydrophilic DMA as the hydrophilic block on account of its simple chain structure, and hexyl acrylate (HA) for the hydrophobic component due to its commercial availability. We prepared nanoparticles using these monomers (**NP1**) and then introduced an azide bearing monomer (3-Azidopropyl methacrylate monomer (AzPMA)) and acrylic acid (AA) monomer (**NP2**) in order to be able to both functionalize these nanoparticles through the azide moieties and stabilize their structure *via* crosslinking through the AA units (Figure 1).

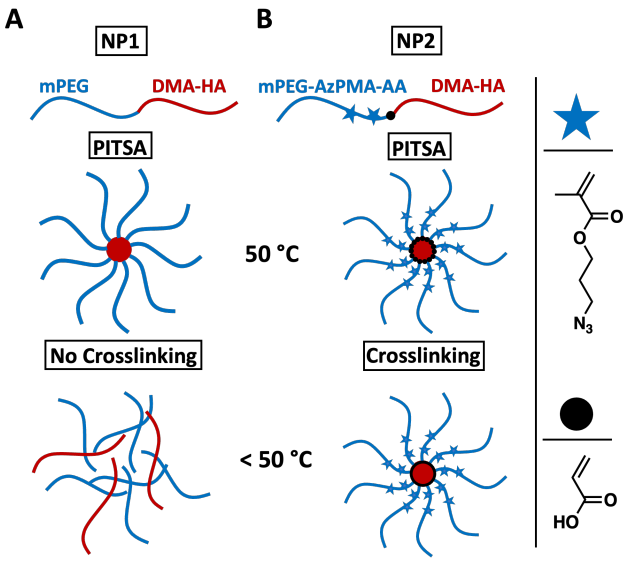


Figure 1. Schematic representation of the preparation of (A) uncrosslinked mPEG-*b*-P(DMA-*co*-HA) nanoparticles (**NP1**) and (B) crosslinked mPEG-*b*-P(AzPMA)-*b*-P(AzPMA-*co*-AA)-*b*-P(DMA-*co*-HA) nanoparticles (**NP2**).

2. Experimental Section

2.1. Materials

3-Chloropropanol (Sigma-Aldrich, 98%), sodium azide (NaN_3, Sigma-Aldrich, ≥99%), tetrabutylammonium bisulfate (Sigma-Aldrich, ≥99%), triethylamine (Alfa Aesar, 99%), methacryloyl chloride (Sigma-Aldrich, 97%, contains ~200 ppm monomethyl ether hydroquinone as stabilizer), hydroquinone (Sigma-Aldrich, ≥99%) were used as received. Hexyl acrylate (HA, Sigma-Aldrich, 99%), *N,N*-dimethyl acrylamide (DMA, Sigma-Aldrich, 99%), methyl methacrylate (MMA, Sigma-Aldrich, 99%), acrylic acid (anhydrous, contains 200 ppm MEHQ as inhibitor, 99%) and 1,4-dioxane (Sigma-Aldrich, 99.8%) were filtered through basic alumina prior to use. Poly(ethylene glycol) methyl ether (mPEG, Sigma-Aldrich, M_n = 5000 Da) 1,3,5-trioxane (Sigma-Aldrich, ≥99%), potassium persulfate (KPS, Sigma-Aldrich), 3-(trimethylsilyl)-1-propanesulfonic acid sodium salt (TMS, Sigma-Aldrich, 97%), *N*-(3-dimethylaminopropyl)-*N*′-ethylcarbodiimide hydrochloride (EDC.HCl, Sigma-Aldrich), cystamine dihydrochloride (Alfa Aesar, ≥97%), dibenzocyclooctyne-N-hydroxysuccinimidyl ester (DBCO-NHS, Sigma-Aldrich), *N*-ethyldiisopropylamine (DIPEA, Sigma Aldrich, ≥97%), *N,N*-dimethylformamide (DMF, Sigma-Aldrich), Fmoc-Trp(Boc)-OH (W, Sigma-Aldrich, ≥97%), Fmoc-Arg(PBF)-OH (R, Sigma-Aldrich), Rink Amide AM Resin (100-200 mesh) (VWR International), Oxyma Pure (Sigma-Aldrich), *N,N*′-diisopropylcarbodiimide (DIC, Sigma-Aldrich, 99%), piperidine (Alfa Aesar, 99%), trifluoroacetic acid (TFA, Sigma-Aldrich, 99%), 2,2′-(ethylenedioxy)diethanethiol (DODT, Sigma-Aldrich, 95%), triethylsilane (TES, Sigma-Aldrich, 97%) was used as received. 2,2′-Azobis(2-methylpropionitrile) (AIBN) was received from Molekula, recrystallized from methanol, and stored at 4 °C. 3-Azidopropyl methacrylate monomer (AzPMA) was prepared according to a previously described procedure.[35] mPEG chain transfer agent (mPEG-CTA) was synthesized following a previously described procedure.[36]

2.2. Characterization

Nuclear magnetic resonance (^{1}H-NMR) spectra were recorded at 300 MHz on a Bruker DPX-300 spectrometer, using chloroform-d ($CDCl_3$) as the solvent. Chemical shifts of protons are reported as δ in parts per million (ppm) and are relative to solvent residual peaks. Size exclusion chromatography (SEC) analysis was performed on a system

composed of an Agilent 1260 Infinity II LC system equipped with an Agilent guard column (PLGel 5 μM, 50 × 7.5 mm) and two Agilent Mixed-C columns (PLGel 5 μM, 300 × 7.5 mm). The mobile phase used was $CHCl_3$ (HPLC grade) containing 0.5% v/v NEt_3 at 40 °C with a flow rate of 1.0 mL min^{-1} (poly(methyl methacrylate) (PM) standards were used for calibration). Detection was conducted using a differential refractive index (RI) detector. Number-average molecular weights (M_n), weight-average molecular weights (M_w) and dispersities ($Đ_M = M_w/M_n$) were determined using the Agilent SEC software. High pressure liquid chromatography (HPLC) analyses were performed on a modular Shimadzu instrument with the following modules: CBM-20A system controller, LC-20AD solvent delivery module, SIL-20AC HT autosampler, CTO-20AC column oven, SPD-M20A photodiode array UV-Vis detector, RF-20A spectrofluorometric detector and a FRC-10 fraction collector. Chromatography was performed on a [Shim-pack GISS 5 μm C18 (4.6×125 mm) reversed phase column] heated at [30 °C]. Flow rate was set at 0.8 mL·min^{-1} and the products eluted using a gradient of buffers: Buffer A, [H2O (18.2 MΩ·cm^{-1} + 0.1 vol% Formic acid)]; Buffer B: [MeCN (HPLC grade) + 0.1 vol% Formic acid]. The elution of sequences with a tryptophan fluorophore was determined using the fluorescence detector (excitation wavelength 350 nm and emission wavelength 450 nm). The elution of sequences with dansyl fluorophore was determined using the fluorescence detector (excitation 335 nm and emission wavelength 519 nm). Fourier Transform Infrared Spectroscopy was carried out using an Agilent Technologies Cary 630 FTIR spectrometer. 16 Scans from 600 to 4000 cm^{-1} were taken at a resolution of 4 cm^{-1}, and the spectra were corrected for background absorbance. Hydrodynamic diameters (D_h) and size distributions (PD) of nano-objects were determined by dynamic light scattering (DLS) using a Malvern Zetasizer Nano ZS with a 4 mW He-Ne 633 nm laser module operating at 25 °C. Measurements were carried out at an angle of 173° (back scattering), and results were analyzed using Malvern DTS v7.03 software. All determinations were repeated 3 times with at least 10 measurements recorded for each run. D_h values were calculated using the Stokes-Einstein equation, where particles are assumed to be spherical. Dry-state-stained transmission electron microscopy (TEM) imaging was performed on a JEOL JEM-1400 microscope operating at an acceleration voltage of 80 kV. All dry state samples were diluted with deionized water to appropriate analysis concentration and then deposited onto formvar-coated or GO-coated copper grids. After roughly 1 min, excess sample was blotted from the grid and the grid was stained with an aqueous 1 wt% uranyl acetate (UA) solution for 1 min prior to blotting, drying and microscopic analysis.

2.3. mPEG-*b*-P(DMA-*co*-HA)$_{99}$ nanoparticle (NP1) synthesis

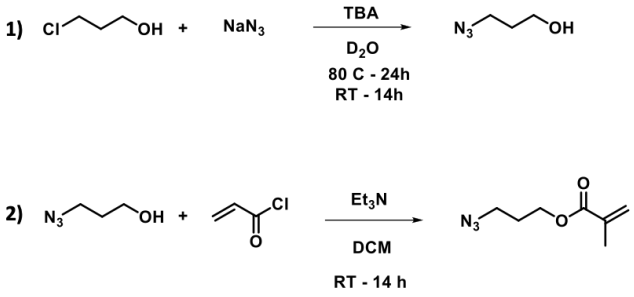
mPEG-CTA (107 mg, 0.02 mmol), DMA (84 μl, 0.8 mmol), HA (215 μl, 1.2 mmol), KPS (1.8 mg, 7 × 10-3 mmol) were placed in a vial with a rubber septum, and DI water (0.250 g) was added to achieve a 10 w/w % solids concentration. TMS (89 mg, 0.4 mmol) was used as the internal standard. The solution was deoxygenated by purging with N_2 for 30 min, then placed in a heating block at 50 °C and left to stir overnight. After the reaction was complete, the vial was opened to the atmosphere while still in the heating block and subsequently stirred for 30 min to ensure reaction quenching. Samples were taken before and after the polymerization reaction to determine the conversion using ^{1}H NMR spectroscopy. A high monomer conversion of ≈99% was determined due to the disappearance of the DMA and HA vinyl signals at 5.78, 6.11, and 6.70 ppm (^{1}H NMR). Also, apparent HA signals at 4.0 ppm (-CH-(CH_3)$_2$) were detected. Particle size was measured by DLS at a temperature range of 50 °C-RT by using the sample taken from the polymerization solution while the solution was still at 50 °C.

2.4. Synthesis of 3-azidopropyl methacrylate (AzPMA) monomer

3-Chloropropanol (10.6 mL, 12g, 0.127 mol) was added to a mixture of water (15 mL), sodium azide (16 g, 0.254 mol, 2 equivalent), and tetrabutylammonium hydrogen sulfate (0.5 g). The mixture was stirred at 80 °C for 24 h and then at room temperature for 14 h. The product was extracted with ether (3 × 50 mL), the resulting solution was

dried over sodium sulfate, the solvent was removed on a rotary evaporator to obtain 3-azidopropanol (yield: 7.3 g, 57%).

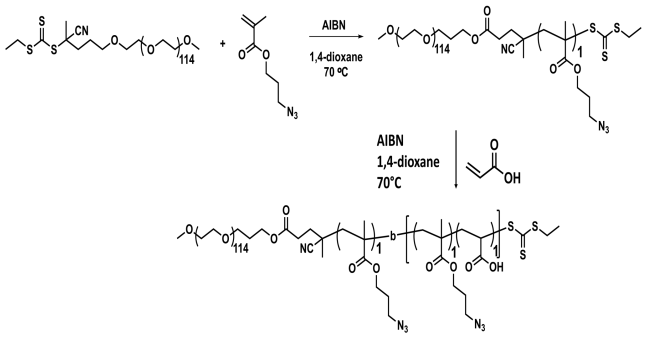
A solution of 3-azidopropanol (7.3 g, 0.072 mol), triethylamine (12.9 mL, 0.092 mol, dried over sodium sulfate), hydroquinone (0.05 g), and methylene chloride (30 mL, dried over sodium sulfate) was cooled in an ice-water bath. Methacryloyl chloride (8.9 g, 8.4 mL, 0.09 mol) was added dropwise over a period of 20 minutes, and the mixture was stirred in the cooling bath for 1 h and then at room temperature for 14 h (Scheme 1). Methylene chloride (15 mL) was added, and the mixture was extracted with an aqueous solution of hydrochloric acid (1/10 v/v, 2 x 30 mL), water (2 x 30 mL), 10 wt % aqueous NaOH (2 x 30 mL), and again with water (2 x 30 mL). The methylene chloride solution was mixed with hydroquinone (0.1 g) and dried over sodium sulfate. The organic solvent was removed under reduced pressure. The crude oil was purified by silica gel column chromatography (hexane: ethyl acetate, 4 : 1), resulting in a colorless oil.



Scheme 1. Synthesis of 3-azidopropyl methacrylate (AzPMA) monomer

2.5. mPEG-*b*-P(AzPMA)$_1$-*b*-P(AzPMA-*co*-AA)$_2$ macro-CTA synthesis

Copolymerization of AzPMA monomer with acrylic acid (AA) was conducted starting with the polymerization of AzPMA by using AIBN as the initiator, mPEG-CTA as the RAFT agent, 1,3,5-trioxane as an internal reference, and 1,4-dioxane as the solvent, following the addition of AA monomer after achieving the targeted total DP of 1 to 5 with a molar ratio of [Monomer]/[1,3,5-Trioxane]/[mPEG-CTA]/[AIBN] = 10:20:1:0.1 in 1,4-dioxane (monomer/1,4-dioxane = 1:2 by volume) (Scheme 2).



Scheme 2. Synthetic scheme for the preparation of mPEG-*b*-P(AzPMA)$_1$-*b*-P(AzPMA-*co*-AA)$_2$ macro-CTA

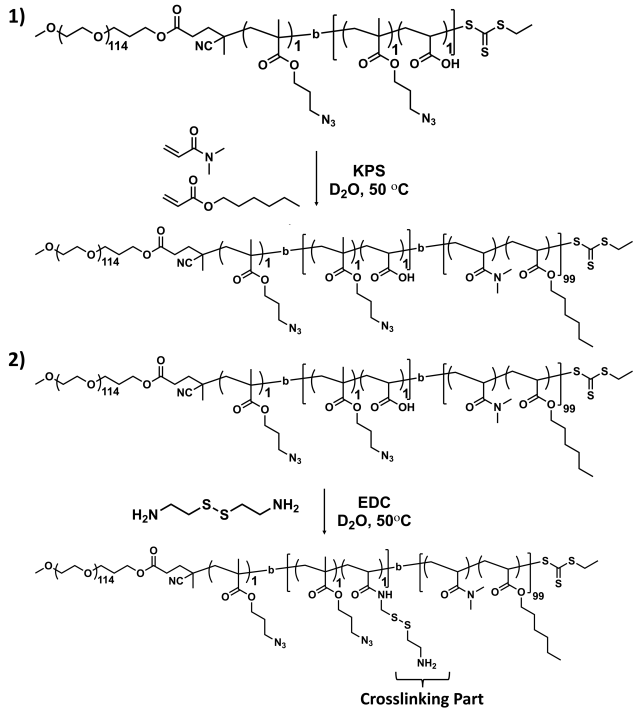
For the synthesis of a copolymer: a stock solution of 10 mg mL^{-1} AIBN was prepared in 1,4-dioxane and 47 µL of this solution (0.5 mg, 2.8 x 10-3 mmol, 0.1 eq) was added to a vial of mPEG-CTA (150 mg, 2.8 x 10^{-2} mmol, 1.0 eq), AzPMA monomer (24 mg, 0.1 mmol, 5.0 eq), and 1,3,5-trioxane (51 mg, 5.7 x 10^{-1} mmol, 20 eq) in 1,4-dioxane and mixed in an oven-dried ampoule containing a magnetic stir bar until all solids dissolved. The resulting solution was degassed using at least three freeze-pump-thaw cycles, back-filled with N2, and placed in a preheated oil bath at 70 °C. Samples were taken periodically to determine the overall and relative conversion of AzPMA. Meanwhile, AA (6.2 mg, 8.5 x 10-2 mmol, 3.0 eq) was purged with N2 in a separate vial for 30 min. When 1 DP of AzPMA was achieved, AA was added to the reaction vessel under N_2. Once 1 DP of AA was achieved, the polymerization reaction was quenched by opening the vial to the air. Purification was achieved by dialysis (3-4 kDa MWCO) against nanopure water followed by lyophilisation.

2.6. mPEG-*b*-P(AzPMA)$_1$-*b*-P(AzPMA-*co*-AA)$_2$-b-P(DMA-*co*-HA)$_{99}$ nanoparticle (NP2) synthesis

For the synthesis of mPEG-*b*-P(AzPMA)$_1$-*b*-P(AzPMA-*co*-AA)$_2$-b-P(DMA-*co*-HA)$_{99}$ nanoparticle (Scheme 3), as a first step, in a vial with a rubber septum, P2 (67 mg, 0.01 mmol), DMA (46 µl, 0.4 mmol), HA (118 µl, 0.7 mmol) KPS (1.0 mg, 4 × 10-3 mmol) were added with DI water (1.94 g) was added to achieve a 10 w/w % solids concentration. TMS (49 mg, 0.2 mmol) was also added as an internal standard. The solution was deoxygenated by purging with N_2 for 30 min, then

placed in a heating block at 50 °C and left to stir overnight. To quench the reaction, the vial was opened to the atmosphere while still in the heating block and stirred further for 30 min. Samples were taken before and after the polymerization reaction to determine the conversion using ^{1}H NMR spectroscopy. Particle size was measured on DLS at a temperature range of 50 °C to RT using the sample taken from the polymerization solution while the solution was still at 50 °C.

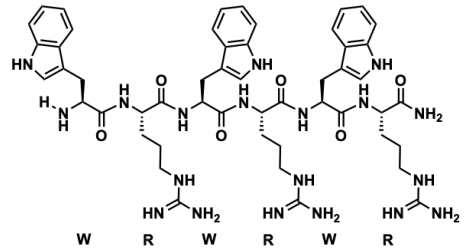
Secondly, EDC (5.9 mg, 0.03 mmol) was added to the reaction vessel while the quenched reaction vial was still in the heating block. After 30 min, cystamine hydrochloride (1.8 mg, 0.008 mmol) was added, and the solution was left to stir overnight at 50 °C. The amount of EDC was calculated by using 2x excess theoretical moles of acrylic acid (0.015 mmol), calculated from the polymer composition (1 AA unit) and amount of macro-CTA added (0.012 mmol), while the amount of cystamine hydrochloride was calculated as 0.5 equivalents of theoretical moles of AA.



Scheme 3. Synthetic scheme for the preparation of **(1)** mPEG-*b*-P(AzPMA)$_1$-*b*-P(AzPMA-*co*-AA)$_2$-b-P(DMA-*co*-HA)$_{99}$ nanoparticle (**NP2**) and **(2)** crosslinking of **NP2** through the acrylic acid units.

2.7. Solid Phase synthesis of (WR)$_3$ peptide

WRWRWR-NH$_2$, (WR)$_3$, peptide was synthesized on a microwave-assisted CEM Liberty Blue automated peptide synthesizer on a 0.25 mmol scale (Scheme 4).



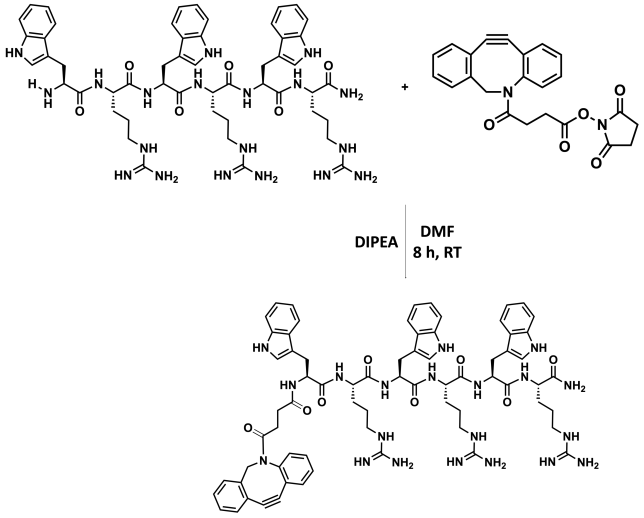
Scheme 4. Structure of WRWRWR-NH$_2$, (WR)$_3$, peptide.

Solutions of 0.2 M of amino acid, 1 M DIC and 1 M Oxyma were prepared in DMF and loaded onto the machine. Rink amide AM resin (0.78 mmol/g) was used for the synthesis of (WR)$_3$ peptide. 20% v/v piperidine solution in DMF was used as a deprotection solution. For Arginine, R, double coupling at 75 °C was carried out. After the synthesis, the resin was washed with DCM 3 times and the resulting peptide was cleaved from the resin by stirring at RT for 4 h in a cleavage solution of trifluroacetic acid (TFA) : 2,2′-(ethylenedioxy)diethanethiol (DODT) : triethylsilane (TES) : H$_2$O with the ratio 92.5% : 2.5% : 2.5% : 2.5%. After the cleavage, the resin was filtered, and the peptide was precipitated in cold diethyl ether 3 times and dried. (WR)$_3$ peptide was characterized by using mass spectroscopy and HPLC. Expected mass (Da): 1044.5760, Found mass (Da): 1044.5756.

2.8. (WR)$_3$ peptide conjugation to dibenzocyclooctyne-N-hydroxysuccinimidyl ester (DBCO-NHS)

DIPEA ((4 µl, 0.02 mmol, 2 eq) and DBCO-NHS (9.3 mg, 0.02 mmol, 2 eq) was added to the solution of (WR)$_3$ peptide (11.3 mg, 0.01 mmol, 1 eq) in DMF (1.2 ml), and the reaction mixture was stirred at RT for 8 h to obtain (WR)$_3$-DBCO-NHS conjugate (Scheme 5). (WR)$_3$-DBCO-NHS was precipitated in cold diethyl ether, collected by centrifugation, and dried under vacuum. The resulting

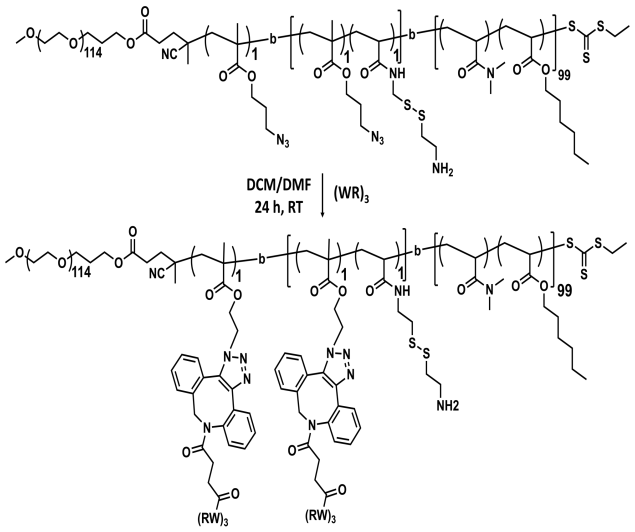
conjugate was characterized by mass spectroscopy. Expected mass (Da) : 1331.56, Found mass (Da) : 1331.67.



Scheme 5. Synthetic scheme for the conjugation of $(WR)_3$ to dibenzocyclooctyne-*N*-hydroxysuccinimidyl ester (DBCO-NHS).

2.9. Conjugation of $(WR)_3$-DBCO-NHS to NP2 *via* Cu-free Click (SPAAC)

A solution of NP2 (10 mg, 0.5×10^{-3} mmol, 1 eq) in DCM was added to the solution of $(WR)_3$-DBCO-NHS (2.1 mg, 0.2×10^{-3} mmol, 3 eq) in DMF and left to stir at RT for 24h (Scheme 6). After the reaction, purification was achieved by dialysis (3-4 kDa MWCO) in nanopure water followed by lyophilisation. Resulting nanoparticles were characterized via FTIR, DLS and TEM.



Scheme 6. Synthetic scheme for the conjugation of $(WR)_3$-DBCO-NHS to **NP2** *via* Cu-free Click (SPAAC).

3. Results and Discussion

3.1. mPEG-*b*-P(DMA-*co*-HA)$_{99}$ nanoparticle (NP1) synthesis

We first prepared a polyethylene glycol chain transfer agent (mPEG CTA) (**P1**), and then carried out PITSA using DMA and HA as the core monomers to test the self-assembly behavior of the mPEG-*b*-P(DMA-*co*-HA) polymer. The CTA was synthesized following previous literature,[36] and then **P1** was obtained by 1-ethyl-3-(3-dimethylaminopropyl) carbodiimide (EDC) coupling with a commercial mPEG (M_n = 5000 Da) in the presence of catalytic 4-dimethylaminopyridine (DMAP). Successful synthesis was confirmed by ^{1}H NMR spectroscopy, and size-exclusion chromatography (SEC) confirmed that the mPEG-CTA had a monomodal and narrow molecular weight distribution (MWD) (Figure S1). Using **P1**, PITSA of DMA and HA was conducted in water at 50 °C to obtain nanoparticles (**NP1**) (Figure 2A). The final molar composition of the purified copolymer was determined using ^{1}H NMR spectroscopy, and the molecular weight distribution (MWD) of the final copolymer was determined using size-exclusion chromatography (SEC). While quantitative blocking efficiency was not achieved for this copolymer (Figure S2), DLS analysis at 50 °C confirmed that this polymer could successfully form nanoparticles. Next, DLS measurements were carried out as a temperature ramp in the range of 20-50 °C (Figure S3, Table S2). DLS was used to characterize the dispersity (PDI = 0.25 at 50 °C) (Figure 2B) and the disassembly of these particles as the temperature was decreased below 50 °C (Figure 2C). This data confirmed that particle formation was driven by LCST behavior.

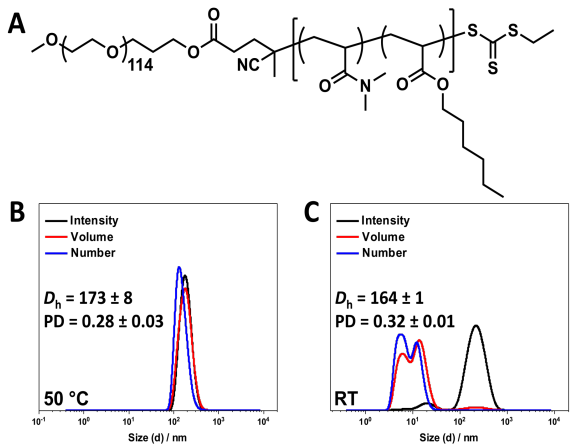


Figure 2. (A) Structure of **NP1** nanoparticles. Size distribution and polydispersity index of **NP1** (B) at 50 °C (C) at room temperature (RT) measured by DLS.

3.2. mPEG-*b*-P(AzPMA)$_1$-b-P(AzPMA-*co*-AA)$_2$-*b*-P(DMA-*co*-HA)$_{99}$ nanoparticle (NP2) synthesis

With our PITSA system validated, we next wanted to investigate the ability to increase the functionality of the NP surface, for example to further attach therapeutic molecules or targeting agents. To this end, an azide-bearing monomer, azidopropyl methacrylate (AzPMA), was introduced into the polymer to enable post-polymerization functionalization through azide-alkyne cycloaddition. A small fraction of acrylic acid (AA) units was also introduced into the polymer structure to enable crosslinking of the resulting nanoparticles to prevent their disassembly, allowing characterization of the nanoparticles at room temperature (RT). AA was introduced after the first block was polymerized to a certain AzPMA monomer, considering the AA has a higher reaction rate than AzPMA. First, the azidopropyl methacrylate (AzPMA) monomer was synthesized from 3-azidopropanol (AzPOH) (see supporting information for detailed procedure) and characterized by ^{1}H NMR (Figure S4). Then, the macro-CTA was synthesized by polymerization of AzPMA at 70 °C with the sequential addition of AA. AzPMA conversion was monitored by ^{1}H NMR spectroscopy, and AA was added when 1 unit of AzPMA monomer had polymerized (Figure S5). The MWD for the mPEG-*b*-P(AzPMA)$_1$-*b*-P(AzPMA-*co*-AA)$_2$ copolymer (**P2**) was determined using SEC, which showed a slightly higher dispersity ($Đ_M$) of 1.32 (Figure S6). Next, PITSA of DMA and HA was conducted using **P2** in water to yield azide-functionalized nanoparticles (**NP2**). PITSA of DMA and HA using **P2** was carried out at 50 °C as with **NP1**. We expected that **P2** would have a lower LCST than **P1**, as our previous research indicates that the hydrophobic AzPMA would have a greater effect than hydrophilic AA on the overall copolymer hydrophobicity. To better explain the effect of monomer hydrophobicity, partition coefficients (Log*P*), which are used to determine the hydrophobicity of small molecules, were used to calculate the hydrophobicity of both monomers using ChemBio 3D. Log*P* was calculated as 2.49 for AzPMA and 0.35 for AA, showing that AzPMA is more hydrophobic than AA. This suggests that the overall copolymer would be more hydrophobic as there are more AzPMA units than the AA monomer in the final copolymer. As such, it is likely to undergo a phase transition at a lower temperature than for **P1**. To characterize the block copolymer assemblies at room temperature after the PITSA process, cystamine was added to the **NP2** polymerization solution at 50 °C to crosslink through the acid groups of AA *via* EDC coupling. The final composition of the polymers after PITSA was determined *via* ^{1}H NMR spectroscopy, which confirmed a final structure of mPEG-*b*-P(AzPMA)$_1$-*b*-P(AzPMA-*co*-AA)$_2$-*b*-P(DMA-*co*-HA)$_{99}$. SEC analysis showed a broad distribution with high $Đ_M$ of 2.90 due to the swelling of the nanoparticles when dispersed in $CHCl_3$ (SEC solvent) (Figure S7). The formation of particles was tracked *via* DLS measurements during a temperature ramp in the range of 20-50 °C (Figure S8, Table S3). As with **NP1**, when **NP2** was uncrosslinked (Figure 3A), particles could be observed at 50 °C followed by particle disassembly with decreasing temperature (Figure 3B). Following the crosslinking reaction, DLS measurements were repeated over the same temperature range (Figure S9, Table S4). As shown in Figure 3C below, successful crosslinking was confirmed by the presence of stable particles

at both 50 °C and RT. This was further demonstrated by TEM analysis which showed stable particles with a size of approximately 42 nm. The difference in sizes between DLS and dry-state TEM measurements were attributed to the drying effect during TEM sample preparation (Figure 3C).

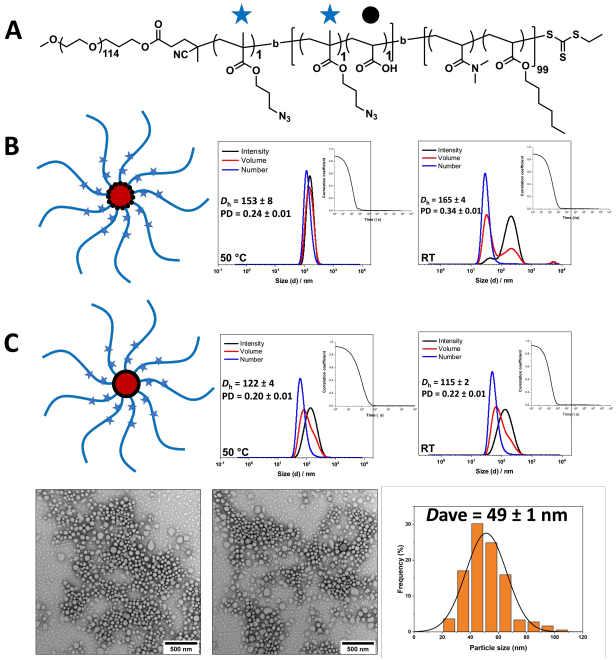


Figure 3. (A) Chemical structure of mPEG-*b*-P(AzPMA)$_1$-b-P(AzPMA-*co*-AA)$_2$-*b*-P(DMA-*co*-HA)$_{99}$ nanoparticle (**NP2**) (star and ball representing the AzPMA and AA monomers, respectively) and (B) size distribution and polydispersity index for uncrosslinked **NP2** at 50 °C and at RT and (C) size distribution and polydispersity index for crosslinked **NP2** at 50 °C and at RT measured by DLS and corresponding TEM images.

3.3. Conjugation of (WR)$_3$-DBCO-NHS to NP2 *via* Cu-free Click (SPAAC)

As a next step, we investigated how post-polymerization functionalization of the particles would affect their stability. To this end, we attached a short antibacterial peptide containing tryptophan (W) and arginine (R) amino acids, (WR)$_3$, through the azide units on the surface of **NP2**. It has been reported that the (WR)$_3$ peptide shows good antibacterial efficiency against widely used bacterial strains.[37] Based on this, this peptide was selected as a functionalizing agent for the synthesized nanoparticles to create antimicrobial therapeutic NPs. First, the antibacterial peptide (WR)$_3$ was synthesized *via* solid phase peptide synthesis (SPPS) on an automated peptide synthesizer. The peptide was obtained with 90% purity which was determined using HPLC (Figure S10). Then, the (WR)$_3$ peptide was reacted with dibenzocyclooctyne-*N*-hydroxysuccinimidyl ester (DBCO-NHS) to enable attachment with the crosslinked **NP2** *via* copper-free Click chemistry (SPAAC) through the azide units (Figure 4A). ^{1}H NMR spectroscopy did not provide distinguishable peaks, and therefore attachment of the peptide was confirmed *via* Fourier Transform Infrared (FTIR) spectroscopy, with the formation of a peak at 1997 nm^{-1} from the C=N bonds of peptide side chains on the spectra of **NP2**-(WR)$_3$ (Figure S11). It should be noted that the disappearance of the azide peak upon attachment could not be monitored as both **NP2** and (WR)$_3$ peptides displayed the same signal on their FTIR spectra at the same region where the azide peak is found. Next, the stability of the peptide-functionalized nanoparticles was determined using DLS and TEM. DLS results showed particle formation with a good correlation curve, and TEM images further confirmed that **NP2** was stable after functionalizing with the (WR)$_3$ peptide. The size of the particles after (WR)$_3$ attachment was found to be smaller according to the DLS and TEM results (Figure 4B). We attribute this to the nanoparticle hydrophobicity increasing with (WR)$_3$ attachment, due to the increased interactions with the polymer chains causing shrinking of the particles.

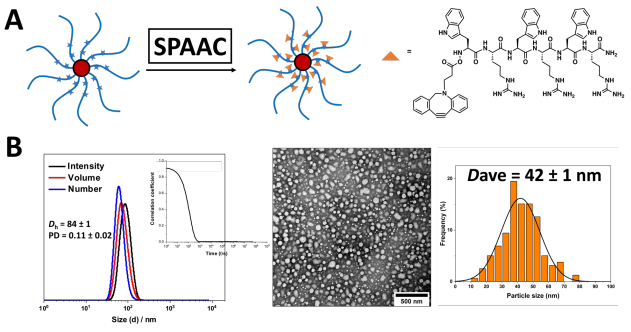


Figure 4. (A) Schematic representation of (WR)$_3$ peptide attachment to the **NP2** via SPAAC. (B) Size distribution and polydispersity index of (WR)$_3$-**NP2** particles measured by DLS and accompanying TEM image.

4. Conclusion

Notably, after showing in our previous work that polymers based on monomers known to produce non-responsive homopolymers can yield thermoresponsive copolymers, we have demonstrated in this work that these copolymers can also form nanoparticles upon the thermal trigger. This is a promising development which will enable the design of new thermoresponsive nanoparticles with tunable temperature responses upon varying the constituent polymer chemistries. These results confirm that PITSA is an efficient method for the preparation and functionalization of nanoparticles with inherent thermoresponse. We have further demonstrated that PITSA nanoparticles can find application in various areas as they are amenable to functionalization with fluorescent dyes, antibodies, anticancer drugs *etc*. Additionally, nanoparticles with different morphologies that can be achieved *via* PITSA can be functionalized by introducing various moieties into the polymer structure, allowing the building of diverse libraries of functional nanoparticles with different morphologies.

To conclude, we report the synthesis of thermoresponsive copolymers of DMA and HA monomers *via* PITSA and investigate their self-assembly behavior by measuring the particle size using DLS. The results showed that both simple mPEG-*b*-P(DMA-*co*-HA) and azide functionalized mPEG-*b*-P(AzPMA)-*b*-P(AzPMA-*co*-AA)-*b*-P(DMA-*co*-HA) copolymers assemble to form nanoparticles at 50 °C, and they disassemble below that temperature unless they are crosslinked through acrylic acid units. We also demonstrated that these nanoparticles could be functionalized with short antibacterial peptides while maintaining their stability, posing as a promising nanoparticle platform that can be functionalized to bear various moieties. We are currently working on our next step, which is to test the antibacterial efficiency of the antibacterial $(WR)_3$ peptide, the nanoparticle, and the peptide-attached nanoparticle against the most commonly tested bacteria strains. Overall, this study demonstrates that various functional nanoparticles can be prepared using PITSA and these systems hold potential for various therapeutic applications. We envisage that the diversification of monomers used for PITSA will allow the design of tailored nanoparticles with tunable properties enabling the preparation of required nanoparticles for targeting different applications.

ASSOCIATED CONTENT

Supporting Information.
Materials, characterization techniques, experimental procedures, and additional data (SEC, ^{1}H NMR, HPLC and FT-IR spectra) (PDF)

AUTHOR INFORMATION

Corresponding Authors

Rachel K. O'Reilly – School of Chemistry, University of Birmingham, Edgbaston, Birmingham, B15 2TT, UK; Orcid ID: 0000-0002-1043-7172, Email: r.oreilly@bham.ac.uk

Authors

Irem Akar – *School of Chemistry, University of Birmingham, Edgbaston, Birmingham, B15 2TT, UK.*

Amanda K. Pearce – *School of Chemistry, University of Birmingham, Edgbaston, Birmingham, B15 2TT, UK.*

Calum Ferguson – *School of Chemistry, University of Birmingham, Edgbaston, Birmingham, B15 2TT, UK.*

Author Contributions

The manuscript was written through contributions of all authors.

Funding Sources

EPSRC and University of Birmingham.

ACKNOWLEDGMENT

This work is supported by the Turkish Ministry of National Education; the Engineering and Physical Sciences Research Council, EPSRC, (EP/S00338X/1), and the University of Birmingham. The authors would like to thank Ms. Bethany Crow for her assistance for HPLC measurements and Ms. Alisha Miller for her assistance for the TEM images.

REFERENCES

[1] D. Li; R. Zhang; G. Liu; Y. Kang; J. Wu.*Adv. Healthc. Mater.* **2020**, *9* (20), 2000605.

[2] N. Narayan; A. Meiyazhagan; R. Vajtai.*Materials* **2019**, *12* (21), 3602.
[3] Z. Nie; A. Petukhova; E. Kumacheva.*Nat. Nanotechnol* **2010**, *5* (1), 15-25.
[4] J. Tan; C. Huang; D. Liu; X. Li; J. He; Q. Xu; L. Zhang.*ACS Macro Lett.* **2017**, *6* (3), 298-303.
[5] Z. Li; J. Ding; M. Day; Y. Tao.*Macromolecules* **2006**, *39* (7), 2629-2636.
[6] L. Yang; J. Tang; H. Yin; J. Yang; B. Xu; Y. Liu; Z. Hu; B. Yu; F. Xia; G. Zou.*ACS Biomater. Sci. Eng.* **2022**, *8* (2), 880-892.
[7] B. Charleux; G. Delaittre; J. Rieger; F. D'Agosto.*Macromolecules* **2012**, *45* (17), 6753-6765.
[8] C. Liu; C.-Y. Hong; C.-Y. Pan.*Polym. Chem.* **2020**, *11* (22), 3673-3689.
[9] Y. Mai; A. Eisenberg.*Chem. Soc. Rev.* **2012**, *41* (18), 5969.
[10] J. C. Foster; S. Varlas; B. Couturaud; Z. Coe; R. K. O'Reilly.*J. Am. Chem. Soc.* **2019**, *141* (7), 2742-2753.
[11] N. J. W. Penfold; J. Yeow; C. Boyer; S. P. Armes.*ACS Macro Lett.* **2019**, *8* (8), 1029-1054.
[12] J. C. Foster; S. Varlas; B. Couturaud; J. R. Jones; R. Keogh; R. T. Mathers; R. K. O'Reilly.*Angew. Chem. Int. Ed.* **2018**, *130* (48), 15959-15963.
[13] H.-J. Huang; Y.-L. Tsai; S.-H. Lin; S.-H. Hsu.*J. Biomed. Sci.* **2019**, *26* (1).
[14] O. Bertrand; J.-F. Gohy.*Polym. Chem.* **2017**, *8* (1), 52-73.
[15] G. Kocak; C. Tuncer; V. Bütün.*Polym. Chem.* **2017**, *8* (1), 144-176.
[16] P.-H. Hsu; A. Almutairi.*J Mater Chem B.* **2021**, *9* (9), 2179-2188.
[17] R. Hoogenboom. Chapter 2 - Temperature-Responsive Polymers: Properties, Synthesis, and Applications. In *Smart Polymers and their Applications (Second Edition)*, Aguilar, M. R., San Román, J. Eds.; Woodhead Publishing, 2019; pp 13-44.
[18] P. Schattling; F. D. Jochum; P. Theato.*Polym. Chem.* **2014**, *5* (1), 25-36.
[19] J. Bergueiro; M. Calderón.*Macromol. Biosci.* **2015**, *15* (2), 183-199.
[20] F. Doberenz; K. Zeng; C. Willems; K. Zhang; T. Groth.*J Mater Chem B.* **2020**, *8* (4), 607-628.
[21] M. A. Ward; T. K. Georgiou.*Polymers* **2011**, *3* (3), 1215-1242.
[22] S. R. Abulateefeh; S. G. Spain; J. W. Aylott; W. C. Chan; M. C. Garnett; C. Alexander.*Macromol. Biosci.* **2011**, *11* (12), 1722-1734.
[23] S. Phunpee; U. R. Ruktanonchai; S. Chirachanchai.*Biomacromolecules* **2022**, *23* (12), 5361-5372.
[24] E. Kostyurina; J. U. De Mel; A. Vasilyeva; M. Kruteva; H. Frielinghaus; M. Dulle; L. Barnsley; S. Förster; G. J. Schneider; R. Biehl; et al.*Macromolecules* **2022**, *55* (5), 1552-1565.
[25] T. Horiuchi; T. Sakai; Y. Sanada; K. Watanabe; M. Aida; Y. Katsumoto.*Langmuir* **2017**, *33* (51), 14649-14656.
[26] X. Chen; T. Michinobu.*Macromol. Chem. Phys.* **2022**, *223* (1), 2100370.
[27] D. Pizzi; J. Humphries; J. P. Morrow; A. M. Mahmoud; N. L. Fletcher; S. E. Sonderegger; C. A. Bell; K. J. Thurecht; K. Kempe.*Biomacromolecules* **2022**.
[28] E. A. Ksendzov; P. A. Nikishau; I. M. Zurina; V. S. Presniakova; P. Timashev; Y. A. Rochev; S. Kotova; S. V. Kostjuk.*ACS Appl. Polym. Mater.* **2022**, *4* (2), 1344-1357.
[29] M. P. J. Miclotte; S. Varlas; C. D. Reynolds; B. Rashid; E. Chapman; R. K. O'Reilly.*ACS Appl. Mater. Interfaces* **2022**, *14* (48), 54182-54193.
[30] J.-F. Lutz; A. Hoth.*Macromolecules* **2006**, *39* (2), 893-896.
[31] I. Akar; R. Keogh; L. D. Blackman; J. C. Foster; R. T. Mathers; R. K. O'Reilly.*ACS Macro Lett.* **2020**, *9* (8), 1149-1154.
[32] I. Akar; J. C. Foster; X. Leng; A. K. Pearce; R. T. Mathers; R. K. O'Reilly.*ACS Macro Lett.* **2022**, *11* (4), 498-503.
[33] C. A. Figg; A. Simula; K. A. Gebre; B. S. Tucker; D. M. Haddleton; B. S. Sumerlin.*Chem. Sci.* **2015**, *6* (2), 1230-1236.
[34] M. Vakili; V. J. Cunningham; M. Trebbin; P. Theato.*Macromol. Chem. Phys.* **2019**, *220* (2), 1800370.
[35] B. S. Sumerlin; N. V. Tsarevsky; G. Louche; R. Y. Lee; K. Matyjaszewski.*Macromolecules* **2005**, *38* (18), 7540-7545.
[36] X. Huang; S. I. Sevimli; V. Bulmus.*Eur. Polym. J.* **2013**, *49* (10), 2895-2905.
[37] M. B. Strøm; B. E. Haug; M. L. Skar; W. Stensen; T. Stiberg; J. S. Svendsen.*J. Med. Chem.* **2003**, *46* (9), 1567-1570.

4.2. Supporting Information

Supporting Information

"Preparation of functional nanoparticles of P(DMA-*co*-HA) copolymers *via* Polymerization-Induced Thermal Self-Assembly"

Irem Akar,[†] Amanda K. Pearce,[†] Calum T. J. Ferguson,[†, ‡] and Rachel K. O'Reilly[*,†]

[†] School of Chemistry, University of Birmingham, Edgbaston, Birmingham, B15 2TT, UK
[‡] Max Planck Institute for Polymer Research, Ackermannweg 10, 55128 Mainz, Germany

*Corresponding Authors: r.oreilly@bham.ac.uk (R.K.O.R.)

Supplementary Characterization Data

Table S1. Molecular characteristics of copolymers prepared *via* RAFT, as determined by ^{1}H NMR spectroscopy and SEC analyses.

Polymers	DP[a]	$M_{n,\,NMR}$[b] (kDa)	$M_{n,\,SEC}$[c] (kDa)	$Đ_M$[c]
mPEG-P(DMA-*co*-HA)	99	18.6	15.4	1.20
mPEG-P(AzPMA)-*b*-P(AzPMA-*co*-AA)	3	5.8	10.5	1.32
mPEG-P(AzPMA)-*b*-P(AzPMA-*co*-AA)-*b*-P(DMA-*co*-HA)	102	19.0	43.4	2.90

[a] Determined by ^{1}H NMR spectroscopy ($CDCl_3$, 300 MHz).
[b] Calculated from monomer conversion.
[c] M_n and $Đ_M$ determined by SEC (in $CHCl_3$ + 0.5% NEt_3, calibrated against PMMA standards).

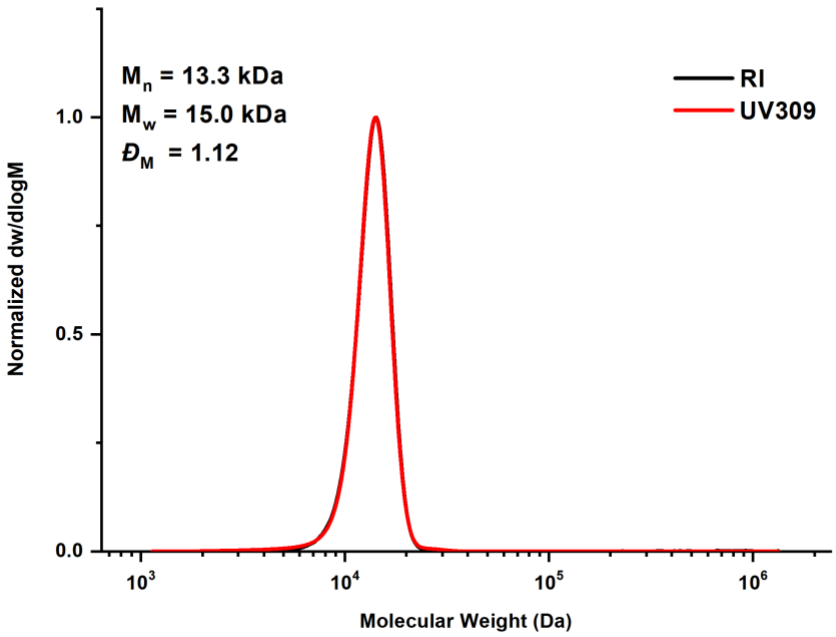


Figure S1. Normalized molecular weight distribution for mPEG-CTA determined by SEC ($CHCl_3$ + 0.5% NEt_3 as the eluent and calibrated against PMMA standards) using RI and UV detectors.

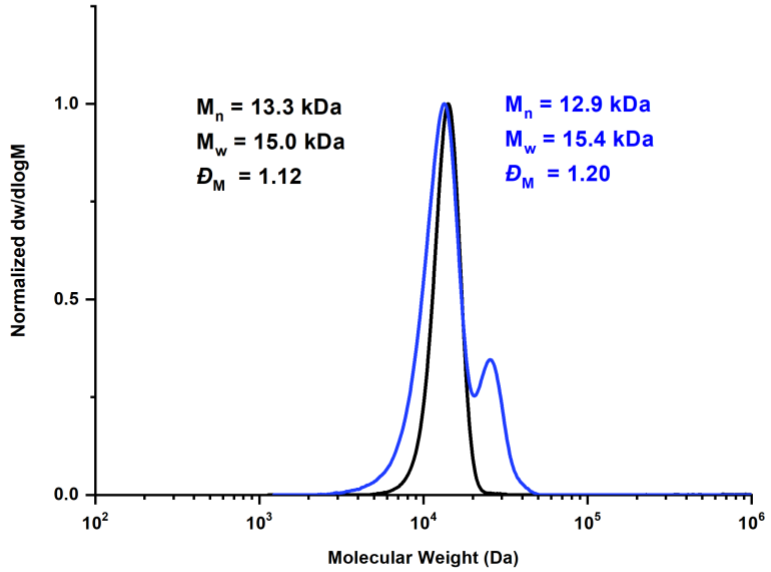


Figure S2. Normalized molecular weight distributions for mPEG-CTA (black) and mPEG-P(DMA-*co*-HA) copolymer (blue) determined by SEC ($CHCl_3$ + 0.5% NEt_3 as the eluent and calibrated against PMMA standards) using an RI detector.

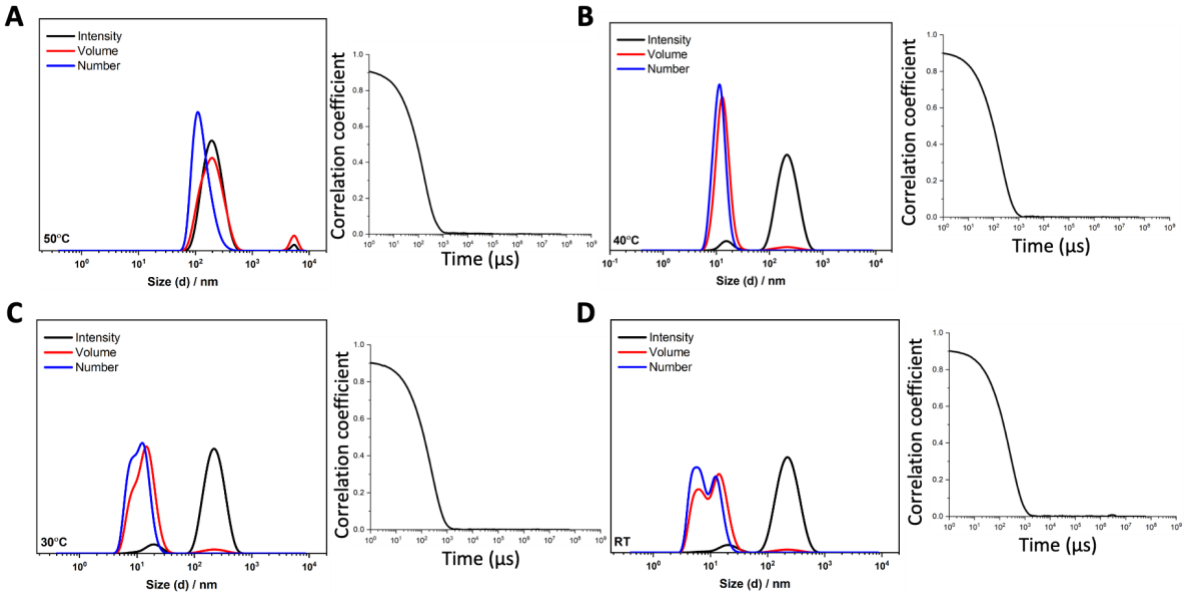


Figure S3. Size distribution of **NP1** at (A) 50 °C, (B) 40 °C, (C) 30 °C, and (D) RT measured by DLS. **NP1** solution was prepared at 5 mg mL^{-1} in nanopure water. The temperature-dependent change in particle size, volume and intensity was recorded within the temperature range of 50 °C to RT with 10 °C intervals.

Table S2. Size, number, intensity, volume and polydispersity measurements for mPEG-P(DMA-*co*-HA)$_{99}$ nanoparticle (**NP1**).

T **(°C)**	**Size**	**Number**	**Intensity**	**Volume**	**PDI**
50	173±8	153±6	193±18	191±18	0.28±0.03
40	167±4	61±86	222±0.6	88±116	0.30±0.03
30	163±3	11±3	222±7	23±7	0.32±0.01
RT	164±1	9±4	228±7	19±9	0.32±0.01

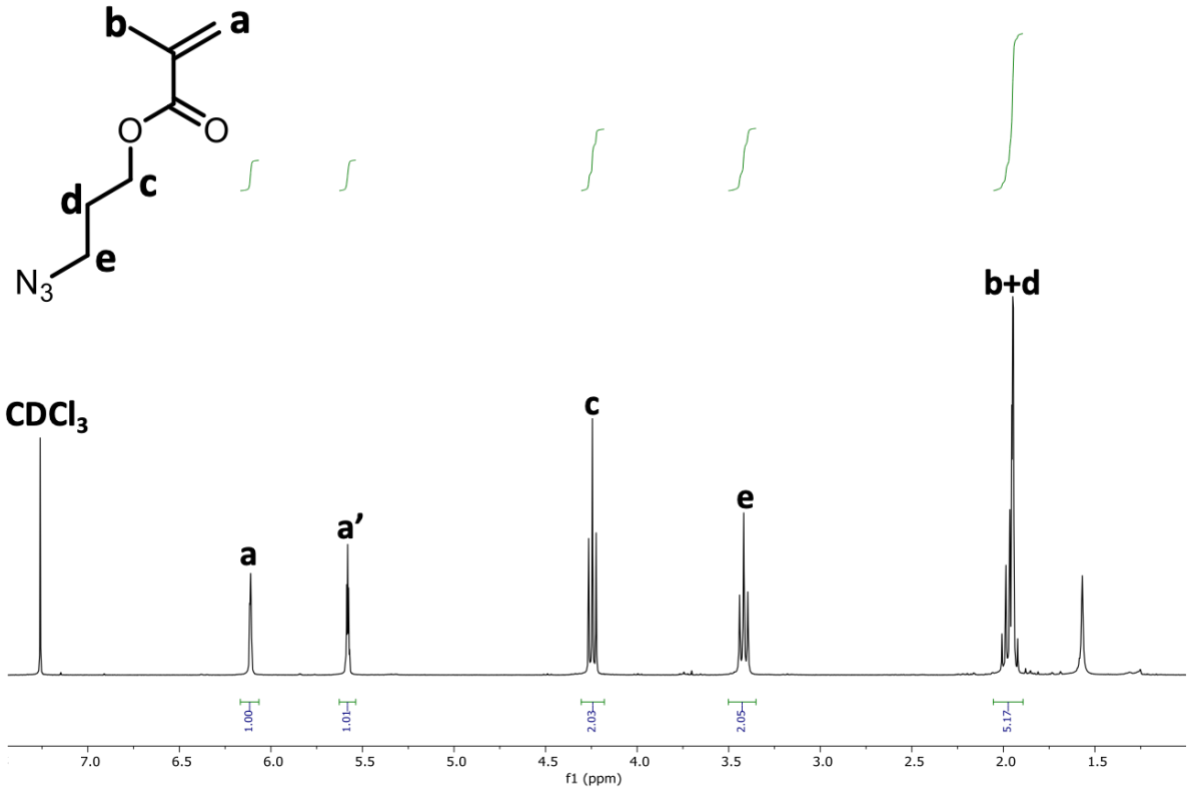


Figure S4. ^{1}H-NMR spectrum of AzPMA monomer in $CDCl_3$ (400 MHz).

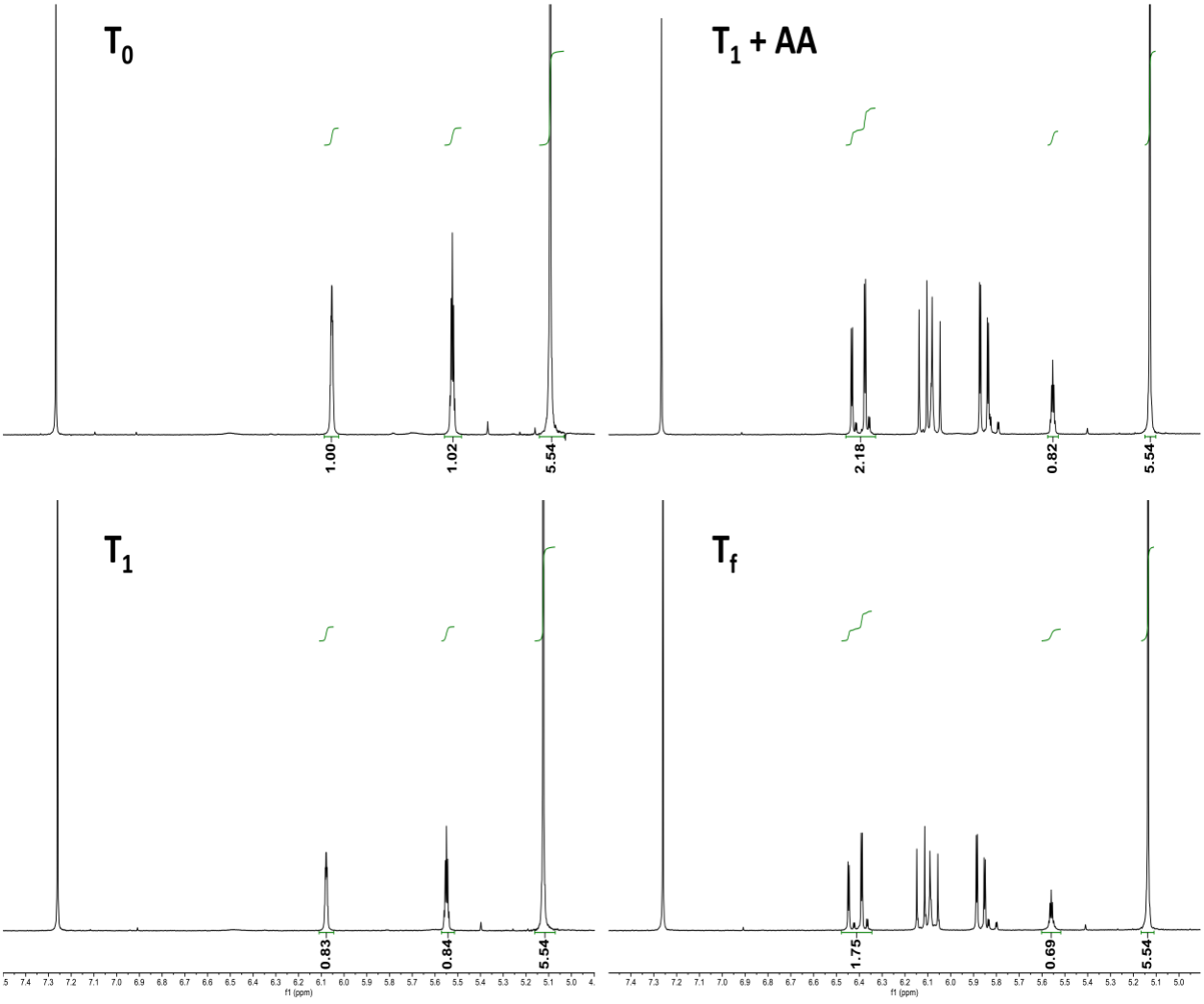


Figure S5. ^{1}H-NMR spectra of **P2** polymer in $CDCl_3$ showing the polymerization kinetics before and after the addition of AA monomer (T_1+AA represents the time point that AA monomer was introduced to the polymer solution.) (400 MHz).

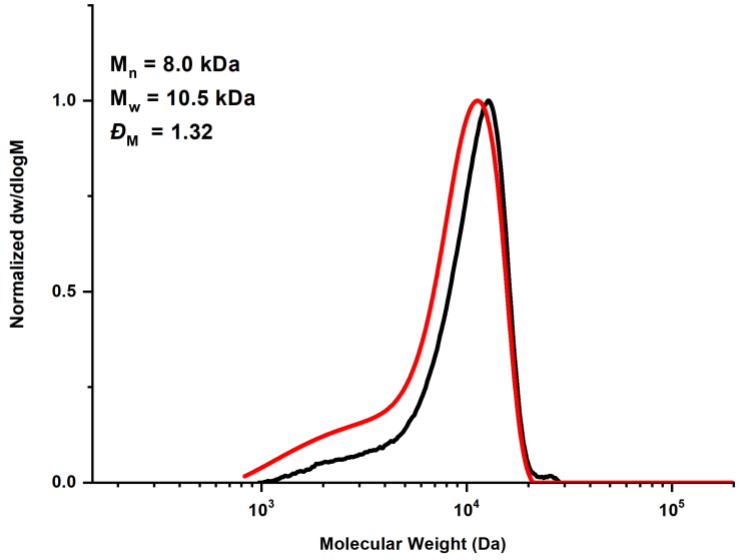


Figure S6. Normalized molecular weight distribution for mPEG-P(AzPMA)$_1$-*b*-P(AzPMA-*co*-AA)$_2$ copolymer determined by SEC ($CHCl_3$ + 0.5% NEt_3 as the eluent and calibrated against PMMA standards) using RI (black) and UV detectors (red).

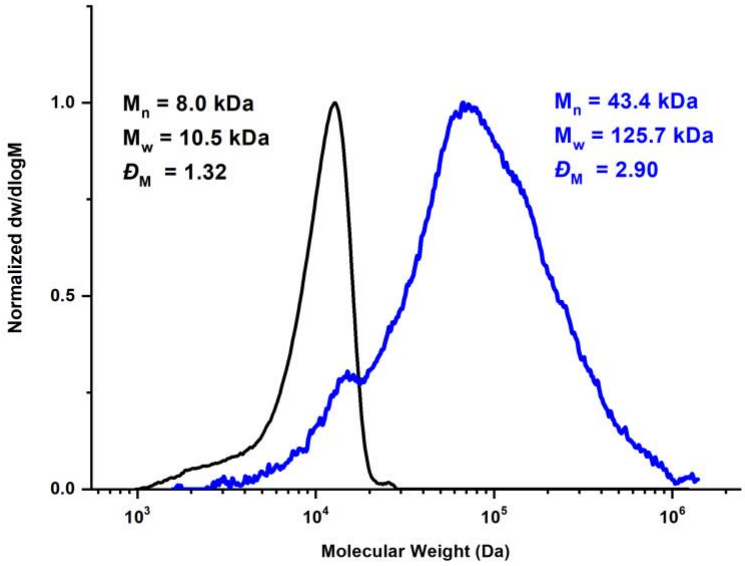


Figure S7. Normalized molecular weight distributions for for mPEG-P(AzPMA)$_1$-*b*-P(AzPMA-*co*-AA)$_2$ (black) and for mPEG-P(AzPMA)$_1$-*b*-P(AzPMA-*co*-AA)$_2$-*b*-P(DMA-*co*-HA) (blue) determined by SEC ($CHCl_3$ + 0.5% NEt_3 as the eluent and calibrated against PMMA standards) using an RI detector.

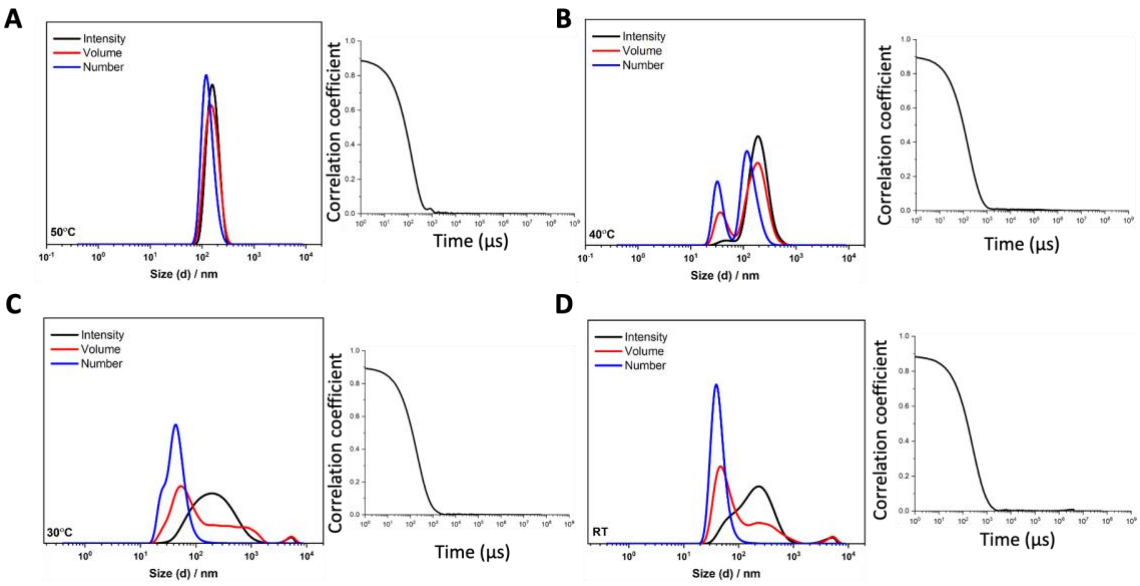


Figure S8. Size distribution of **NP2** before crosslinking at (A) 50 °C, (B) 40 °C, (C) 30 °C, and (D) RT measured by DLS. **NP2** solution was prepared at 5 mg mL^{-1} in nanopure water. The temperature-dependent change in particle size, volume and intensity was recorded within thetemperature range of 50 °C to RT with 10 °C intervals.

Table S3. Size, number, intensity, volume and polydispersity measurements for NP2 before crosslinking.

T **(°C)**	**Size**	**Number**	**Intensity**	**Volume**	**PDI**
50	153±1	133±1	163±3	159±3	0.24±0.01
40	163±2	103±59	203±17	163±44	0.26±0.04
30	159±2	45±13	363±44	364±82	0.42±0.02
RT	165±4	33±5	267±52	185±88	0.34±0.01

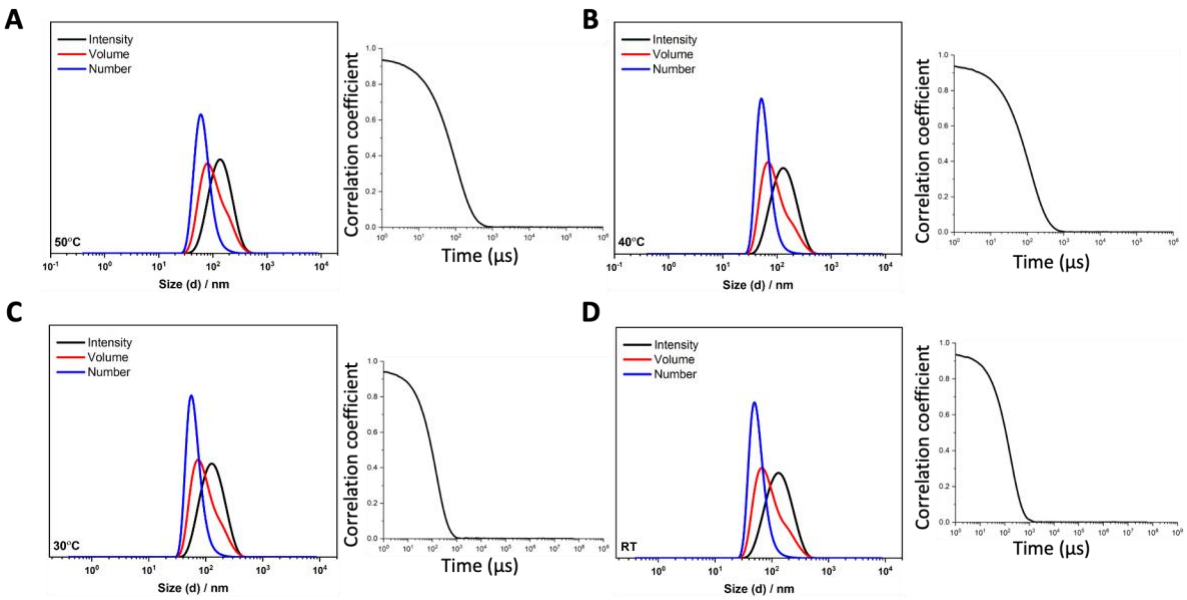


Figure S9. Size distribution of **NP2** after crosslinking at (A) 50 °C, (B) 40 °C, (C) 30 °C, and (D) RT measured by DLS. **NP2** solution was prepared at 5 mg mL^{-1} in nanopure water. The temperature-dependent change in particle size, volume and intensity was recorded within the temperature range of 50 °C to RT with 10 °C intervals.

Table S4. Size, number, intensity, volume and polydispersity measurements for **NP2** after crosslinking.

T **(°C)**	**Size**	**Number**	**Intensity**	**Volume**	**PDI**
50	122±4	71±9	154±4	120±8	0.20±0.01
40	116±2	68±7	146±6	111±2	0.20±0.01
30	113±2	50±12	146±2	98±8	0.22±0.01
RT	115±2	58±2	148±3	104±4	0.22±0.01

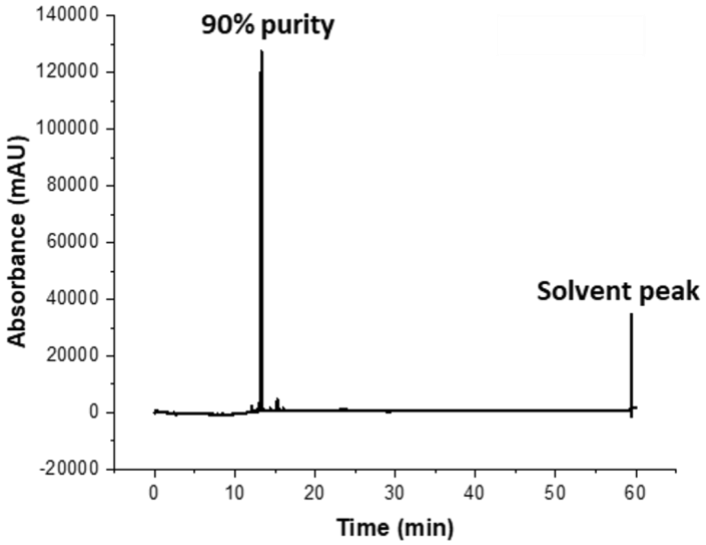


Figure S10. HPLC chromatogram of $(WR)_3$ peptide in acetonitrile : H_2O (1:1 v/v).

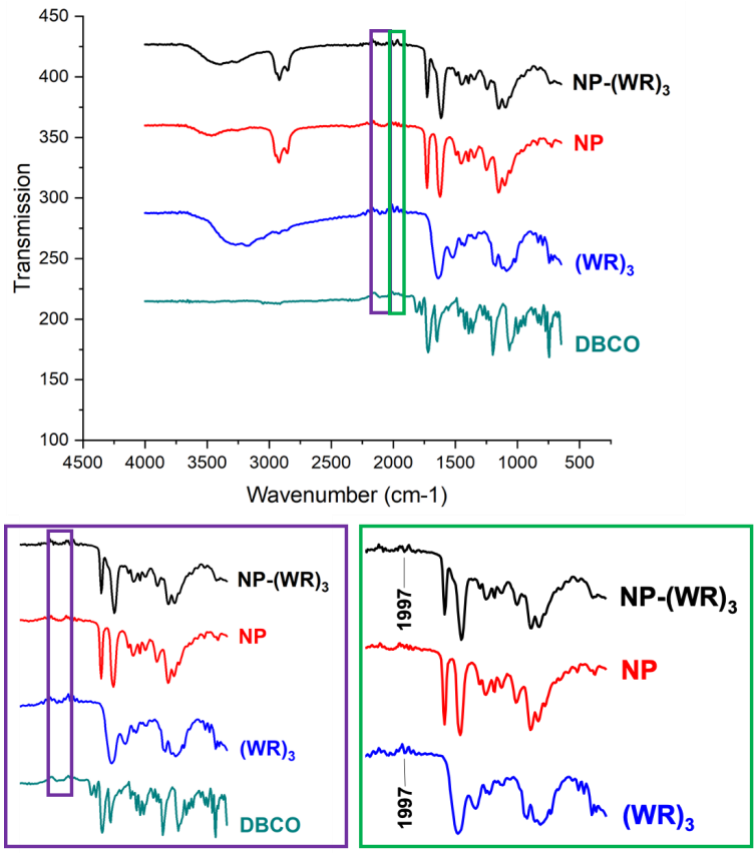


Figure S11. FTIR spectrum of DBCO-NHS, $(WR)_3$ peptide, **NP2** and **NP2**-$(WR)_3$ conjugate.

Chapter 5. Conclusion and Outlook

The overall aim of this project was to explore the synthesis of thermoresponsive polymers and investigate the effect of polymer hydrophobicity on thermoresponsive behavior of copolymers. Additionally, self-assembly behavior of thermoresponsive polymers using a recent self-assembly method was investigated and reported in the last experimental chapter of this thesis.

In Chapter 1, the concepts of synthetic polymers, polymerization methods, especially reversible addition-fragmentation chain transfer (RAFT) polymerization which was the main methodology used for copolymer synthesis in this thesis, and polymerization-induced self-assembly (PISA), with a focus on polymerization-induced thermal self-assembly (PITSA) was introduced. Thermoresponsive polymers and their applications were explained followed by a brief history of the ways of determining polymer hydrophobicity to the most recent computational tools to calculate hydrophobicity proxies.

Chapter 2 included the synthesis of brushy copolymers of OEGMA and various alkyl methacrylates where the comonomer compositions were varied in individual copolymer series in order to observe the effect of alkyl chain length and also initial feed ratio. The attempt of correlating thermoresponsive behavior of the copolymers to their hydrophobicity was done by comparing copolymer T_{CP} values to computationally calculated Log*P*/SA values of each copolymer. According to the statistical analysis carried out on different polymer properties such as polymer molecular weight, mol% and wt% of hydrophobic comonomers, polydispersity, it was found for these OEGMA-based copolymers that the mol% of the hydrophobic comonomers is the strongest descriptor of the T_{CP} of the copolymers. This was attributed to the brushy nature of OEGMA dominating the phase transition of the copolymers, thus only grafting density had the greatest effect on the T_{CP}. This was further confirmed with the same statistical study done on similar OEGMA-based copolymers reported on the literature. The lack of dependence of the comonomer chemistry on the polymer T_{CP}, would enable to

design new copolymers using brushy monomers with required thermoresponsive behaviors for selected applications.

In Chapter 3, the same methodology used in the Chapter 2 was used for the synthesis and characterization of non-brushy P(DMA-*co*-RA) copolymers where hydrophilic DMA was copolymerized with hydrophobic alkyl acrylates *via* RAFT polymerization in order to obtain statistical copolymers. These copolymers are particularly interesting as they are obtained by using monomers that individually produce nonresponsive homopolymers. Thermoresponsive behavior of these copolymers were determined by measuring their T_{CP} on UV-Vis, which showed a decrease in the T_{CP} values as the hydrophobicity of the copolymers increased. Hydrophobicity of the copolymers were also determined by calculating the Log*P*/SA of each copolymer on a computational program using a representative oligomer model for each copolymer. The attempt to correlate polymer hydrophobicity to their T_{CP} was successful for these non-brushy copolymers. Using this correlation, the T_{CP} of a new copolymer was predicted prior to synthesis with only 1 °C difference from the measured $T_{CP.}$ Therefore, it was suggested that the prediction power of this system serves as a guiding principle for non-brushy copolymers when designing new polymers with a thermoresponse at desired temperature points.

Chapter 4 included the synthesis of thermoresponsive nanoparticles using DMA and HA monomers *via* PITSA. It was explored how the ability of these non-responsive monomers to produce thermoresponsive copolymers translates into self-assembly of these copolymers during PITSA process. Initially, a simple system was prepared by using a PEG-CTA and chain extending it with DMA and HA monomers. Nanoparticle formation at 50 °C was shown *via* DLS measurement followed by disassembly of particles as the temperature decreased. In order for particles to remain stable at room temperature, acrylic acid monomers were introduced to the polymer chain for enabling crosslinking through them. Also, AzPMA monomers were

introduced to allow functionalization of the nanoparticles *via* Cu-free “Click” chemistry. After the crosslinking, the stability of the nanoparticles at room temperature was shown *via* DLS measurements and TEM imaging. The nanoparticles were further functionalized with a short antibacterial peptide, $(WR)_3$, which was synthesized on an automated peptide synthesizer. Functionalized nanoparticles were characterized *via* DLS and TEM. This study showed that functional thermoresponsive nanoparticles of non-responsive monomers can be synthesized using PITSA. The next step for this study is to carry out antibacterial tests for the peptide functionalized nanoparticles to explore the potential improved antibacterial efficiency of the nanoparticles.

Overall, this project investigated the tuning of the thermoresponsive behavior of various copolymers and the systems that can be prepared by using these copolymers. The potential of these thermoresponsive systems for therapeutic applications renders them promising tools in the area of biomedicine and thus requires further investigations for improvement of these systems.